EPA-600/4-78-003
January 1978

RESIDENCE TIME OF ATMOSPHERIC POLLUTANTS AND LONG-RANGE TRANSPORT

by

Teizi Henmi, Elmar R. Reiter and Roger Edson
Department of Atmospheric Science
Colorado State University
Fort Collins, Colorado 80523

Grant 803685

Project Officer
George C. Holzworth
Meteorology and Assessment Division
Environmental Sciences Research Laboratory
Research Triangle Park, NC 27711

U.S. ENVIRONMENTAL PROTECTION AGENCY
OFFICE OF RESEARCH AND DEVELOPMENT
ENVIRONMENTAL SCIENCES RESEARCH LABORATORY
RESEARCH TRIANGLE PARK, NC 27711

DISCLAIMER

This report has been reviewed by the Environmental Science Research Laboratory, U.S. Environmental Protection Agency, and approved for publication. Approval does not signify that the contents necessarily reflect the views and policies of the U.S. Environmental Protection Agency, nor does mention of trade names or commercial products constitute endorsement or recommendation for use.

ABSTRACT

The Lagrangian trajectory model which is suitable for the study of long-range transport of pollutants is developed. The model is aimed for use with input parameters obtainable routinely from the national meteorological services.

The horizontal dispersion of pollutants along the trajectory of a layer-averaged wind is determined by the quantity Σ_h, which is calculated from the standard deviation of wind velocities. The vertical distribution of pollutants is assumed to be uniform throughout the mixing layer.

The computer program is capable of calculating trajectories over the region of the U.S. using routine sounding data. The output consists of tables of locations of trajectory end points at each time-step, and dispersion widths along a trajectory, and the plotting of trajectories.

Calculations of regional residence times, T, of SO_2 in the mixing layer are based on the following assumptions: a) Dry deposition, precipitation scavenging, and chemical transformation are the removal mechanisms of the pollutant from the atmosphere, b) The deposition velocity is 1 cm/sec and the chemical transformation rate is $1 \times 10^{-6} sec^{-1}$ regardless of the season and the location, c) The ratio of concentration of the pollutant in precipitation water to that in air is 5×10^4 on a volume basis, d) There is no leakage of the pollutant from the top of the mixing layer, and e) Import and export fluxes due to turbulent diffusion through the boundaries of the region under consideration are balanced.

Climatological data of the mixing layer depth (Holzworth, 1972) and hourly precipitation data are used for the calculation of the mean regional residence time, T. T is calculated for the region of the United States east of 105°W longitude, for the cold season (November to April), and for the warm season (May to October). The results are shown as isopleths of T over the studied area.

In order to incorporate the scavenging due to cumulus cloud precipitation into our trajectory model, a cumulus cloud model with detailed microphysical processes was developed. The microphysical processes taken into consideration are: Brownian diffusion, turbulence capture, impaction, autoconversion and accretion. Using typical size distributions for maritime and continental aerosols, scavenging characteristics in maritime and continental cumulus clouds were studied. The results can be summarized as follows: The scavenging coefficient of aerosols by cloud water droplets is one order of magnitude larger in the continental cloud than in the maritime cloud. On the other hand, the scavenging coefficient of aerosols by rainwater droplets is slightly

larger in maritime clouds than in continental clouds. Similarly, the scavenging coefficient of cloudwater droplets by rainwater droplets is larger by several factors in the maritime cloud than in the continental cloud. As a whole, aerosols are more efficiently scavenged in the continental cloud than in the maritime cloud.

CONTENTS

FIGURES

TABLES

LIST OF SYMBOLS

A	Cunningham correction factor
a	aerosol radius
a'	coefficient in the autoconversion
b	constant in the Ekman layer equation
$C(x)$	concentration of a pollutant at the distance x
C_1	source strength
C	concentration of the pollutant
C'	entrainment constant
C_p	specific heat at constant pressure
D	diameter of raindrop
$\overline{E(D/C)}$	average collection efficiency between rain and cloud droplets
$f(a)$	size distribution of aerosols
$f(r)$	size distribution of cloudwater droplet
$F(R)$	size distribution of rainwater droplet
f	Coriolis parameter
f'	fraction of the distance x over which rain is falling
F_α	constant defined by Eq. (42)
g	acceleration of gravity
h	height of the mixing layer
h'	coefficient defined in Eq. (48)
i	aerosol size index
j	cloudwater size index

k rainwater size index

k' coefficient in the autoconversion Eq. (48)

k_b Boltzmann's constant

k_k total decay rate

k_p decay rate due to precipitation scavenging

K momentum eddy diffusivity

K_α constant defined by Eq. (43)

L_{c_ℓ} latent heat of condensation

L_1 source width

$L(3)$, $L(16)$ $L(12)$ travel distance calculated with the 3-hours, 6-hours, and 12-hours respectively

ΔL_6, ΔL_{12} vectorial differences of trajectories obtained with the 3-hour and 6-hour intervals, and with the 3-hour and 12-hour intervals respectively

ℓ mean free path of air molecules

M rainwater content

M_H content of rainwater fallout

m cloudwater content

n_o concentration of cloudwater droplets

N_a number concentrations of aerosols in the cloud air

N_c number concentrations of aerosols in the cloudwater

N_o size distribution of raindrop

P_d probability of dry period

P_p probability of wet period

P_r ratio of rainwater fallout to the total rainwater

$\overline{P}$ mean precipitation rate

Q_c cloudwater mixing ratio

Q_H rainwater mixing ratio

Q_s	total mixing ratio of condensed water substance
Q_T	total moisture mixing ratio
q_e	environmental vapor mixing ratio
q_s	saturation mixing ratio
q_v	cloud vapor mixing ratio
R	rainwater droplet radius
R_a	gas constant of air
r	radius of cloudwater droplet
S	coefficient defined by Eq. (62)
T	residence time
T_c	temperature in the cloud
Te	turnover time
Te_n	environmental temperature
t_p	residence time due to precipitation scavenging
t_c	residence time due to chemical transfer
t_d	residence time due to dry deposition
$\bar{u}$	mean wind speed
V_g	deposition velocity
V_p	precipitation scavenging velocity
V_t	terminal velocity of rainwater droplet
$\bar{V}_y$	y-component of the mean wind
w	vertical velocity
α	coefficient of Gamma distribution
β	coefficient of Gamma distribution
Γ	Gamma function
γ	coefficient in the Marshall-Palmer distribution

ε	ratio of the density of water to that of air
ε'	rate of energy dissipation
η	dynamic viscosity of air
η_d	frequency distributions of dry period
η_p	frequency distributions of wet period
$\theta(z)$	wind direction at altitude z
κ	concentration of pollutant in rainwater
Λ_1	scavenging rate of aerosols by cloudwater droplets
Λ_2	scavenging rate of aerosols by rainwater droplets
Λ_B	Brownian diffusion scavenging rate of aerosols by rainwater droplets
Λ_I	interception collection rate of aerosol by rainwater droplet
Λ_{II}	inertial impaction rate of aerosols by rainwater droplets
Λ_T	turbulent diffusion scavenging rate
λ	conversion rate of cloudwater into rainwater
λ_d	decay rate due to dry deposition
λ_c	chemical transformation rate
λ_p'	removal coefficient during wet period
λ_d'	removal coefficient during dry period
$\bar{\lambda}$	mean precipitation scavenging coefficient
μ	entrainment parameter
ν	kinetic viscosity of air
ν_r	radius dispersion
ρ	density of air
ρ_a	density of cloud air
ρ_e	density of the environmental air

ρ_ℓ	density of water
ρ_p	density of aerosol
Σ_h	mean width of pollutant plume
$\Delta\Sigma_h$	relative error of horizontal dispersion
σ	coefficient of Gamma distribution
σ_{v_h}	dispersion factor defined by Eq. (12)
σ_{v_x}	standard deviation of x-component of wind
σ_{v_y}	standard deviation of y-component of wind
τ_d	mean duration of dry period
τ_p	mean duration of wet period
τ	time
χ	concentration of pollutant in air

ABBREVIATIONS

DWi	distance weighting factor
TS_o	trajectory segment
TSi	contribution to the trajectory segment from an observed wind to the midpoint of TSi
AWi	alignment weighting factor

ACKNOWLEDGEMENTS

We are grateful to George C. Marshall Space Flight Center of NASA for kindly supplying the Atmospheric Variability Experiment Data; and to The Air Resources Laboratories of NOAA at Silver Spring, Maryland, for making it possible to use the computor program of trajectory analysis.

SECTION 1

INTRODUCTION

The transport of air pollutants across metropolitan, regional and national boundaries has received increasing attention by scientists and control agencies. It is now recognized that long-range transport of polluted air masses takes place well beyond 100 km, and that secondary air pollutants, such as ozone and sulfate, are produced during the transport. Acid rain in the northeastern United States is associated with air parcels that have traveled through major industrial areas in the midwestern and east-central states one or two days earlier (Dittenhoefer and Dethier, 1976). Thus, transport model calculations play an important role in understanding the relation between emissions and concentrations of pollutants in the atmosphere, and the formation of secondary air pollutants.

One of our principal efforts in the last two contract periods has been to develop a long-range transport model suitable for keeping track of pollutants downstream of large industrial complexes. The basic concepts of our model are as follows: The mean motion of pollutants in the mixing layer is determined by the mean wind field in the layer. In practice, the pollutant movement can be followed by a step-by-step trajectory analysis, in which mean wind speeds and directions in the mixing layer are estimated from available sounding data and are applied for a period of several hours. From the time-dependent mean wind fields, the trajectory of a large polluted air volume can be obtained. The horizontal dispersion of pollutants is caused by horizontal turbulence and by mean wind shear. However, for long-range transport, the mean wind shear is by far the dominant cause of the dispersion of pollutants. In our transport model, the horizontal dispersion of pollutants is determined by the quantity, Σ_h, which is calculated by the standard deviation of wind velocities in the mixing layer. In our model, the physical removal processes due to dry deposition and precipitation scavenging are included. In Section 4, the details of our model are described.

A parameter which adequately characterizes the fate of pollutants over longtime and space scales is the residence time in the atmosphere. We have considered the determination of the residence time of SO_2 in the mixing layer. Assuming that precipitation, deposition, and the transformation into sulfate are the mechanisms of removal, the regional residence times of pollutants have been calculated for the region of the United States east of 105°W longitude. The details of this study are found in Section 5.

In pollution meteorology, cumulus clouds have two important roles. The first role is to vertically transport heat, moisture, and momentum as well as pollutants. The second role is to cleanse the polluted atmosphere by rainout and washout processes. The best knowledge about these roles can be obtained

from a cloud-modelling study. Taking into consideration the microphysical processes such as Brownian diffusion, turbulent capture, impaction, and auto-conversion, we have studied the in-cloud scavenging (rainout) characteristics of clouds. Particularly, scavenging in the continental and maritime cumulus clouds has been considered. This study is described in Section 6.

SECTION 2

CONCLUSION

The Lagrangian trajectory model which is suitable for the study of long-range transport of pollutants is developed. The model is aimed for use with input parameters obtainable routinely from the national meteorological services. The model equation contains the terms of physical removal processes, so that the sink areas of pollutants which emanate from an industrial complex can be determined. The horizontal dispersion of pollutants along the trajectory of a layer-averaged wind is determined by the quantity Σ_h, which is calculated from the standard deviations of wind velocities. A computer program for trajectory analysis uses winds averaged through any desired layer above average terrain. Computer output includes a listing of individual trajectory endpoints after selected durations, dispersion factor Σ_h, and plotted trajectories.

The e-folding residence time T and turnover time Te of sulfur dioxide are calculated over the region of the United States east of 105° W longitude. The year was divided into the cold season (January - April, and November and December), and the warm season (May - October), and the T and Te for each season are calculated. It is shown that, for practical purposes, either T or Te can be used to represent the residence time for the studied area. The following conclusions are obtained:

1. The residence time is, in general, longer in the warm season than in the cold season over the studied area.

2. Short residence times characterize the region surrounding the Great Lakes and the southern part of the United States.

3. Long regional residence times are found in the western parts of the the studied area.

4. In the studied area, the regional residence time lies in the range between 20 and 40 hours for the cold season and in the range between 30 and 60 hours for the warm season.

5. The dry deposition is the most dominant removal machanism in the studied area.

In order to incorporate the scavenging due to cumulus cloud precipitation into our trajectory model, the scavenging characteristics of continental and maritime cumulus clouds are investigated, based on a numerical model of in-cloud scavenging, combined with a cumulus model. It is found that the scavenging rate of aerosols by cloud water droplets is one order of magnitude larger

in the continental cloud than in the maritime cloud. On the other hand, scavenging rates of aerosols by rainwater droplets, and scavenging rates of cloudwater droplets by rainwater droplets are larger in the maritime cloud than in the continental cloud.

SECTION 3

RECOMMENDATIONS

The Lagrangian trajectory model developed by this project is primarily aimed for the study of transport of chemically inactive pollutants. It is recommended that further efforts shall be made to incorporate into the model the transformation of SO_2 to sulfate.

The residence time calculation of SO_2 was primarily based on the physical removal processes. Sulfate removal is an additional important aspect of the overall sulfur-removal process. Accordingly, an extension of the present calculation to provide for sulfate residence time is recommended.

The study of scavenging characteristics by cumulus clouds was concerned only with particulate pollutants. It is desirable to study the scavenging of gaseous pollutants, such as SO_2, by cumulus clouds, so that the precipitation removal term in the transport model can be refined. The applications of a method of calculating SO_2 washout from plumes, developed by Dana et al., (1976) should be considered. Furthermore, the study of scavenging characteristics by other types of clouds, such as clouds associated with front formation, must be studied in the future.

SECTION 4

LONG-RANGE TRANSPORT MODEL

4.1 General Features of Long-Range Transport

In the long-range transport process of airborne pollutants, the following physical features can be envisioned:

The general track of airborne pollutants is determined by the horizontal wind field over the whole depth of the atmospheric layer through which the material has been spread vertically. It is usually found that wind speed and direction change substantially with respect to height. Horizontal spreading of pollutants will be caused by horizontal turbulence, by the systematic change of wind with height, and by synoptic-scale variations in the wind field. The horizontal spread of pollutants by systematic changes of wind with respect to height will be particularly effective when the plume of pollutants is subject to an alternation of nocturnal stable conditions and daytime convective conditions. Mixing will also progressively extend the vertical spread of pollution, ultimately to the top of the boundary layer and toward a state of uniformity throughout the depth of this layer. This process will occur rapidly in the course of transport during daytime convective conditions, but will be slowed down during stable conditions at night. There is a diurnal variation in the depth over which effective vertical mixing exists. The pollution contained in the layer between the daytime and nighttime mixing height will take a different track from that of pollutants in the mixing layer during the nighttime hours. During the next day, far downstream from its original source region, the pollution carried above the nighttime inversion may again be mixed into the mixing layer as solar radiation spawns renewed mixing processes during daytime. The transport of the pollution to even greater heights is accomplished by penetrative convection (such as in Cb clouds), by large scale ascent from horizontal convergence and by uplifting of warm air over cold air.

In general, therefore, the transport of pollutants must be considered separately in three main layers:

(1) Nighttime and daytime mixing layer containing a near uniform vertical distribution of pollutants;

(2) The layer between daytime mixing height and nighttime mixing height, in which pollutants are trapped during the nighttime;

(3) The free atmosphere containing pollution which has been carried up, beyond the range of boundary layer mixing, by large-scale ascent or by penetrative convection.

In order to estimate the fate of pollutants in the atmosphere, the transport in each of these three layers must be studied.

4.2 Trajectory Model for Long-Range Transport

One of the main objectives of this investigation is to determine the sink areas of pollutants emanating from large industrial complexes. The pollutants are removed from the atmosphere by mechanisms such as dry deposition and precipitation scavenging. Chemical transformation of pollutants during their transport stage will have to be considered as well. In the following model, the terms of chemical transformation are not included. Thus, the model in its present stage is only applicable to the transport of particulate and chemically inactive pollutants.

Let us assume that pollutants are transported with the mean wind speed $\bar{u}$, as shown in Figure 1, from an initial vertical plane at 0 in which the concentration c_o is uniformly distributed. The width of the source area perpendicular to the mean wind is taken as L_o, its height is h, the height of the mixing layer. After time $t = x/u$, the pollutants cross a vertical plane, P, at a distance x from the source area. The width of the pollution plume at P is defined as

$$L(x) = L_o + 2[\sigma v_h] \frac{x}{\bar{u}} , \qquad (1)$$

where $[\sigma v_h]$ is the quantity defined in the next section.

If C(x) is the concentration at distance x, the rate at which pollutants cross the vertical plane of P is $\bar{u} \cdot h \cdot L(x) \cdot C(x)$. Assuming that $\bar{u}$ and h are constant during the time interval required to travel the distance δx, the net rate of loss of pollutants between the planes at x and at $x + \delta x$ is $\bar{u} \cdot h \cdot \frac{d}{dx}(LC)\delta x$. This amount is balanced by removal processes such as dry deposition, precipitation scavenging and loss from the top of the mixing layer. The mass balance equation for C(x) is given by

$$\bar{u} \cdot h \frac{d}{dx}(Lc) = [v_g + f' v_p + v_d] \cdot LC \qquad (2)$$

where v_g is the deposition velocity, v_d is the diffusion velocity from the top of the mixing layer, h, and f' is the fraction of the distance x over which rain is falling. v_p is the precipitation scavenging velocity.

From equations (1) and (2) one obtains

$$\int_{L_o \cdot C_o}^{L \cdot C} \frac{d(L \cdot C)}{L \cdot C} = \int_0^X \frac{[v_g + f' v_p + v_d]}{h} \cdot \frac{dx}{\bar{u}}$$

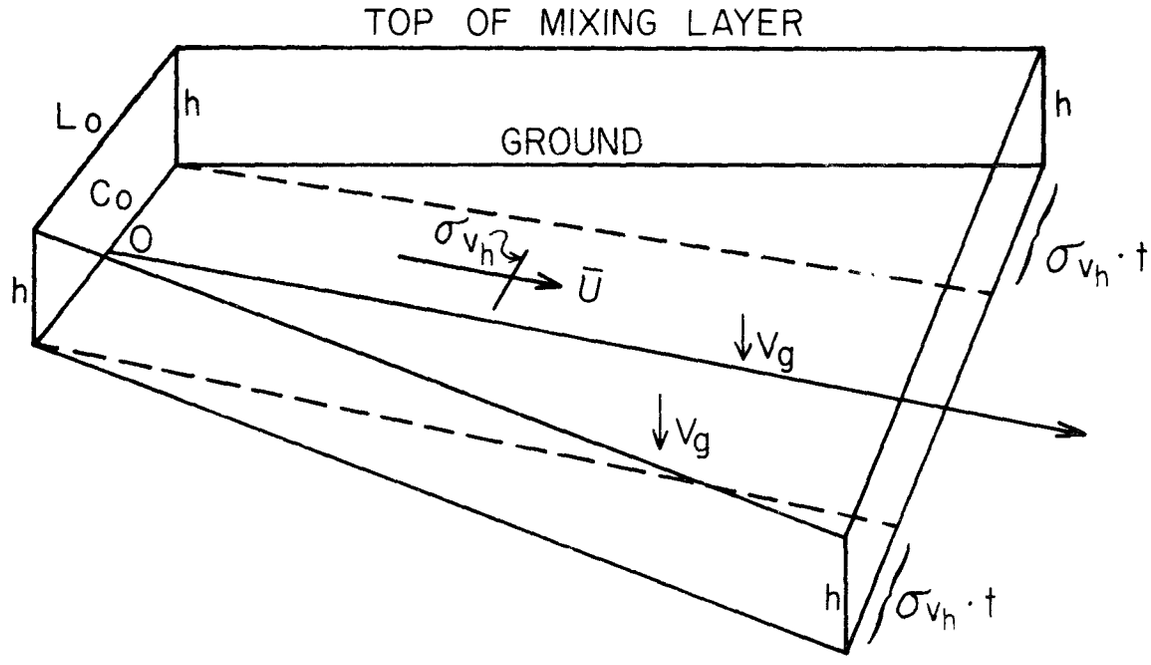

Figure 1. Schematic diagram of the model.

Therefore,

$$C(x) = \frac{C_o \cdot L_o}{L_o + 2[\sigma v_h]\frac{x}{\bar{u}}} \exp\left[-\frac{v_g + v_d + f' v_p}{h}\frac{x}{\bar{u}}\right] \qquad (3)$$

A similar equation was derived by Scriven and Fisher (1974).

An application of equation (3) along the trajectory of the mean wind $\bar{u}$, which is defined in the next section, can be made as follows: After the first interval, t, of trajectory analysis, the concentration of the pollutant under consideration at the end point of trajectory, x_1, is given by

$$C_1(x_1 = \bar{u}_1 \cdot t) = \frac{C_o \cdot L_o}{L_o + 2[\sigma v_{h_1}]\cdot\frac{x_1}{\bar{u}}} \exp\left\{-\frac{v_{g1} + v_{d1} + f'_1 v_{p1}}{h}\right\} \qquad (4)$$

where subscript 1 refers to the first interval of trajectory analysis. For the second interval, C_1 is regarded as the concentration of the new hypothetical line source with the width of $L_1 = L_o + 2\sigma v_{h1}\frac{x_1}{\bar{u}}$. The concentration of pollutant at the distance x from the new hypothetical line source is

$$C(x) = \frac{C_1 \quad L_1}{L_1 + 2[\sigma v_h]\frac{x}{\bar{u}}} \exp\left\{-\frac{v_g + v_d + f' v_p}{h}\frac{x}{\bar{u}}\right\} \qquad (5)$$

where C_1 is given by equation (4). By repeating the above process, the concentration along the trajectory at any distance from the source area can be calculated.

4.3. Vertical Dispersion of Pollutants in the Mixing Layer

If one attempts a comprehensive description of the transport process of pollutants, one finds that little is known about the rate of vertical mixing after tens of minutes and/or kilometers following the release of a pollutant (Pasquill, 1974). This is due in part to the great difficulties in sampling over a large volume of space within the mixing layer, and in part due to the difficulties of measuring low concentrations existing at several tens of minutes after release from a source. However, recent observations of pollutant concentrations above and downwind of industrial complexes (Davis and Newstein, 1968; Georgii, 1969; Kocmond and Mack, 1972; Auer, 1975) have shown that, within a mixing layer which is well defined by a capped inversion, the concentration of pollutants is uniformly distributed in the vertical throughout the mixing layer. Furthermore, computer and laboratory studies of the vertical diffusion of nonbuoyant particles within the mixing layer by Deardorff and Willis (1974) indicate that the distribution of particles released near the

ground become vertically uniform after the dimensionless time, t_*, has assumed a value of about 3. t_* is defined as $t_* = (w_*/z_i)t$, where t is the time after release, and $w_* = [(g/\theta_m)\ \overline{w'\theta'}_s\ z_i]^{1/3}$. g is the gravitational acceleration, θ_m is the mean potential temperature in the mixing layer, and $\overline{w'\theta'}_s$ is the kinematic heat flux close to the surface.

In agreement with these findings, we assume that the concentrations of a pollutant for mesoscale and synoptic scale trajectories are uniformly distributed in the vertical throughout the mixing layer.

4.4 Horizontal Dispersion of Pollutants in the Mixing Layer

Physically, the horizontal dispersion of pollutants is caused by horizontal turbulence and by mean vertical wind shear. However, for the mesoscale and synoptic scale transport of pollutants it can be assumed that the mean wind shear is the dominant cause for the dispersion (Tyldesley and Wallington, 1965; Csandy, 1968). This dominance of vertical wind shear in the horizontal dispersion, with the assumption of uniform distribution of pollutants in the vertical throughout the mixing layer, brings us to the following arguments:

Let us take the X-axis along the east-west direction and the Y-axis along the north-south direction. Then, within the mixing layer, as illustrated in Figure 2, the following equations hold:

The mean mass-averaged velocity components are given by

$$\bar{v}_x = \frac{\int_0^h \rho v(z) \cdot \cos\theta\,(z)\, dz}{\int_0^h \rho dz} \tag{6}$$

$$\bar{v}_y = \frac{\int_0^h \rho v(z) \cdot \sin\theta\,(z) dz}{\int_0^h \rho dz} \tag{7}$$

where $\bar{v}_x$ and $\bar{v}_y$ are the x - and y - components of the mean wind, v(z) is the wind speed at altitude z, $\theta(z)$ is the wind direction at altitude z, ρ is the air density, and h is the height of the mixed layer.

The mean wind speed is given by

$$\bar{u} = \sqrt{v_x^2 + v_y^2} \tag{8}$$

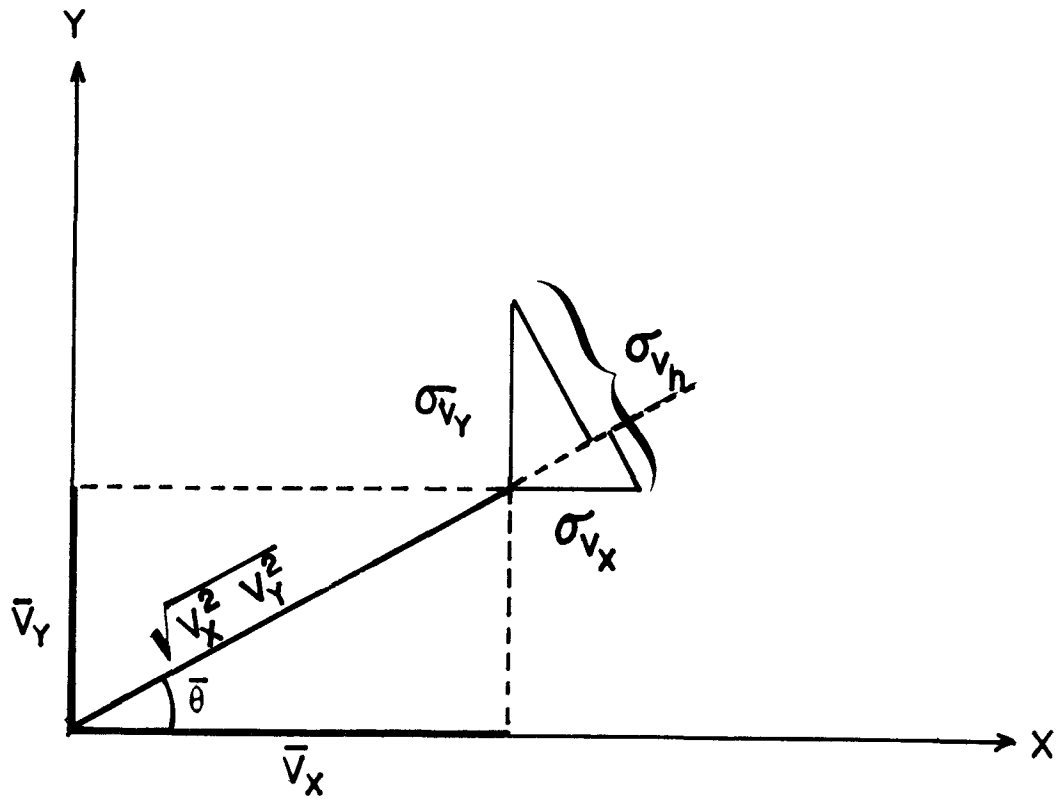

Figure 2. Scheme of the calculation of standard deviations of wind components.

The mean veering angle is

$$\theta = \tan^{-1} \frac{\bar{v}_y}{\bar{v}_x} \tag{9}$$

The deviation of wind from the mean wind is

$$\sigma v_x = \left[\int_0^h (v_x[z] - \bar{v}_x)^2 dz/h \right]^{1/2} \tag{10}$$

$$\sigma v_y = \left[\int_0^h (v_y[z] - \bar{v}_y)^2 dz/h \right]^{1/2} \tag{11}$$

The horizontal deviation of that wind component from the mean wind, which is perpendicular to the mean wind, $\bar{v}$, is

$$\sigma v_h = \frac{\sigma v_x \cdot |\bar{v}_y| + \sigma v_y \cdot |\bar{v}_x|}{\bar{u}} \tag{12}$$

this is called a "dispersion factor".

The mean "width" of the pollutant plume along the mean wind is given by

$$\sigma_h = \sigma v_h \cdot t = \frac{\sigma v_x \cdot |\bar{v}_y| + \sigma v_y \cdot |\bar{v}_x|}{\bar{u}} \frac{x}{\bar{u}} \tag{13}$$

where t is the time step of the trajectory analysis, and x is the distance from the source.

When the trajectory analysis is repeated for n time steps of equal length, the accumulated width of the pollutant plume along the mean wind is given by

$$\Sigma_h = 2(\sigma v_{h,1} \cdot t + \sigma v_{h,2} \cdot t + \text{----} + \sigma v_{h,n} \cdot t) + L_o$$

$$= 2\left(\sum_1^n \sigma_{v_{h,i}}\right) \cdot t + L_o$$

$$= 2 \sum_1^n \left(\sigma v_{h,i} \cdot \frac{x_i}{\bar{v}_i}\right) + L_o \tag{14}$$

where L_o is the width of the original source area perpendicular to the mean wind.

4.5. Preliminary Studies of Trajectory and Dispersion of the Layer-Averaged Wind in the Mixed Layer

In order to apply the long-range transport model to actual data, the development of an accurate trajectory construction technique using the layer-averaged wind is essential. For this purpose, the upper air sounding data obtained during the NASA-sponsored Atmospheric Variability Experiments (AVE) are used. The three-hourly sounding interval and the more detailed vertical resolution of the data permit more accurate trajectory computation and mixing-layer depth determination than is feasible with the customary twice daily soundings.

In this study, three different trajectory analyses are made with 3-, 6-, and 12-hourly time intervals using the AVE data.

4.5.1. Trajectory Studies

In this study, the height of the mixing layer is defined as the first level (using 25 mb interval data) between 500 meters and 3000 meters from the surface where a significant stabilization of temperature lapse rate occurs ($\frac{\partial T}{\partial z} \geq -4°C/km$). If no such level is found, the height of the mixing layer is assumed to be at 3000 meters above the surface. After the layer-averaged wind speeds and directions are calculated for all stations, the streamlines of the layer-averaged wind are drawn, and trajectory analyses are performed. The trajectory analysis technique employed is described in standard meteorological analysis text books.

Figures 3 and 4 show the surface synoptic charts during the periods of AVE II and III at the beginning (a) and at the end (b) of these two periods.

For the AVE II data, we chose North Platte, Nebraska; Monette, Missouri; and Greensboro, North Carolina, as the starting points of air parcel trajectories. For AVE III data, the trajectories of air parcels leaving from North Platte, Nebraska; Green Bay, Wisconsin; and Buffalo, New York, were studied. The reason for choosing these stations as initial points is that they are situated under different synoptic weather conditions. In order to study the effects on accuracy of the different time resolutions, three different trajectory analyses are made with 3-, 6-, and 12-hour time intervals.

The results of the trajectory analysis for the AVE II and III periods are shown in Figures 5 and 6. Assuming that the trajectories obtained with the 3-hour time intervals are "exact", trajectories obtained with the 6-hour and 12-hour intervals are compared with those using 3-hour intervals. Departures are obtained in terms of vectorial differences between the two trajectories. The results are shown in Tables 1 and 2. In these tables, L(3) is the travel distance calculated with the 3-hour time interval and Δ_{L_6} and $\Delta_{L_{12}}$ are

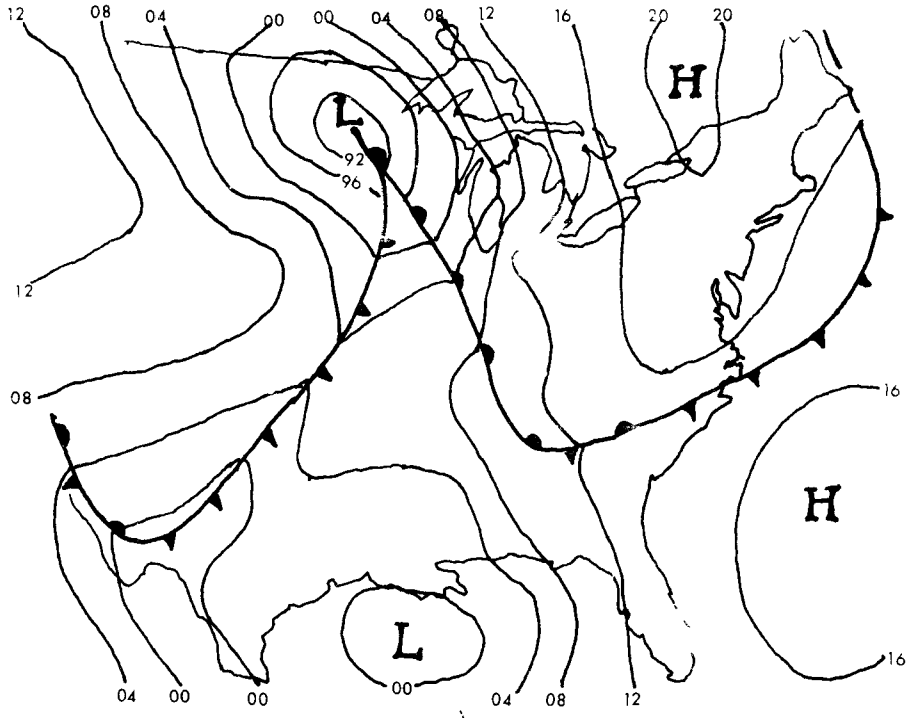

(a)

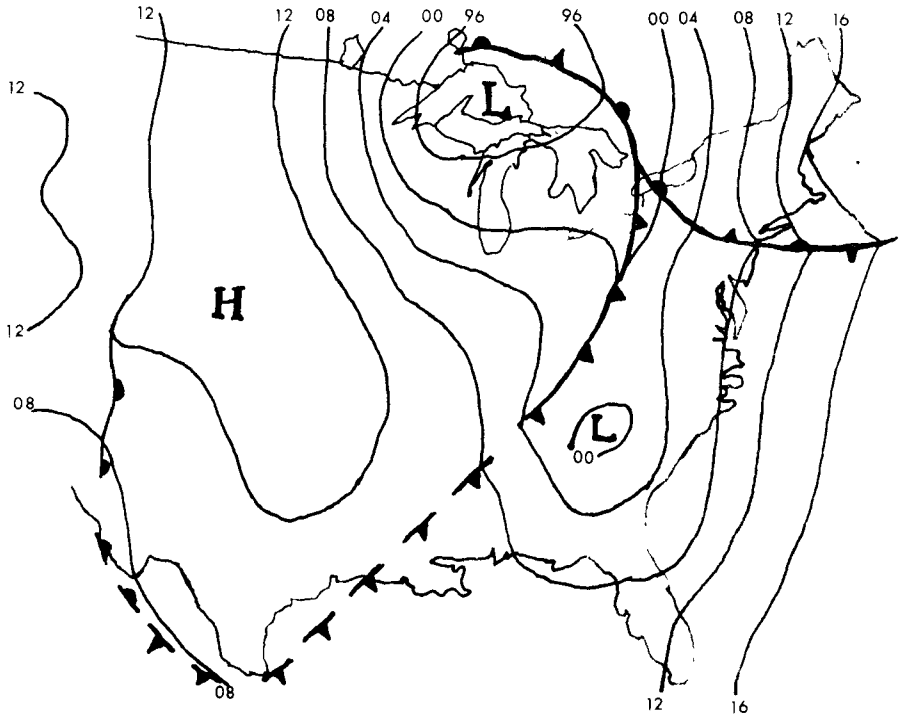

(b)

Figure 3. Surface synoptic charts for the AVE II
(a) for 12 GMT, 11 May 1974
(b) for 12 GMT, 12 May 1974

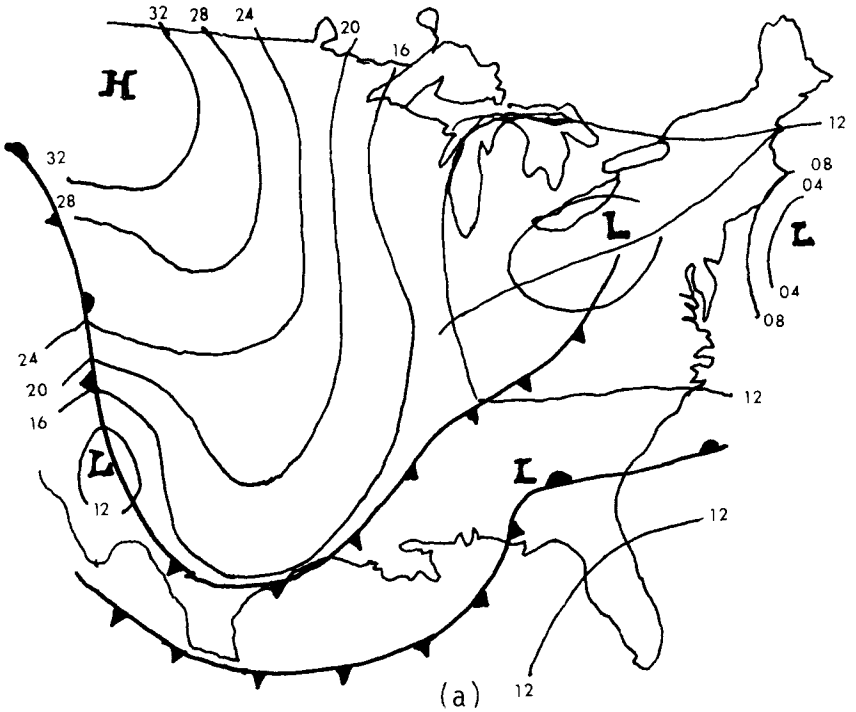

(a)

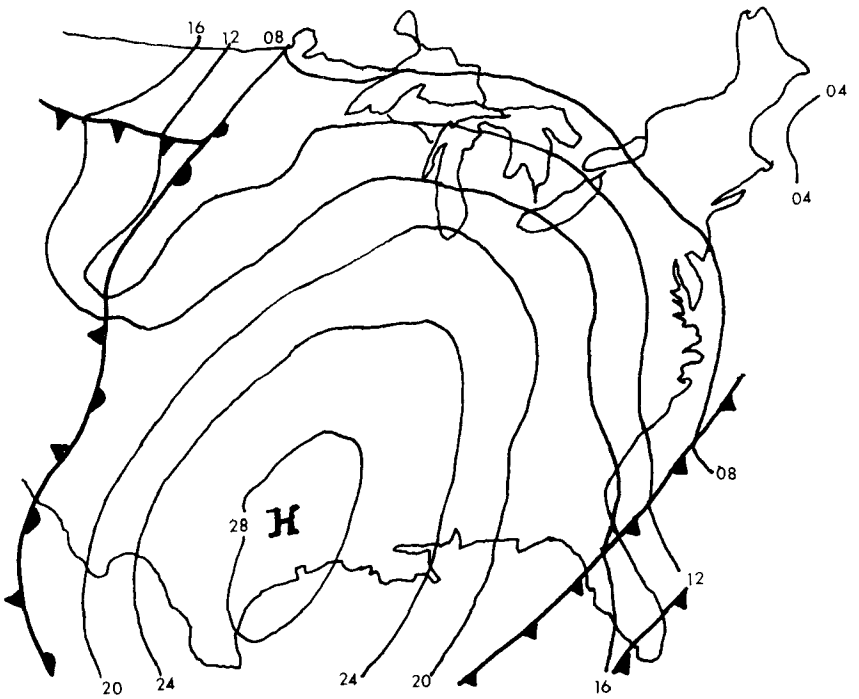

(b)

Figure 4. Surface synoptic charts for the AVE III
(a) for 00 GMT, 6 February 1975
(b) for 12 GMT, 7 February 1975

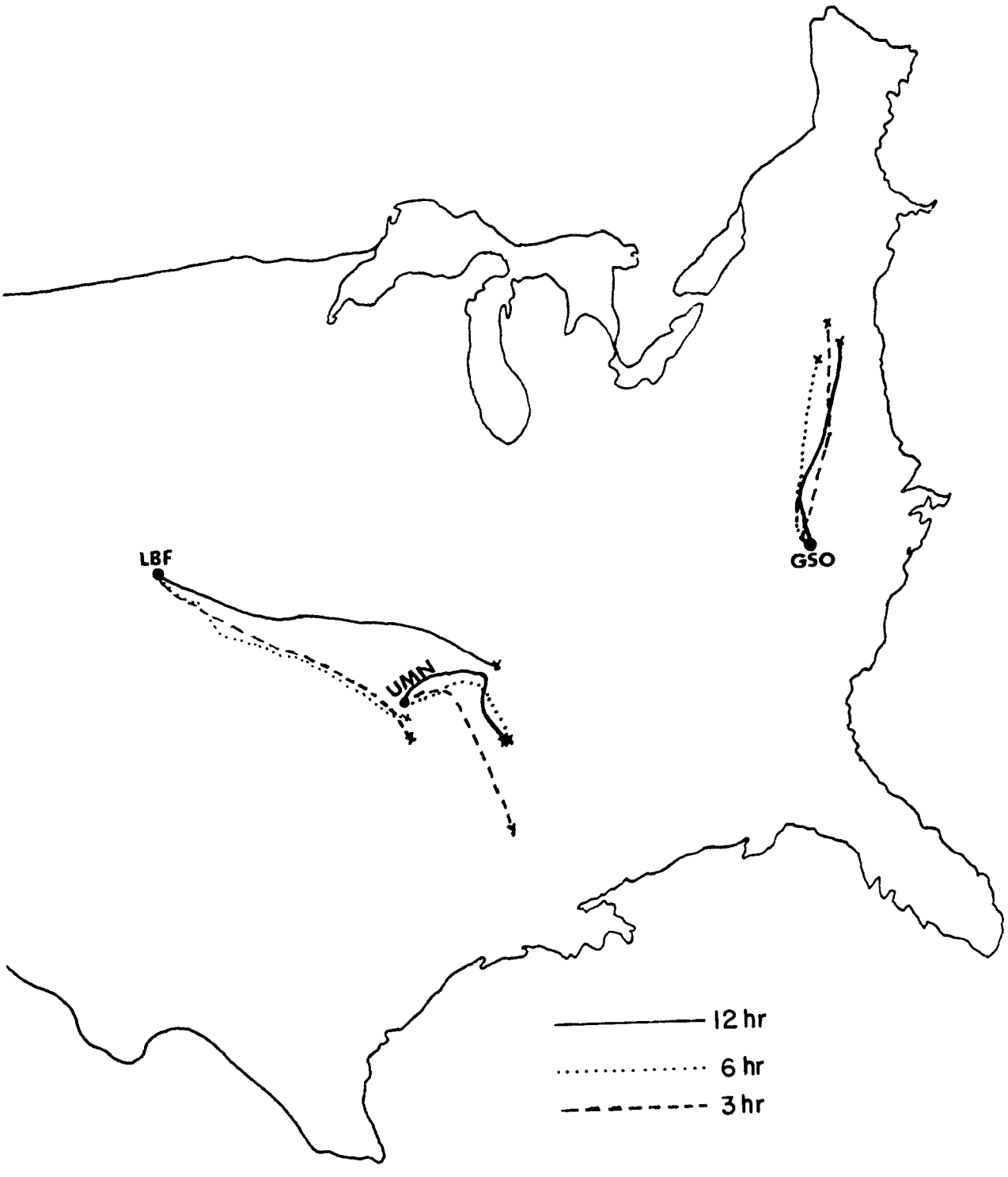

Figure 5. Trajectories of the layer-averaged wind for the AVE III. 12Z May 11 - 12Z May 12.

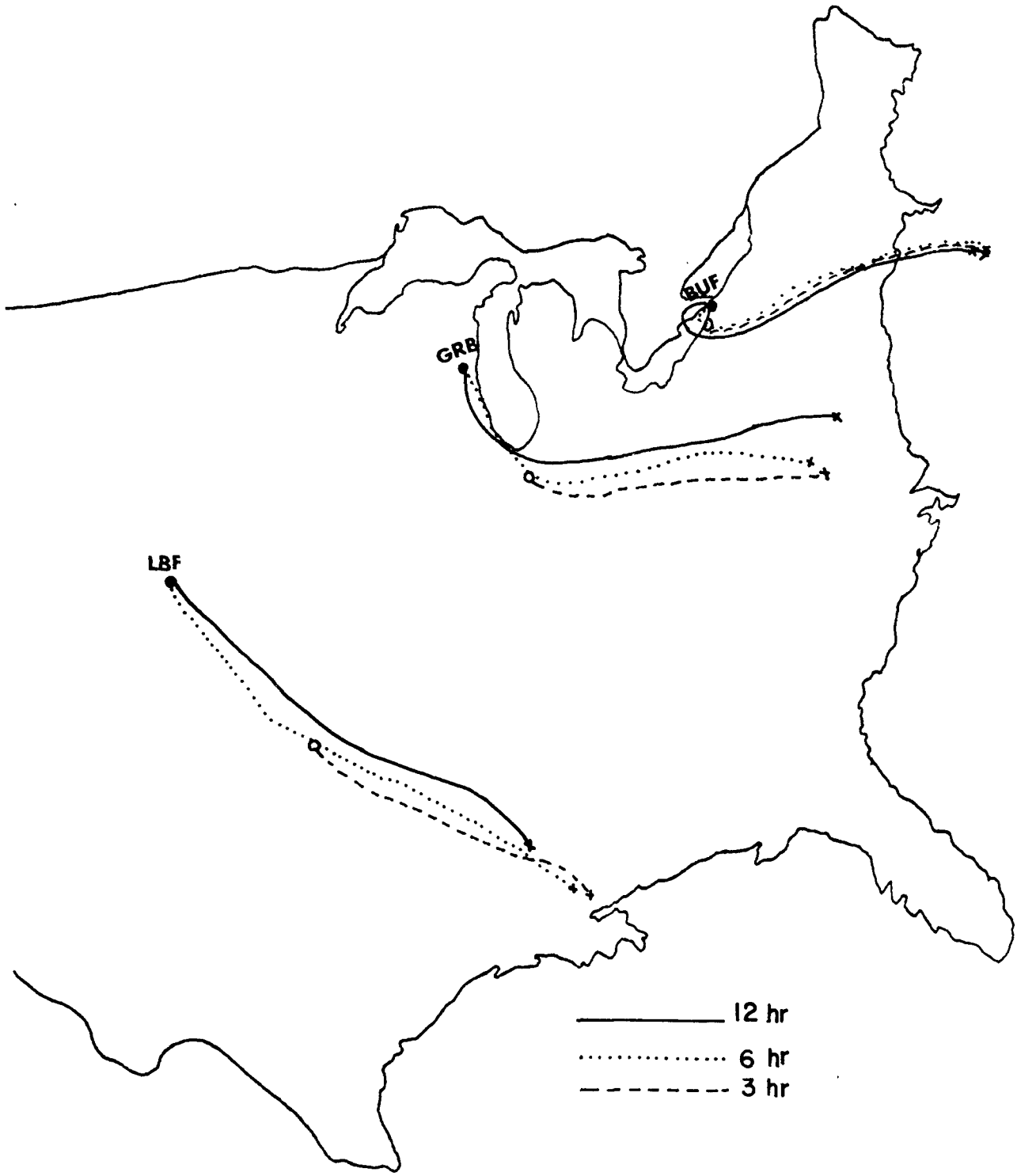

Figure 6. Trajectories of the layer-averaged wind for the AVE III. 00Z Feb. 6 - 12Z Feb. 7.

TABLE 1. The Relative Accuracy of Trajectory Analysis for the AVE II. (12Z May 11 12Z May 12, 1974)

a. Trajectory of air parcel leaving North Platte, Nebraska

	Travel Time (Hours)				
	0	6	12	18	24
$L(3)$	0 (km)	230	420	670	910
ΔL_6	0	<15	25	55	35
ΔL_{12}	0	---	110	---	270
$\Delta L_6/L(3)$	0	<.07	.06	.08	.04
$\Delta L_{12}/L(3)$	0	---	.26	---	.30

(Average wind speed = 10.5 m/sec)

b. Trajectory of air parcel leaving Monette, Missouri

	Travel Time (Hours)				
	0	6	12	18	24
$L(3)$	0 (km)	110	210	420	700
ΔL_6	0	0	80	95	150
ΔL_{12}	0	---	95	---	205
$\Delta L_6/L(3)$	0	0	.36	.23	.21
$\Delta L_{12}/L(3)$	0	---	.43	---	.29

(Average wind speed = 8.1 m/sec)

c. Trajectory of air parcel leaving Greensboro, North Carolina

	Travel Time (Hours)				
	0	6	12	18	24
$L(3)$	0(km)	100	210	430	750
ΔL_6	0	40	70	70	95
ΔL_{12}	0	---	70	---	55
$\Delta L_6/L(3)$	0	.40	.33	.16	.13
$\Delta L_{12}/L(3)$	0	---	.33	---	.07

(Average wind speed = 8.7 m/sec)

TABLE 2. The Relative Accuracy of Trajectory Analysis for the AVE III.
(00Z Feb. 6 12Z Feb. 7, 1975)

a. Trajectory of air parcel leaving North Platte, Nebraska

	Travel Time (Hours)						
	0	6	12	18	24	30	36
L(3)	0 (km)	310	660	970	1180	1370	1580
ΔL_6	0	0	0	40	50	15	25*
ΔL_{12}	0	---	110	---	180	---	250
$\Delta L_6/L(3)$	0	0	0	.04	.04	.01	.02
$\Delta L_{12}/L(12)$	0	---	.12	---	.15	---	.16

(Average wind speed = 12m/sec)

b. Trajectory of air parcel leaving Green Bay, Wisconsin

	Travel Time (Hours)						
	0	6	12	18	24	30	36
L(3)	0 (km)	170	370	610	850	1070	1320
ΔL_6	0	0	0	70	100	80	55*
ΔL_{12}	0	---	70	---	145	---	170
$\Delta L_6/L(3)$	0	0	0	.11	.12	.07	.04
$\Delta L_{12}/L(3)$	0	---	.19	---	.17	---	.13

(Average wind speed = 10.1 m/sec)

c. Trajectory of air parcel leaving Buffalo, New York

	Travel Time (Hours)						
	0	6	12	18	24	30	36
L(3)	0 (km)	50	100	230	430	670	910
ΔL_6	0	0	0	30	35	<15	40*
ΔL_{12}	0	---	45	---	25	---	60
$\Delta L_6/L(3)$	0	0	0	.13	.08	<.02	.04
$\Delta L_{12}/L(3)$	0	---	.45	---	.06	---	.07

(Average wind speed = 6.9 m/sec)

* In the AVE III, the data for the first and last 12-hour periods were taken at 6-hour intervals while for the middle 12-hour period, the data were taken at 3-hour intervals.

the vectorial differences of trajectories obtained with the 3-hour and 6-hour intervals, and with the 3-hour and 12-hour intervals, respectively. According to these tables, trajectories obtained with the 12-hour intervals are, in general, less accurate than those obtained with the 6-hour intervals. Least accurate trajectories are obtained in the regions where the speed of the layer-averaged wind is strongest. It is also noted that, if the wind speeds and directions vary from one time interval to the next, the trajectories become less accurate. As can be expected, the relative errors defined by $\Delta L_6/L(3)$ and $\Delta L_{12}/L(3)$ are larger when a discontinuity, such as a cold front, passes through the region.

This preliminary study indicates that trajectories obtained with 6-hour intervals between observation times may be accurate enough so as not to warrant the need of 3-hour intervals.

From the figures, it can be seen that the directions and distances of trajectories obtained with 12-hour intervals agree, in general, with those obtained with shorter intervals expept when a discontinuity passes through the region. Therefore, trajectories calculated with 12-hour intervals may be reliable especially when the statistics of many trajectories is used.

4.5.2. Dispersion Study

Preliminary studies of horizontal dispersion, Σ_h, were also made along the trajectories of layer-averaged winds in the mixing layer. The results are shown in Figures 7 and 8 where (a), (b), and (c) are, respectively, the trajectories analyzed with the 3-, 6-, and 12-hour intervals. The horizontal dispersion is calculated as

$$\Sigma_h = 2(\sigma v_{h,1} \cdot t_1 + \sigma v_{h,2} \cdot t_2 + ... + \sigma v_{h,n} \cdot t_n) + L_o,$$

where L_o is the initial width of the source area perpendicular to the mean wind and t is the time step of the trajectory analysis. In this study, L_o is assumed to be zero. An average value of σv_h is determined for each trajectory time step. In Table 3, the values of Σ_h calculated with different time intervals for each trajectory analysis are shown. Also shown are the relative errors defined by $\Delta\Sigma_h/\Sigma_h(3)$, where $\Delta\Sigma_h$ is given by $|\Sigma_h(3) - \Sigma_h(6 \text{ or } 12)|$. It can be seen that the agreement of the values of Σ_h calculated along trajectories is good between different time intervals.

4.6. Computer Program for Trajectory Analysis

The computer program for trajectory analysis which was provided by NOAA's Air Resource Laboratories has been modified for our purpose.

The details of this program are described by Heffer and Taylor (1975), and can be summarized as follows.

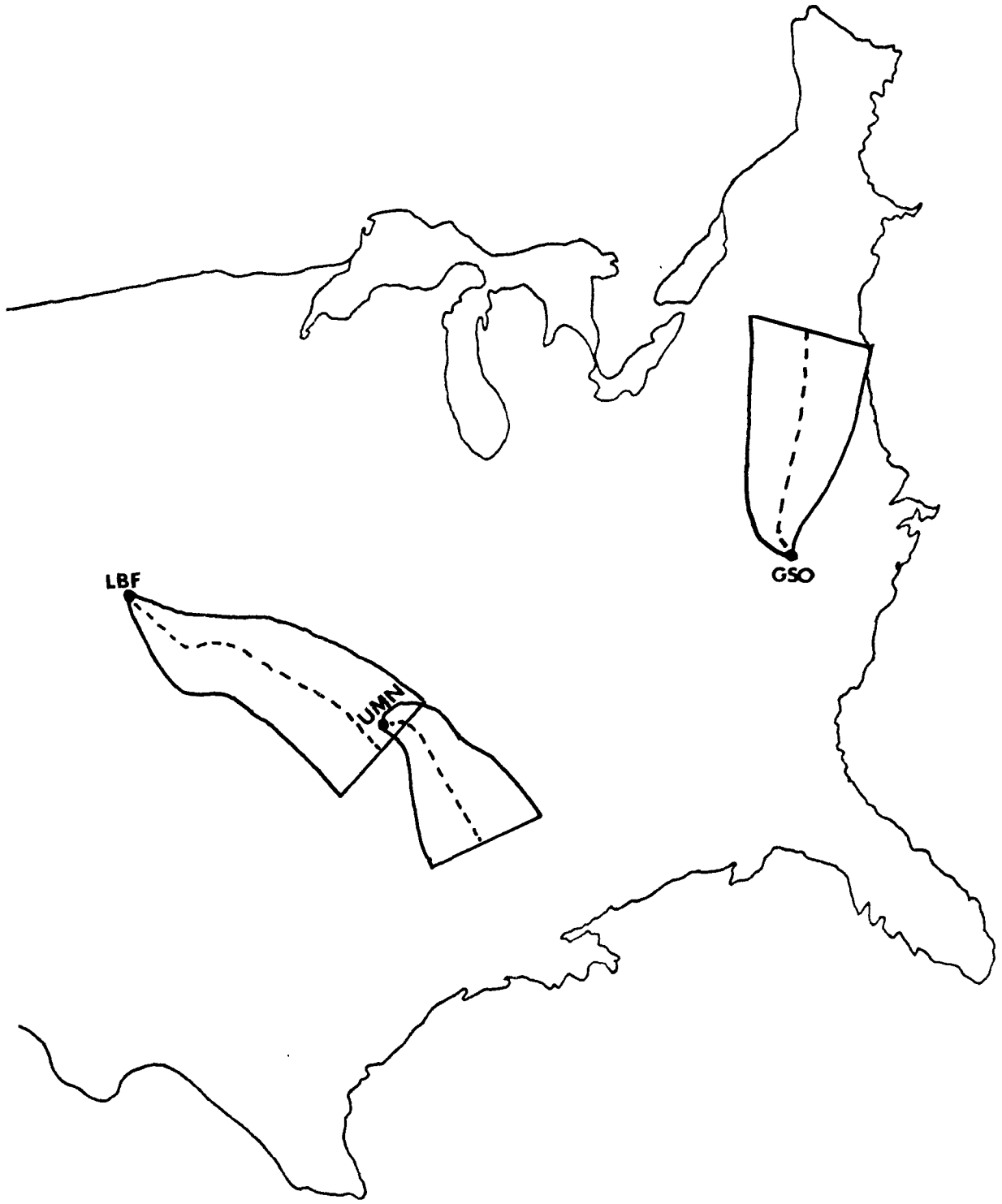

Figure 7 (a). Horizontal dispersion along the trajectory of the layer-averaged wind for the AVE II. Time interval = 3 hours. May 11 - May 12

Figure 7 (b). Horizontal dispersion along the trajectory of the layer-averaged wind for the AVE II. Time interval = 6 hours. May 11 - May 12

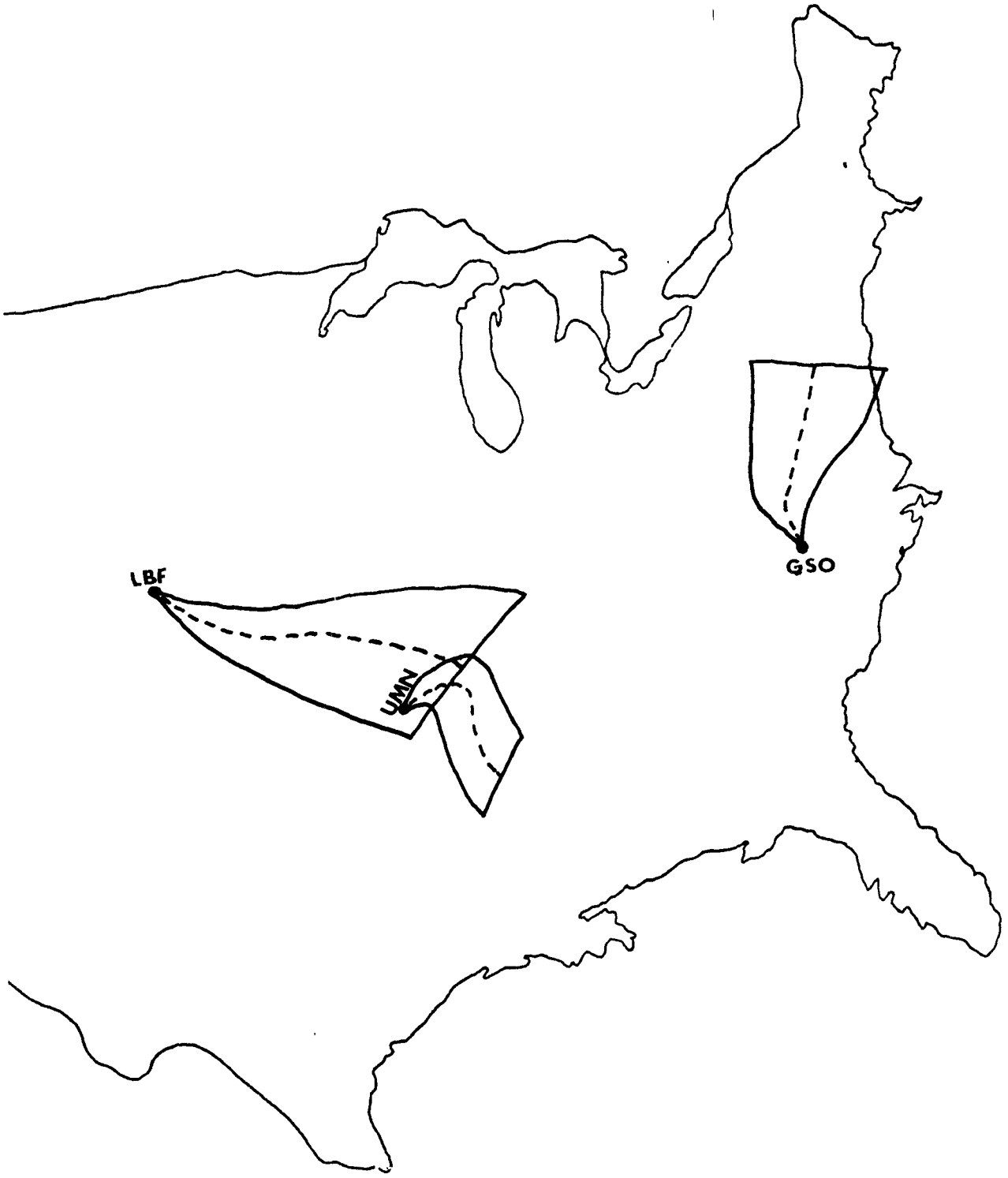

Figure 7 (c). Horizontal dispersion along the trajectory of the layer-averaged wind for the AVE II. Time interval = 12 hours. May 11 - May 12

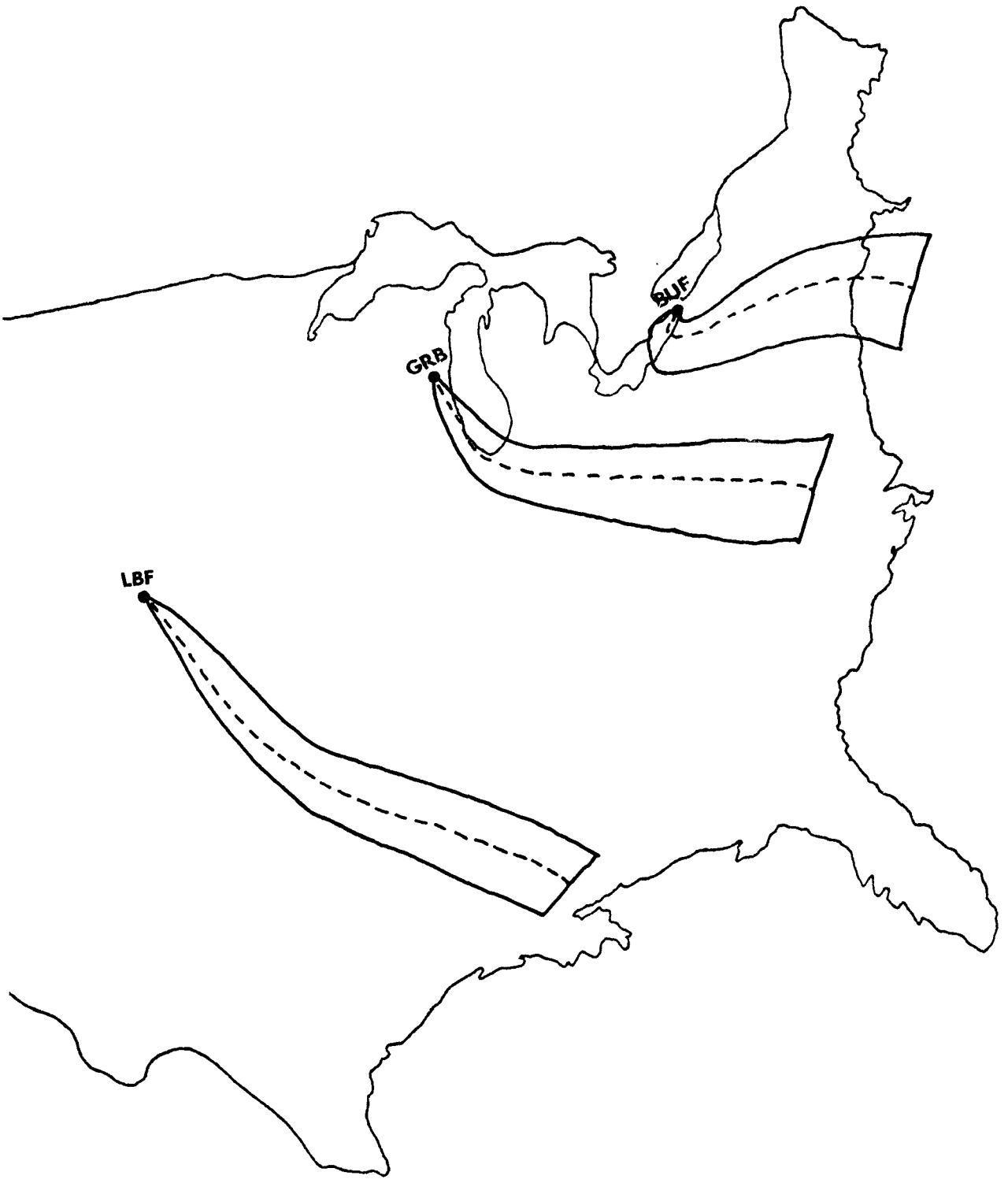

Figure 8 (a). Horizontal dispersion along the trajectory of the layer-averaged wind for the AVE III. Time interval = 3 hours. Feb. 6 - Feb. 7

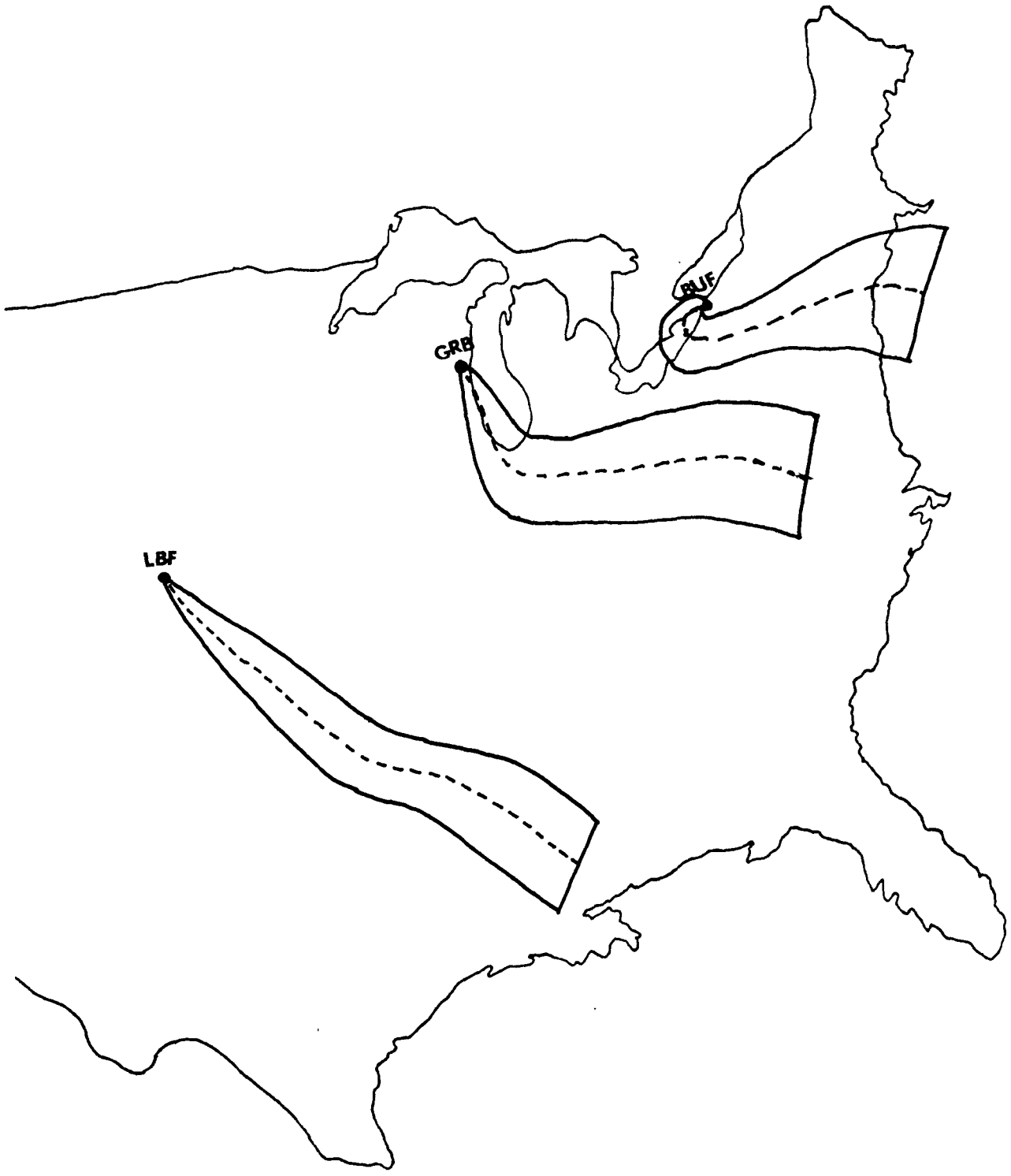

Figure 8 (b). Horizontal dispersion along the trajectory of the layer-averaged wind for the AVE III. Time interval = 6 hours. Feb. 6 - Feb. 7

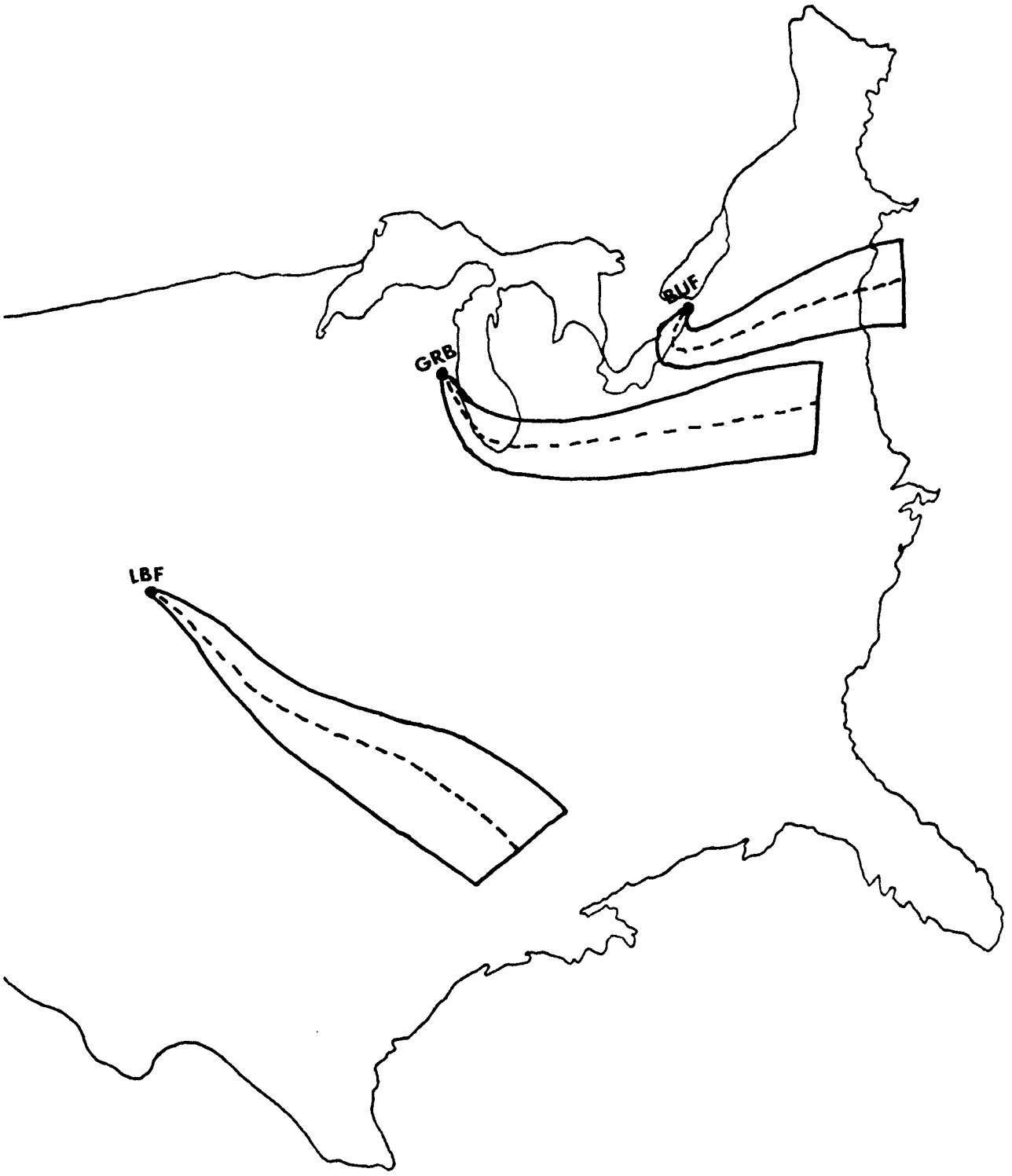

Figure 8 (c). Horizontal dispersion along the trajectory of the layer-averaged wind for the AVE III. Time interval = 12 hours. Feb. 6 - Feb. 7

TABLE 3. Horizontal Dispersion and Relative Error

AVE II

a. North Platte, Nebraska

	Time Interval of Analysis (Hours)		
	3	6	12
Σ_h after 24 hrs	500 km	460	500
$\Delta\Sigma_h/\Sigma_{h(3)}$	0	.08	0

b. Monette, Missouri

	3	6	12
Σ_h after 24 hrs	360 km	240	220
$\Delta\Sigma_h/\Sigma_{h(3)}$	0	.22	.39

c. Greensboro, North Carolina

	3	6	12
Σ_h after 24 hrs	440 km	360	460
$\Delta\Sigma_h/\Sigma_{h(3)}$	0	.18	.04

AVE III

a. North Platte, Nebraska

	Time Interval of Analysis (Hours)		
	3	6	12
Σ_h after 36 hrs	240 km	260	420
$\Delta\Sigma_h/\Sigma_{h(3)}$	---	.08	.75

b. Green Bay, Wisconsin

	3	6	12
Σ_h after 36 hrs	320 km	380	320
$\Delta\Sigma_h/\Sigma_{h(3)}$	---	.19	0

c. Buffalo, New York

	3	6	12
Σ_h after 36 hrs	360 km	440	340
$\Delta\Sigma_h/\Sigma_{h(3)}$	---	.22	.06

$$\Delta\Sigma_h = \left|\Sigma_h(3) - \Sigma_h[6, \text{ or } 12]\right|$$

A trajectory is composed of a series of three-hour segments. Each segment is computed assuming persistence of the winds reported closest to the segment time. For example, for a three-hour segment from 00Z to 03Z, three-hour persistence of the 00Z winds is assumed. The three-hour segment from 03Z to 06Z is computed assuming three-hour "backward" persistence of the 06Z winds.

For each station, the average wind in the mixing layer is computed from the reported winds linearly weighted according to height. Using the average winds calculated, each trajectory segment is computed as (see Fig. 9).

$$TS_o = \frac{\sum^{R} DW_i \cdot AW_i \cdot TS_i}{\sum^{R} DW_i \cdot AW_i} \tag{15}$$

Here TS_o is the trajectory segment, $\sum^{R}$ indicates the summation over all observed winds within a radius R of the segment origin, DW_i is the distance weighting factor, $TS_i = V_i \cdot \Delta t$, is the contribution to the trajectory segment from an observed wind to the mid-point of TS_i; and $AW_i = f(\theta_i)$, is the alignment weighting factor, a function of θ_i, the angle formed between TS_i and a line drawn from the segment origin to a wind observation point.

For the calculations of σ_{v_x} and σ_{v_y}, defined by Eqs. (10) and (11), similar equations as Eq. (15) are used:

$$\sigma_{v_x} = \frac{\sum^{R} DW_i \cdot AW_i \cdot \sigma V_{xi}}{\sum^{R} DW_i \cdot AW_i} \tag{16}$$

$$\sigma_{v_y} = \frac{\sum^{R} DW_i \cdot AW_i \cdot \sigma V_{yi}}{\sum^{R} DW_i \cdot AW_i} \tag{17}$$

The dispersion factor σ_{v_h} is calculated from Eq. (12). σ_{v_h} along a trajectory, say from 00Z to 06Z, is given as an arithmetic mean of two values at 00Z and 06Z.

The following are parameter values used in the program:

Δt = 3 hours
R = 300 nautical miles

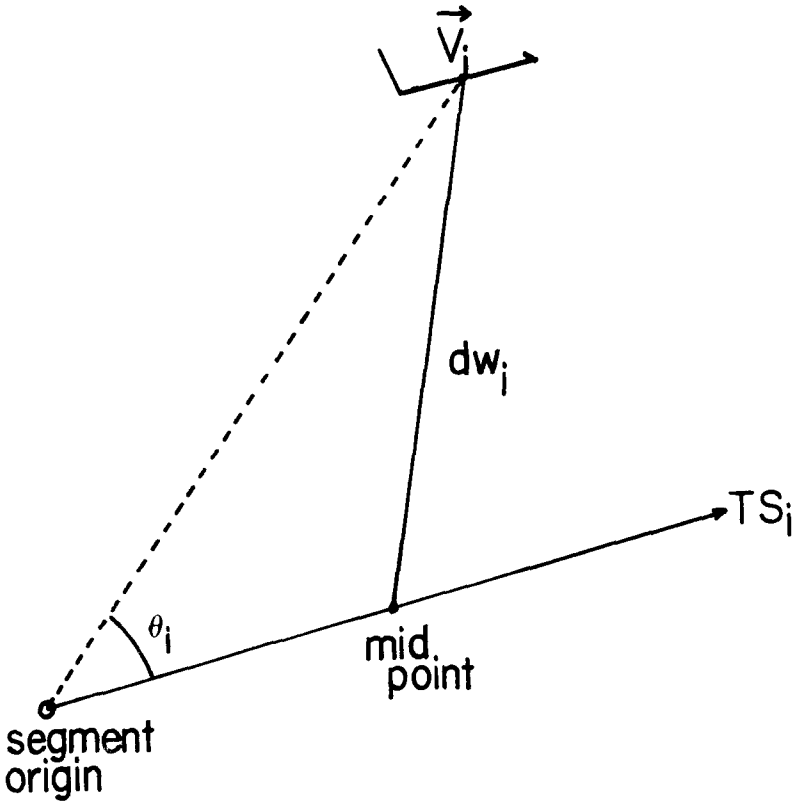

Figure 9. Configuration for determining a trajectory segment from observed winds.

$DW_i = 1/dw_i^2$ (the closest observation receives the greatest weight)

$AW_i = 1 - 0.5|\sin \theta_i|$ (observations upwind and downwind receive the greatest weight)

The trajectory segments are linked together to produce a complete trajectory. The first segment starts from the endpoint of the segment before it. Trajectories terminate after the desired duration or when the specified criteria are not met.

The input data necessary are as follows:

1. The origin of the trajectories.

2. The data trajectory computations begin and the number of days for which trajectory computations are desired.

3. The number of days of wind input data.

4. The mixing layer height.

5. The geographical boundaries within which observed winds are considered for trajectory calculations.

6. The geographical boundaries for maps in the plotting subroutines.

In the following, we illustrate the outputs of the trajectory program which is modified for the Atmospheric Variability Experiment II and III (Scoggins and Turner, 1974; Fuelberg and Turner, 1975). The trajectories are originated at North Platte, Nebraska on May 11, 1974, using AVE II data.

Table 4 shows the number of reporting stations within a specified radius for each time interval. The reliability of a trajectory can be evaluated from the number of reporting stations.

In Table 5 the latitude and longitude of trajectory segment endpoints at each interval are shown. A trajectory that was terminated for not satisfying operational criteria is identified by a latitude $\geq$ 996 and longitude $\geq$ 9996.

Table 6 shows the height of the mixing layer and dispersion parameter σ_{v_h} at each time interval. In this particular example, the height of the mixing layer is designated at 200 mb above the surface.

The accumulated dispersion width, Σ_h, defined by Eq. (14) is given in Table 7. Figure 10 is an example of the plot of the trajectories. Trajectories are coded A, B and C for starting time at 12Z, 18Z, and 00Z, respectively.

Table 4. The number of reporting stations within a specified radius for each time interval.

LBF (41.1 100.7)

NUMBER OF REPORTING STATIONS AND INPUT WIND TIME CODE.

TRAJECTORY SEGMENT AT 3-HOUR INTERVALS

START DATE-TIME MAY 74	1	2	3	4	5	6	7	8	9	10	11	12	13	14	15	16
11-12Z	6	5	5	9	11	11	11	10	10	8	7	8	8	7	8	7
11-18Z	6	6	6	7	8	7	6	7	9	10	9	8	0	0	0	0
12- 0Z	6	6	6	7	7	8	8	7	0	0	0	0	0	0	0	0

Table 5. The latitude and longitude of trajectory segment endpoints at each time interval (tenths of degrees).

START-DATE-TIME	0		3		6		9		12	
11-12Z	410	1006	402	998	395	990	390	983	387	976
11-18Z	410	1006	405	992	399	979	394	967	388	957
12- 0Z	410	1006	402	994	395	985	391	979	387	972

START DATE-TIME	15		18		21		24	
11-12Z	383	968	376	960	369	954	360	948
11-18Z	380	949	370	940	996	9996	996	9996
12- 0Z	996	9996	996	9996	996	9996	996	9996

Table 6. The height of the mixing layer (meters above ground) and dispersion parameter σ_{v_h} (m/sec) at each time interval.

START DATE-TIME	0		3		6		9		12	
11-12Z	2005.	5.64	1990.	3.60	1987.	3.84	1986.	2.56	1981.	2.70
11-18Z	2016.	1.72	1992.	2.25	1960.	2.42	1927.	3.72	1913.	3.30
12- 0Z	2034.	1.68	1999.	3.83	1978.	4.72	1964.	4.77	1932.	3.93

BOUNDARY HT (METERS ABOVE GROUND) - DISPERSION (M/S)

START DATE-TIME	15		18		21		24	
11-12Z	1960.	4.21	1947.	4.26	1941.	4.93	1932.	4.49
11-18Z	1932.	4.85	1944.	4.69	0.	0.00	0.	0.00
11- 0Z	0.	0.00	0.	0.00	0.	0.00	0.	0.00

BOUNDARY HT (METERS ABOVE GROUND) - DISPERSION (M/S)

Table 7. The accumulated dispersion width, Σ_h (degrees latitude), at each time interval.

START DATE-TIME	0	3	6	9	12
11-12Z		.87	1.52	2.15	2.65
11-18Z		.44	.88	1.50	2.16
12- 0Z		.53	1.36	2.29	3.17

ACCUMULATED DISPERSION WIDTH AT THIS TIME INTERVAL GIVEN IN DEGREES LATITUDE ON TRAJECTORY

START DATE-TIME	15	18	21	24
11-12Z	3.33	4.13	5.02	5.94
11-18Z	2.88	3.80	0.00	0.00
12- 0Z	0.00	0.00	0.00	0.00

ACCUMULATED DISPERSION WIDTH AT THIS TIME INTERVAL GIVEN IN DEGREES LATITUDE ON TRAJECTORY

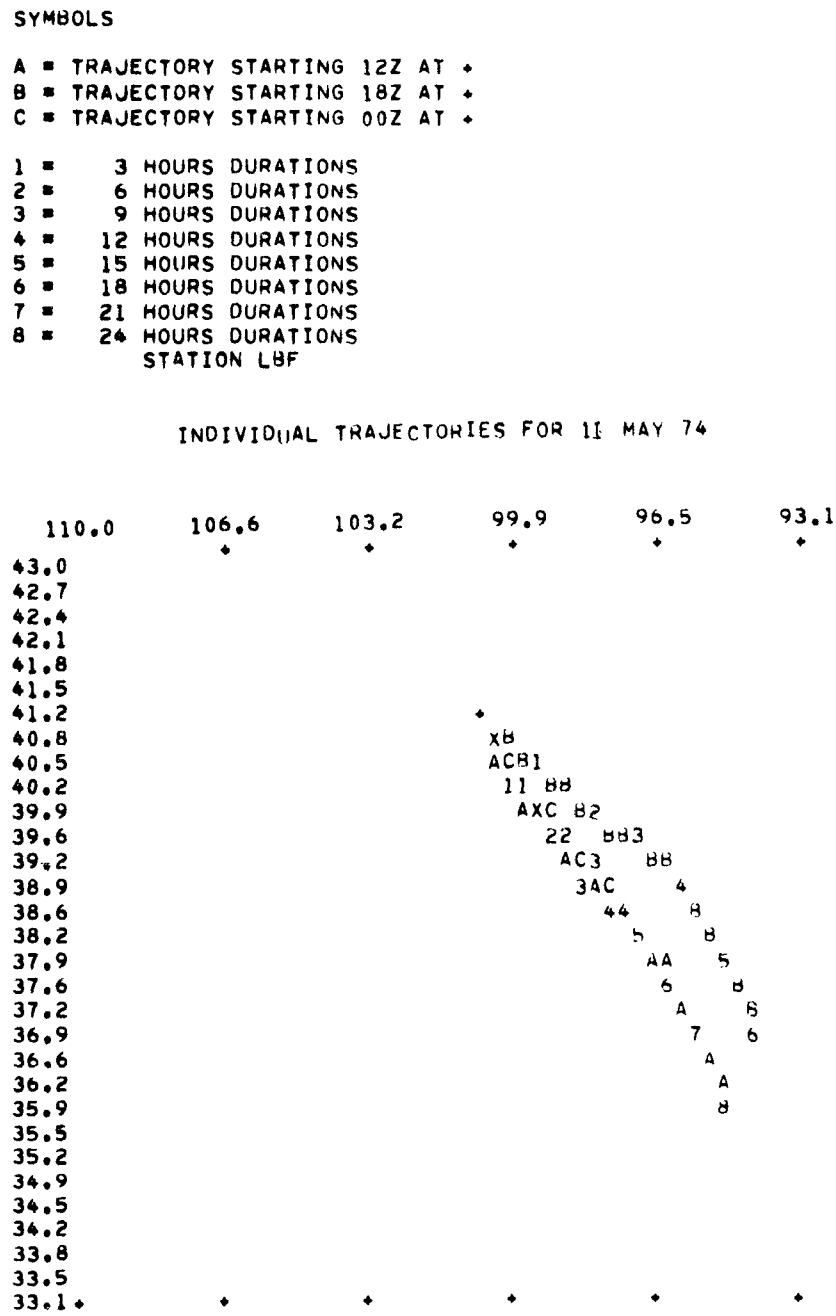

Figure 10. An example of the plotting of trajectories. The trajectories originated at North Platte, Nebraska, on 11 May 1974.

4.7. Characteristic of Dispersion Parameter σ_{v_h}

4.7.1. Application to the Wind Profile Given by the Ekman Layer Theory and the Wind Profiles of the AVE Data

The classical Ekman layer theory defines the wind field as

$$v_x = U_g(1 - e^{-bz} \cos bz)$$

$$v_y = U_g e^{-bz} \sin bz$$

where, $b = \sqrt{f/2k}$, f is the Coriolis parameter and K is the momentum eddy diffusivity. v_x is the wind component along the geostrophic wind and v_y is the wind component perpendicular to the geostrophic wind. The height of the Ekman layer, h, is given by

$$h = \pi b.$$

Assuming that the height of the Ekman layer is identical with the height of the mixing layer, the following quantities are obtained:

$$\bar{u} = 0.8638\ U_g$$

$$\sigma v_x = 0.3026\ U_g$$

$$\sigma v_y = 0.1102\ U_g$$

$$\sigma v_h = \frac{\sigma v_x \cdot |\bar{v}_y| + \sigma y \cdot |\bar{v}_x|}{\bar{u}} = 0.166\ \bar{U}_g = .193\ \bar{u}$$

For a steady state atmosphere which is also assumed by the Ekman theory, the width of the pollutant plume along the mean wind after the dispersion time T = nt is simply given by

$$\sigma_h = [\sigma v_h] \cdot T = .193\ \bar{u} \cdot T$$

assuming that $L_o = 0$. This quantity is compared with observations of pollutant plume widths in Figure 11 (Bauer, 1973). There is good agreement between our estimates and experimental observations despite the assumption in the Ekman theory of an idealized neutral environment within the mixing layer. The agreement is especially good at travel times between one hour and one day.

σv_h calculated from wind fields obtained from actual radiosonde data are in reasonable agreement with those from the classical Ekman layer theory.

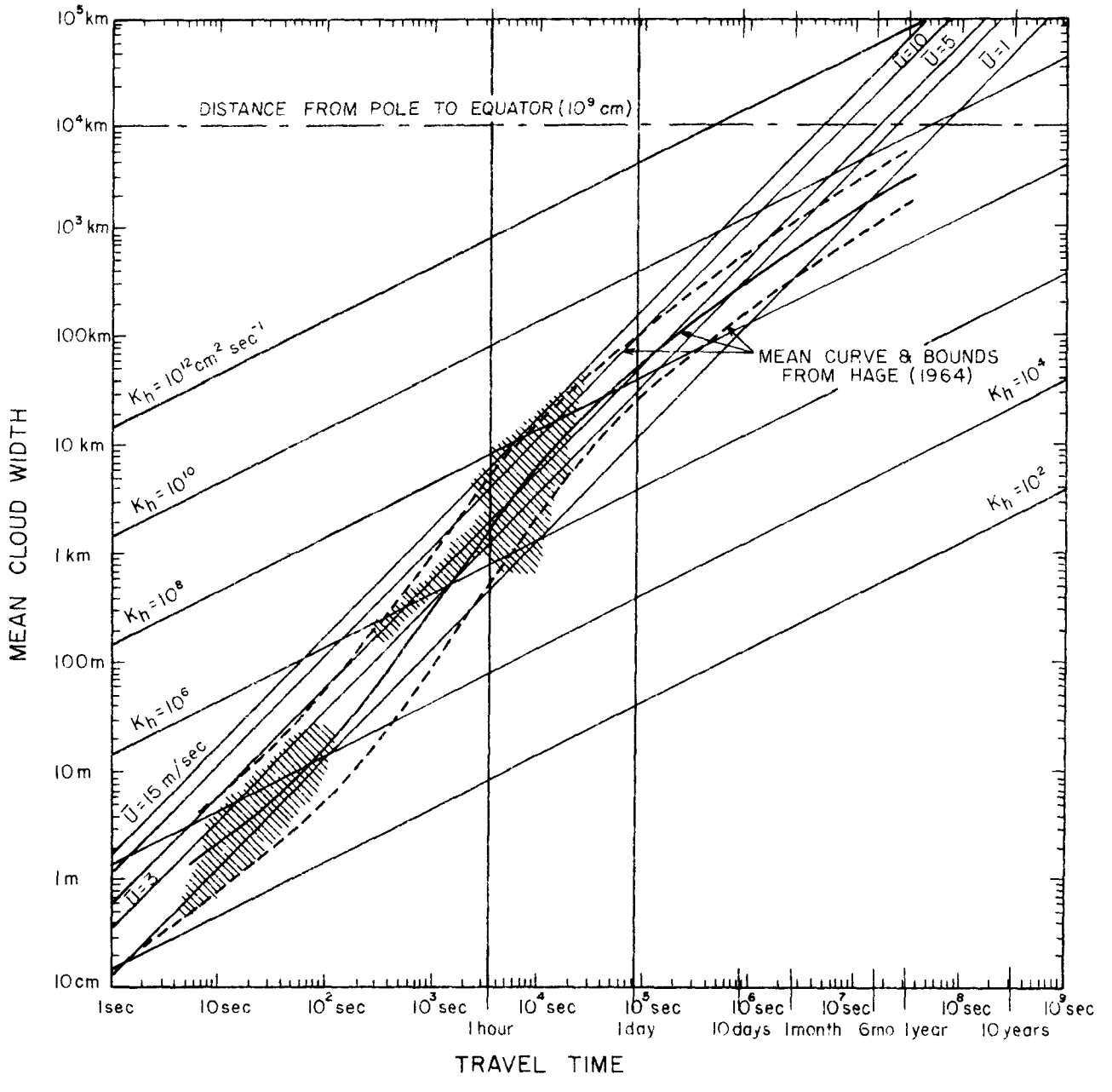

Figure 11. Horizontal dispersion as a function of travel-time (after Bauer, 1973). The calculated mean cloud widths for $\bar{v}$ = 1, 10, m/sec using the Ekman theory are shown by solid lines.

Figures 12 and 13 show calculation results using the data of AVE II and III which were obtained at weather stations in the eastern United States. In these calculations the mixing layer height was assumed to be at 200 mb above the ground. In Figures 12 and 13, each dot represents one observation. Included are observations from all locations in the eastern United States. The scattering is, of course, caused by the different wind profiles at different locations and times. However, notice the magnitudes of $\sigma v_h/\bar{u}$ which are mostly within the range of 0.1 through 0.4, except in the cases of low mean wind speeds. The classical Ekman layer theory gives the value of .193.

Therefore, it seems that the horizontal dispersion calculated from radiosonde data would give values compatible to those observed with the spreading of pollutant plumes.

4.7.2 Persistence of Dispersion Parameter σ_{v_h} Along a Trajectory

Our method of calculating the horizontal dispersion of pollutants along the mean wind trajectory is based on the assumption that the wind-shear structure throughout the mixing layer along the trajectory is persistent at least for the period of the time step of the trajectory segment.

In order to examine the validity of this assumption, the persistence index of σ_{v_h} along a trajectory, defined as the ratio of the average value of the absolute difference of σ_{v_h} between the time step to the average value of σ_{v_h} along a trajectory, is calculated. The persistence index P.I. is expressed as

$$P.I. = \frac{\sum_{N} \left| \sigma V_{h_i} - \sigma V_{h_{i-1}} \right|}{N \cdot \overline{\sigma V_h}} = \frac{\sum_{N} \left| \sigma V_{h_i} - \sigma V_{h_{i-1}} \right|}{\sum_{N} \sigma V_{h_i}} \qquad (18)$$

The calculations of this persistence index are conducted for different time steps along trajectories originating from 36 different locations in the eastern U.S.

The data used are AVE II. Trajectories are started at 12Z and 18Z, May 11, and 00Z, May 12, 1974. For each time step along each trajectory, P.I. is calculated by Eq. (18). Then, the mean values and standard deviations of the P.I. calculated for different time steps along different trajectories are obtained.

The results are shown in Fig. 14(a),(b) and (c). In the figure dots are the mean values of P.I., and bars are the standard deviations of P.I. It can be seen that the values of the persistence index increase gradually with

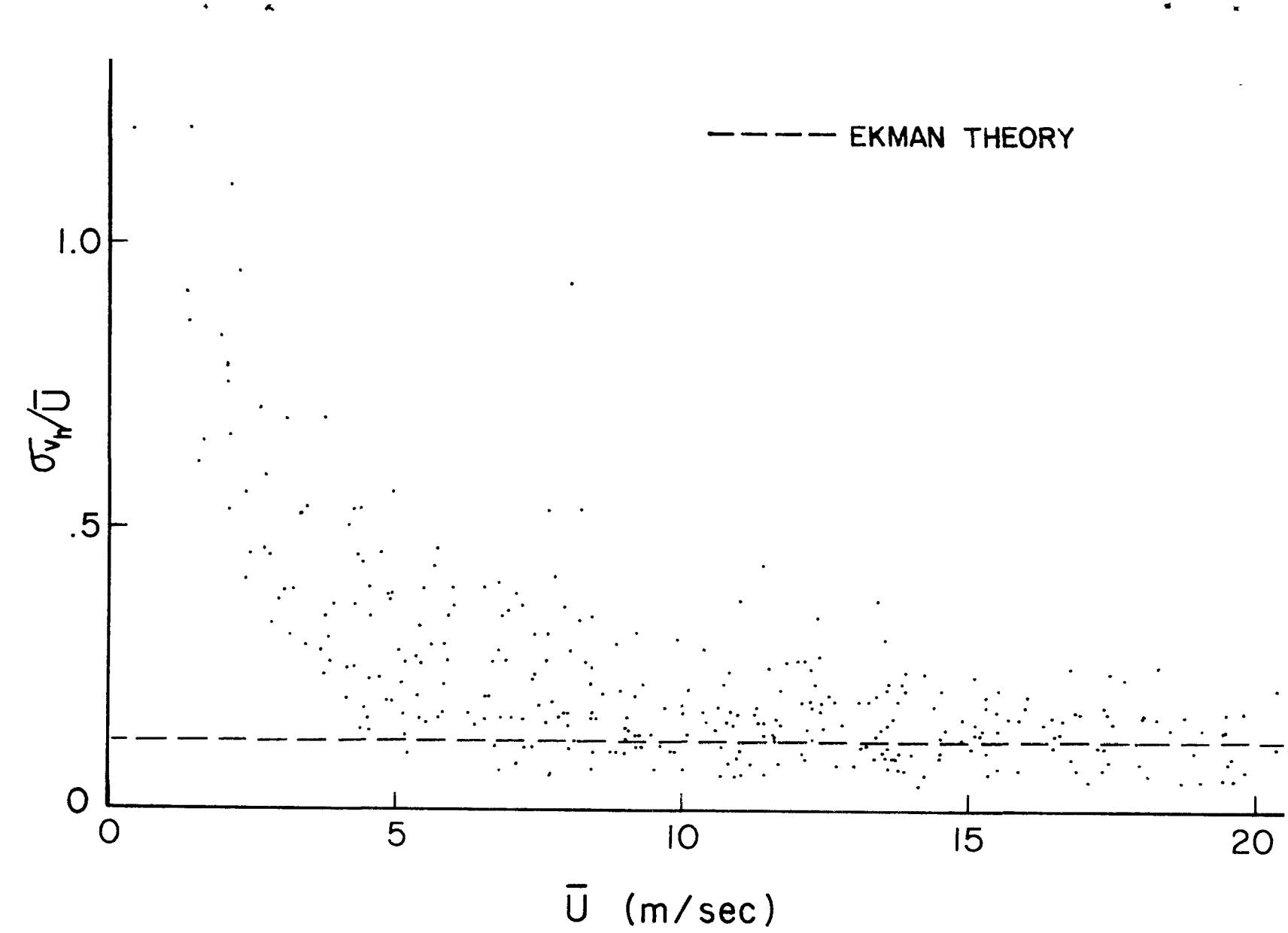

Figure 12. The relationship between $\sigma v_h/\bar{u}$ and $\bar{u}$ calculated for the Atmospheric Variability Experiment II.

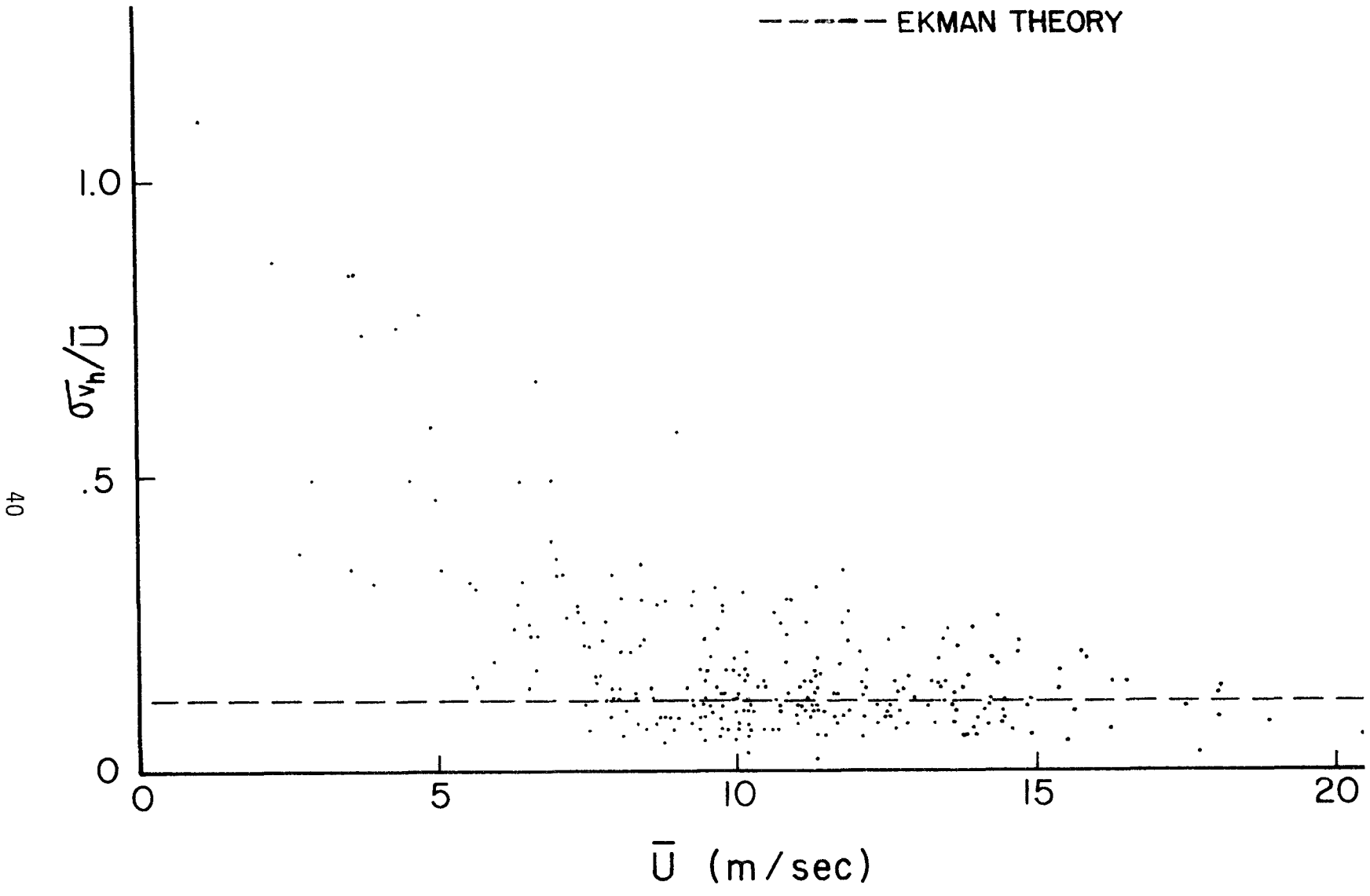

Figure 13. The relationship between $\sigma v_h / \bar{u}$ and $\bar{u}$ calculated for the Atmospheric Variability Experiment III.

increasing time steps. σ_{v_h} is more persistent when the P.I. is smaller. The figures show that the values of σ_{v_h} are about 0.3 for the time step of three hours, and about 0.4 for the time step of 12 hours. This means that the relative accuracy of σ_{v_h} calculated with a time step of 12 hours is not too different from the one with a time step of three hours.

It may be concluded that, for practical use with routine sounding data, our method of calculating the horizontal dispersion of pollutants can be applied.

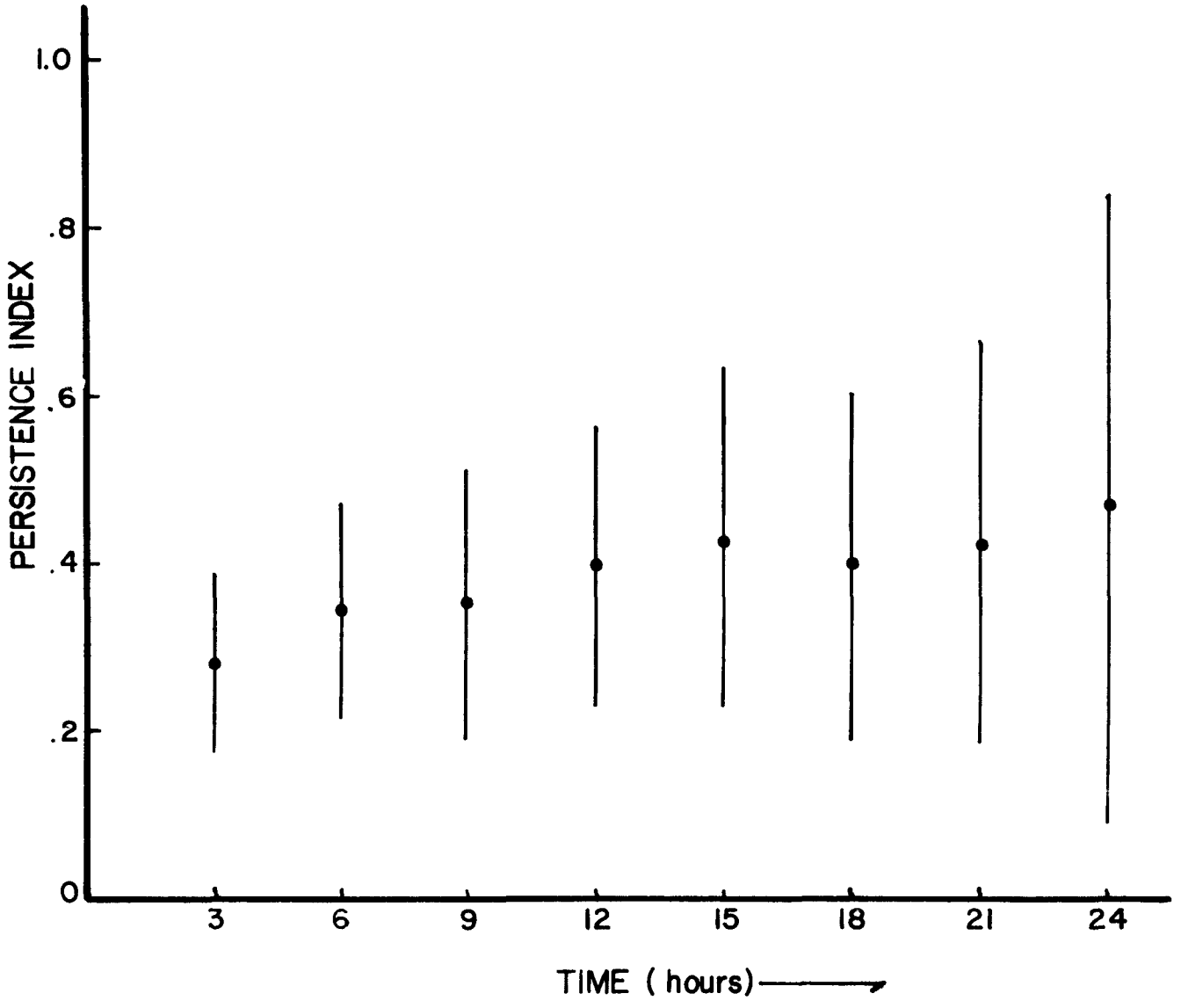

Figure 14(a). Persistence Index, P.I., of σ_{v_h} versus time step for trajectories started at 12Z, 11 May 1974.

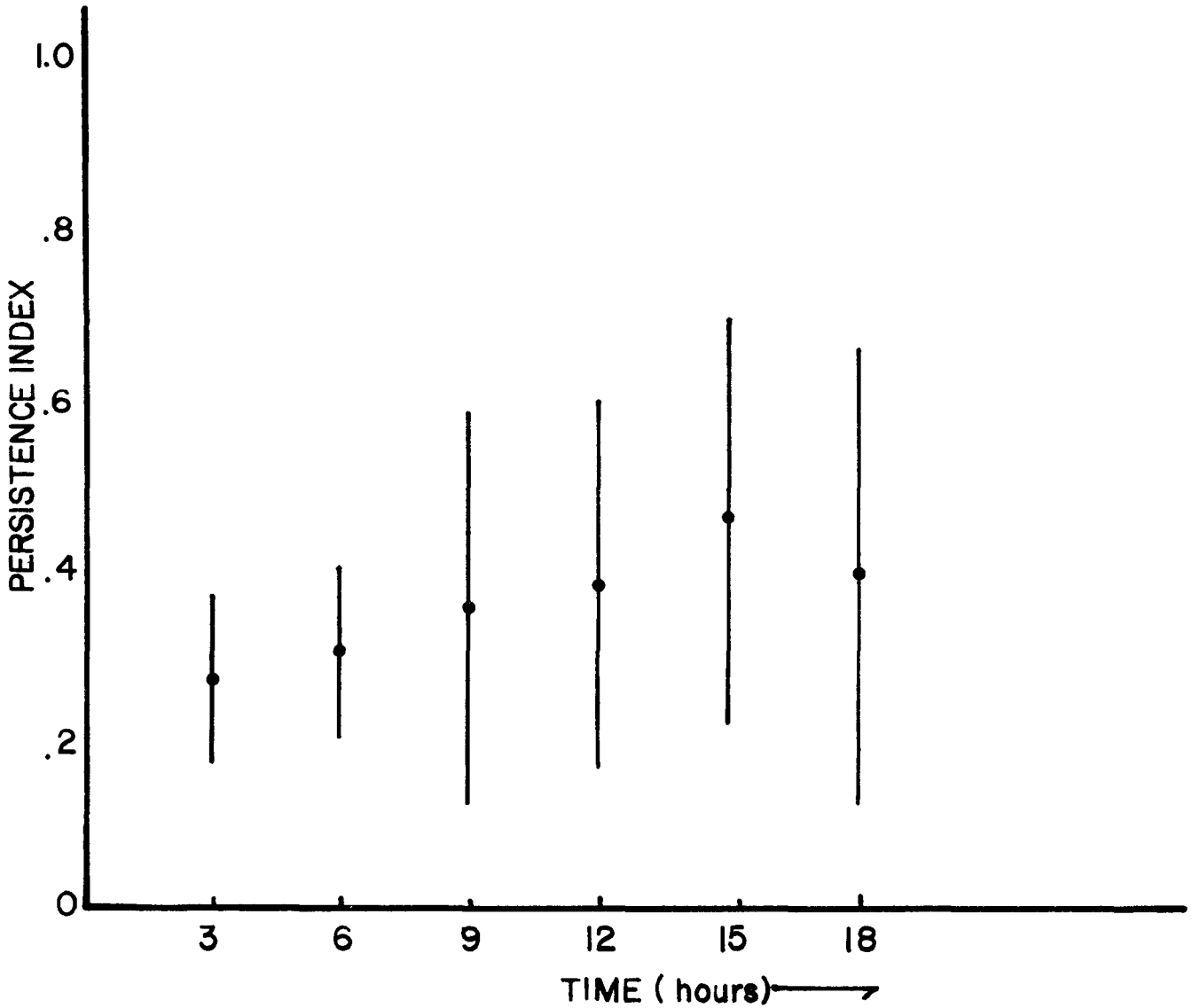

Figure 14(b). Same as Figure 14(a), except at 18Z, 11 May 1974.

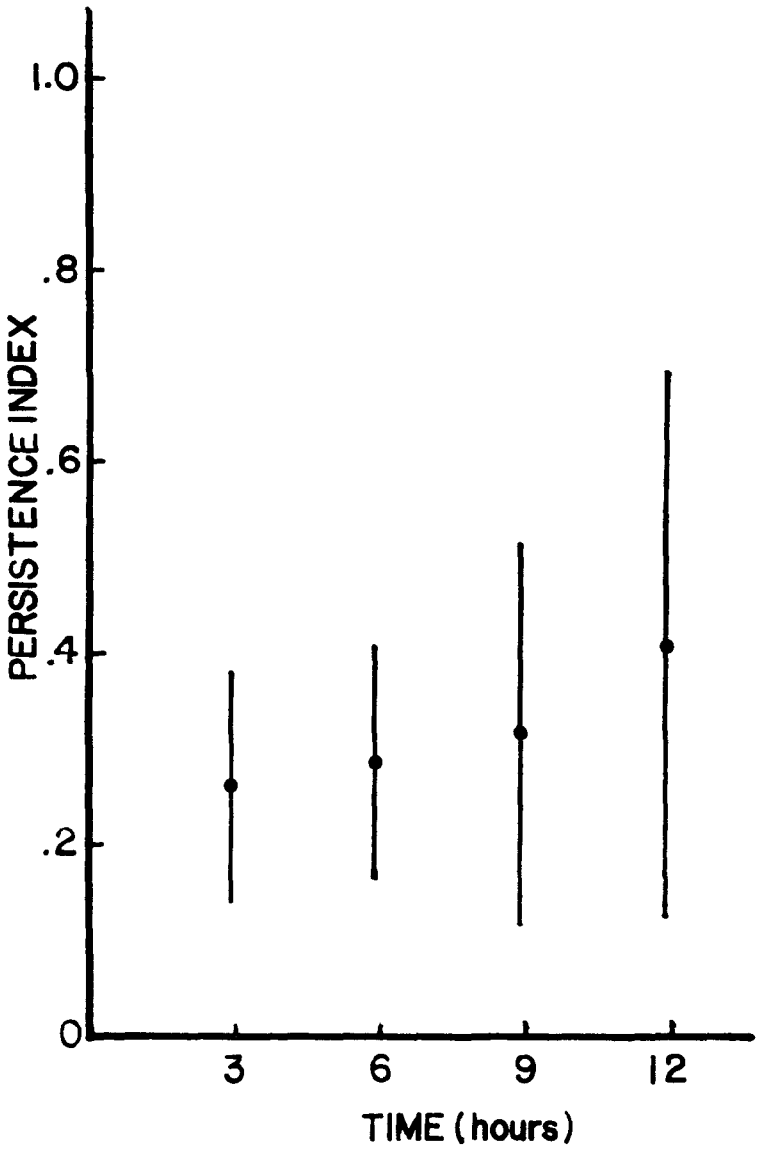

Figure 14(c). Same as Figure 14(a), except at 00Z, 12 May 1974.

SECTION 5

REGIONAL RESIDENCE TIMES OF SO_2 OVER THE EASTERN U.S.

5.1. Introduction

The present energy shortage will make it mandatory to develop fossil fuels with a greater potential for polluting the environment than was heretofore the case. For an assessment of the environmental impact of this energy development it will be essential to arrive at a better understanding of the fate of pollutants, especially of sulfur dioxide, in the atmosphere.

A parameter which adequately characterizes the fate of pollutants over long time- and space-scales is the "residence time or "turnover time" in the atmosphere. The residence time of a pollutant can be defined as the time required to decrease its burden in the atmosphere over a certain region by a factor of 1/e, assuming that no further input into the atmosphere and no import across the boundaries of the region occur. The turnover time is the time equal to the total mass of a pollutant in the atmosphere over a certain region divided by the removal flux of the pollutant.

There have been several reports on the residence time of sulfur dioxide. Meetham (1950) studied the budget of industrial SO_2 over England and obtained a residence time of sulfur dioxide of 11 hours. Junge (1960) reexamined Meetham's results and obtained a residence time for sulfur dioxide of four days. In the same paper, from the data of emissions and depositions of sulfur dioxide over the United States and the average horizontal transport velocity, Junge obtained a residence time for anthropogenic SO_2 in the United States of about five days. Rodhe (1970) found from a study in Sweden that only a small part of the anthropogenic sulfur from a city in Sweden was deposited within the nearest 10 km and the residence time for this sulfur must have been at least five hours. From the atmospheric sulfur budget over northern Europe, Rodhe (1972) estimated a turnover time for anthropogenic sulfur of two to four days. Based on the emission data of SO_2 over Europe and calculations by a transport model, Eliassen and Saltbones (1974) arrived at a residence time for SO_2 of about half a day.

These studies show that the residence time for SO_2 is different at different locations and for different seasons. Most of the above studies have been based on data obtained during several days when no precipitation has occurred.

In this section, we report the residence time for sulfur dioxide in the eastern United States, based on climatological data of the mixing layer

height and of precipitation in the region. The reason for studying the residence time in this area is that most of the industrial activities are located in this area.

Most of the pollutants have their sources near the surface of the earth and are emitted into the mixing layer, where they eventually spread toward a state of uniformity throughout the depth of the layer. The mixing layer depth is an important parameter in air-pollution meteorology. For example, seasonally averaged values of pollutant concentrations depend on seasonal averages of the depth of the mixing layer over the region considered. Large portions of the total burden of pollutants stay in this layer. Some of the pollutant escapes by vertical transport into the free atmosphere above the mixing layer through convection, through turbulent mixing and through large-scale vertical motions. In this paper we are concerned only with the fate of pollutants which remain in the mixing layer.

Calculations were made of the regional residence time of sulfur dioxide over the region of the United States east of 105°W longitude where major industrial activities are located. The year was divided into the cold season (January - April, and November and December) and the warm season (May - October), and the regional residence time for each of these two seasons was calculated.

5.2. Data Used

5.2.1. Mean Mixing-layer Height, $\overline{H}$.

The mixing-layer height is defined as the level above the surface which limits the relatively vigorous vertical mixing near the ground. Holzworth (1967 and 1972) defined the maximum mixing depth as the height at which the adiabat through the surface temperature maximum observed between 1200 and 1600 LST intersects the actual temperature sounding curve obtained from the 1200 GMT sounding. The morning mixing-layer height is calculated as the height above ground which the dry adiabat through the minimum surface temperature observed between 0200 at 0600 LST, increased by 5°C, intersects the observed 1200 GMT temperature sounding. Both mixing heights, thus defined, have to be considered only as approximations to the actual depth of the mixing layer. They are, however, thought to be reasonable estimates suited for practical applications, especially when such applications are intended for large regions and for climatological studies.

The report by Holzworth (1972) contains the isopleths and the tables of these mixing-layer heights for four seasons. For the purpose of this paper, the mixing-layer heights, $\overline{H}$, calculated for the cold and warm seasons separately, are defined as the averages of the afternoon mixing heights of winter and spring, and summer and fall, respectively, as reported by Holzworth.

5.2.2. Precipitation data.

In order to calculate the mean durations of dry periods τ_d and wet periods τ_p, and the mean scavenging coefficient $\overline{\lambda}$ which will be described in

the following section, the hourly precipitation data of the year 1974 (U.S. Department of Commerce, 1974) were analyzed. The data for 61 stations located in the study area were used for the computation of these parameters for each season.

5.3. Approach

5.3.1. Regional residence time T and turnover time Te.

In order to calculate the residence time of a pollutant we assume that it is distributed uniformly throughout the mixing layer, that there is no leakage through the top of this layer, that the imported and exported amounts of a pollutant due to turbulent diffusion across the boundaries of the region are balanced, that it is removed from the layer by dry deposition and precipitation scavenging, and that it is transformed into other species by first order reactions. Under these assumptions, we can write

$$\frac{dC}{dt} = -(\lambda_d + k_p + \lambda_c)\, C$$

$$C = C_o \exp\left[-(\lambda_d + k_p + \lambda_c)t\right]$$

The e-folding residence time T can be defined as follows:

$$T = \frac{1}{k_t} = \frac{1}{\lambda_d + k_p + \lambda_c} = \frac{1}{\frac{1}{t_d} + \frac{1}{t_p} + \frac{1}{t_c}} \qquad (19)$$

C is the concentration of the pollutant under consideration, k_t the total decay rate, λ_d the decay rate due to dry deposition, k_p the decay rate due to precipitation scavenging, and λ_c the chemical transformation rate. t_d, t_p and t_c would be defined as the residence times, if only one of the mechanisms, dry deposition, precipitation scavenging, or chemical transformation were responsible for the removal.

Assuming a Markov process for the sequence of weather events, Rodhe and Grandell (1972) derived an expression for the expected "turnover time" Te of a pollutant in the presence of precipitation. This "turnover time" is defined as the total mass of the pollutant in the atmosphere divided by the removal flux and can be written as:

$$Te = \frac{\tau_d + \tau_p + \tau_d\tau_p(P_d\lambda'_p + P_p\lambda'_d)}{\tau_d\lambda'_d + \tau_p\lambda'_p + \tau_d\tau_p\lambda'_d\lambda'_p} \qquad (20)$$

$$\tau_d = \int_0^\infty \tau\eta_d(\eta)d\eta_d \qquad (21)$$

$$\tau_p = \int_0^\infty \tau \eta_p(\eta) d\eta_p \tag{22}$$

$$p_d = \frac{\tau_d}{\tau_d + \tau_p} \tag{23}$$

$$P_p = \frac{\tau_p}{\tau_d + \tau_p} \tag{24}$$

Here, τ_d and τ_p are the mean durations of dry and wet periods, respectively, η_d and η_p are the frequency distributions of dry and wet periods, τ is the time, p_d is the probability of dry periods and P_p is the probability of wet periods. λ_p' and λ_d' are, respectively, the removal coefficients during wet and dry periods.

The coefficients λ_p' and λ_d' can be written as:

$$\lambda_p' = \lambda_p + \lambda_d + \lambda_c \tag{25}$$

$$\lambda_d' = \lambda_d + \lambda_c \tag{26}$$

where, λ_p is the rate of precipitation scavenging, λ_d is the rate of dry deposition, and λ_c is the rate of chemical transformation. In this paper, we assume that λ_d and λ_c are constant, independent of weather.

The e-folding residence time T given by (19) and the turnover time, Te, given by (20) are calculated and compared.

5.3.2. Dry deposition.

Dry deposition of pollutants subject to airborne transport can occur by sedimentation and by retention at the ground through impaction or adsorption.

The mechanism of dry deposition is most conveniently expressed by the concept of a deposition velocity, v_g. This velocity is defined as

$$v_g = \frac{\text{deposition rate}}{\text{volumetric concentration}}$$

v_g is dependent on many factors, such as the surface roughness of the terrain, the stability of the atmosphere, the chemical properties of the pollutants and the biological properties of the plant canopy. There are ample data from

field experiments of deposition velocities available for sulfur dioxide gas (Garland et al., 1974; Owers and Powell, 1974; Shepherd, 1974; Whelpdale and Shaw, 1974). The difficulty of analyzing such field data is that the factors on which the deposition velocity depends enter into the data partially in a controlled, and partially in an uncontrolled manner. Among these field experiments the data by Whelpdale and Shaw (1974) show exceptionally systematic values. According to these authors, the deposition velocity of SO_2 is larger under unstable conditions of the atmosphere than under stable conditions. This is due to the fact that the stable atmosphere causes a suppression of pollution transfer between different atmospheric layers, whereas in an unstable atmosphere there is a great deal of turbulent exchange. On the other hand, the data obtained by Garland et al. (1974), Shepherd (1974), and Owers and Powell (1974) do not show a dependence of deposition velocity of sulfur dioxide on atmospheric stability. However, those results show that the deposition velocity lies in the fairly broad range between 0.1 cm/sec and 3.0 cm/sec which could easily encompass the effects of different stabilities.

The deposition velocity of sulfur dioxide was also estimated from a mass budget study. Meetham's (1950, 1954) analyses showed that the deposition velocity is about 1.8 cm/sec. From aircraft sampling of sulfur dioxide and sulfate off the east coast of England, Smith and Jeffrey (1974) concluded that the loss of sulfur dioxide due to deposition was commensurate to a velocity between 0.8 and 1 cm/sec over land, and between 0.6 and 0.8 cm/sec over the sea.

Prahm et al. (1976) obtained a deposition velocity for sulfur dioxide of 2 cm/sec $\pm$ 50% over the Atlantic from the study of atmospheric transport of sulfur oxides over the Atlantic.

In accordance with the above brief reviews, we assume that the dry deposition velocity, v_d, of sulfur dioxide is 1 cm/sec regardless of the region and the season.

Given v_d, the decay rate λ_d due to dry deposition can be written as

$$\lambda_d = \frac{v_g}{\bar{H}} = \frac{1}{t_d} \tag{27}$$

where $\bar{H}$ is the mean mixing layer height.

5.3.3. Precipitation scavenging.

Climatological data of pollutants in precipitation show that their concentrations in rain are large where the concentrations of pollutants in the air at ground level are large, suggesting that the air mass in the vicinity of the clouds from which the precipitation falls is responsible for the concentration of pollutants in rainwater (Lodge et al., 1968; Stevenson, 1968; Andersson, 1969). Thus, the following assumptions can be made:

1. The air in the mixing layer directly below the cloud is transported into the cloud by large-scale vertical motion as well as by convective motions.

2. The pollutants in the air are scavenged by both rainout and washout processes.

3. The precipitation containing pollutants falls on the same general region from which the polluted air was entrained into the cloud system.

Under these assumptions it is practical to express both rainout and washout processes in the single term of a "scavenging velocity", $\bar{v}_p$. This parameter is defined as

$$\bar{v}_p = \left(\frac{\kappa}{\chi}\right)_v \cdot \bar{p} \qquad (28)$$

where κ is the concentration of pollutants in rainwater, χ the concentration of pollutants in air, and $\bar{p}$ the mean precipitation rate. The subscript v means that the ratio $\left(\frac{\kappa}{\chi}\right)$ is formed on a volume basis. This ratio is a function of many physical parameters such as the size distributions of the pollutant and of precipitation particles, the chemical composition of the pollutant, the precipitation rate, etc. The ratio $\left(\frac{\kappa}{\chi}\right)$ varies with time even during the same event of precipitation. Unfortunately, there are very few observations available in which this ratio has been measured simultaneously with other physical parameters.

Engelmann (1971) estimated from data by Georgii and Bielke (1966) that the ratio $\left(\frac{\kappa}{\chi}\right)_m$ for SO_2 is 19 for rains of 11 to 20 mm per day and 190 for rain of 0.3 mm per day. Here the subscript m means that the ratio is formed on a mass basis. These values on a mass basis can be converted into approximately those on a volume basis multiplying by a factor of 10^3. Summers' data (1970), obtained by flight observations of convective storms, show that the ratio $\left(\frac{\kappa}{\chi}\right)_v$ for SO_2 is within the range of 2.7×10^4 to 8.6×10^4. For typical values of SO_2 concentration in the air, the saturation value of SO_4^{--} in distilled water is at least two orders of magnitude below the values found in rainwater. The saturation concentration of SO_4^{--} is determined, however, by the pH, and oxidation will continue as long as the pH is kept above the critical value. Adding NH_3 will accomplish this. Junge and Ryan (1958) propose that there is enough NH_3 in the atmosphere for this oxidation process to account for the observed values of SO_4^{--} in rainwater.

However, recent investigation by Dana et al. (1976) showed that the oxidation process due to NH_3 is not solely responsible for the observed values of SO_4^{--} in rainwater.

In this paper, we chose the values of 5×10^4 as a typical value of $\left(\frac{K}{\chi}\right)_v$ for sulfur dioxide. The mean precipitation rate $\bar{p}$ was determined from the hourly precipitation data, dividing the total precipitation amount during the season of interest by the total hours of precipitation.

Given the values of $\left(\frac{K}{\chi}\right)_v$ and $\bar{p}$, or the value of $\bar{v}_p$, and the mean mixing-layer height, $\bar{H}$, the mean scavenging coefficient, $\bar{\lambda}$, can be calculated as

$$\bar{\lambda} = \left(\frac{K}{\chi}\right)_v \cdot \bar{p}/\bar{H} = \bar{v}_p/\bar{H} \qquad (29)$$

For the present purpose, the mean scavenging coefficient given by Eq. (29) is used for λ_p. The decay rate due to precipitation, k_p, in Eq. (19) is given by

$$k_p = P_p\bar{\lambda} \qquad (30)$$

5.3.4. Chemical transformation.

There are numerous research reports available on the reaction rates and reaction kinetics of SO_2 with other pollutants (e.g., Urone and Schroeder, 1969; Bufalini, 1971). Some results are contradictory to others. However, the following can be inferred: In the daytime and at low relative humidity (below 70%), the photochemical reactions of SO_2 with O_2 and hydrocarbons will be of primary importance. In this case SO_2 will be converted into H_2SO_4 aerosols. In the daytime when the relative humidity is between 70 and 100%, and at night, the aerosols will absorb substantial quantities of water and the aerosol size distribution will shift to larger sizes. The rate of SO_2 conversion should be increased through solution oxidation mechanisms, aided by the catalytic effects of metal salts present as nuclei. It is realized that a full description of the transformation rate of SO_2 is difficult at present.

From field observation data of the concentrations of SO_2 and particulate SO_4 in Europe, Eliassen and Saltbones (1975) arrived at empirical values of λ_c of the order of 10^{-6} sec^{-1}.

From the study of transport of sulfur oxides over the Atlantic Prahm et al. (1976) arrived at $\lambda_c = 3 \times 10^{-6}$ sec^{-1}. In this paper, we assume that λ_c in Eqs. (19) and (20) is 1×10^{-6} sec^{-1}.

5.4. Results

5.4.1. Mean dry period τ_d and mean wet period τ_w.

In Fig. 15(a) and (b), the mean dry period, τ_d, is shown for the cold season and for the warm season, respectively. In general, τ_d is larger in the western part of the studied region than in the eastern part regardless of the season. The region surrounding the Great Lakes and the coastal region show small values of τ_d.

The mean wet period τ_w is shown in Fig. 16(a) and (b) for the cold season and for the warm season, respectively. τ_w is within the range of two to five hours. These values of τ_d and τ_w are used for the following calculations.

5.4.2. Residence time due to dry deposition, t_d.

In Fig. 17(a) and (b), the residence times due to dry deposition, t_d, are shown for the cold season and for the warm season, respectively.

From these diagrams, it can be seen that t_d is larger in the warm season than in the cold season over the whole region. This is simply due to the fact that the mixing layer is deeper in the warm season than in the cold season. The region surrounding the Great Lakes is shown to have the smallest value of t_d. On the other hand, the mean mixing-layer height in the western part of the region studied is relatively high, resulting in the larger values of t_d.

5.4.3. Mean scavenging coeffiecient $\overline{\lambda}$.

From Eq. (30), the mean scavenging coefficient $\overline{\lambda}$ over the studied area is calculated for each station, assuming that $(\kappa/\chi)_v = 5 \times 10^4$. In Fig. 18(a) and (b), the distributions of $\overline{\lambda}$ are shown for the cold and the warm seasons, respectively. The values of $\overline{\lambda}$ are small in the western and the northern parts of the studied area, and are large in the southern part of the region. This is due to the moister climate in the southern area. Furthermore, it can be seen that $\overline{\lambda}$ is larger in the warm season when the convective activity is more frequent, than in the cold season so that, on the average, the precipitation amount per precipitation event is larger in the warm season than in the cold season.

5.4.4. Regional residence time T and turnover time Te.

Using Eqs. (19) and (20) and assuming $k_c = 1 \times 10^{-6}$ sec^{-1}, the regional residence time T and turnover time Te for the cold season and the warm season

(a)

(b)

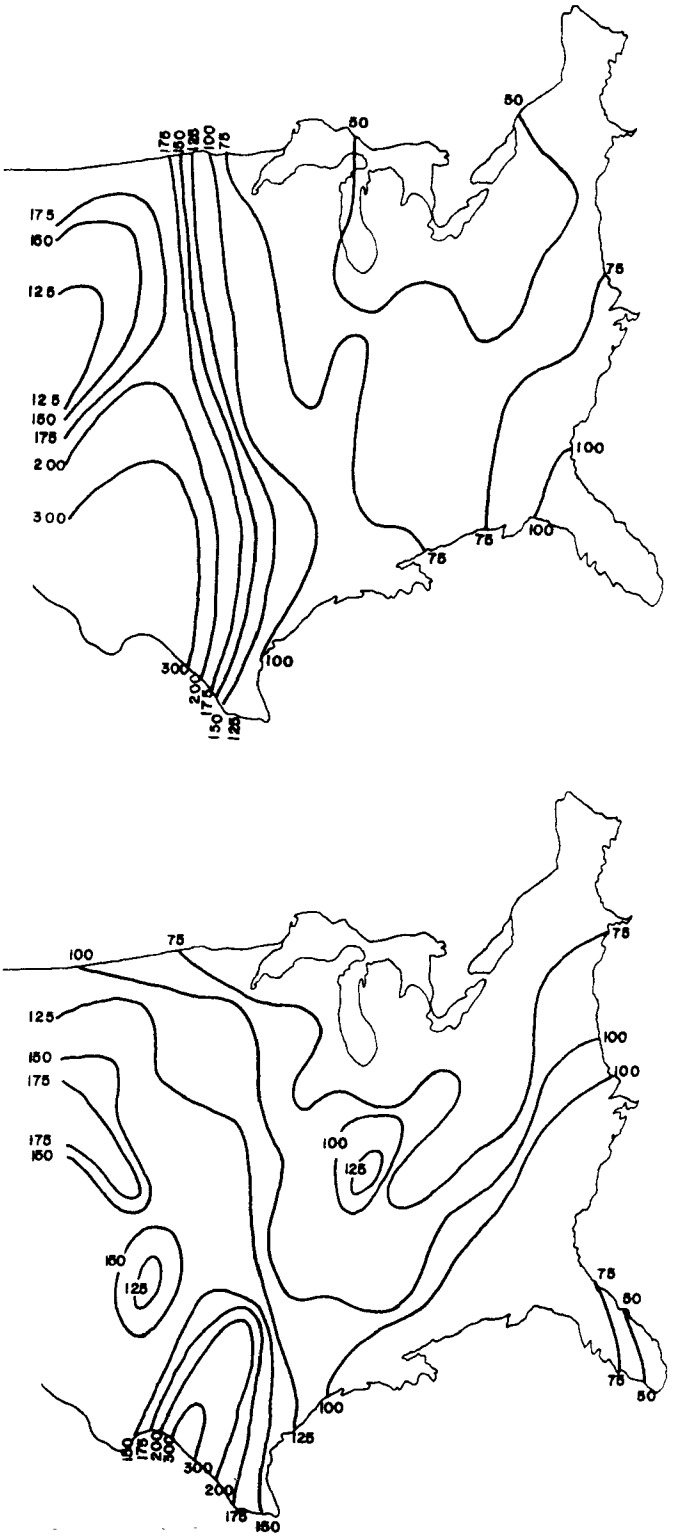

Figure 15. Mean dry period, τ_d (in hours), (a) for the cold season, and (b) for the warm season.

(a)

(b)

Figure 16. Mean wet period, τ_W (in hours), (a) for the cold season, and (b) for the warm season.

(a)

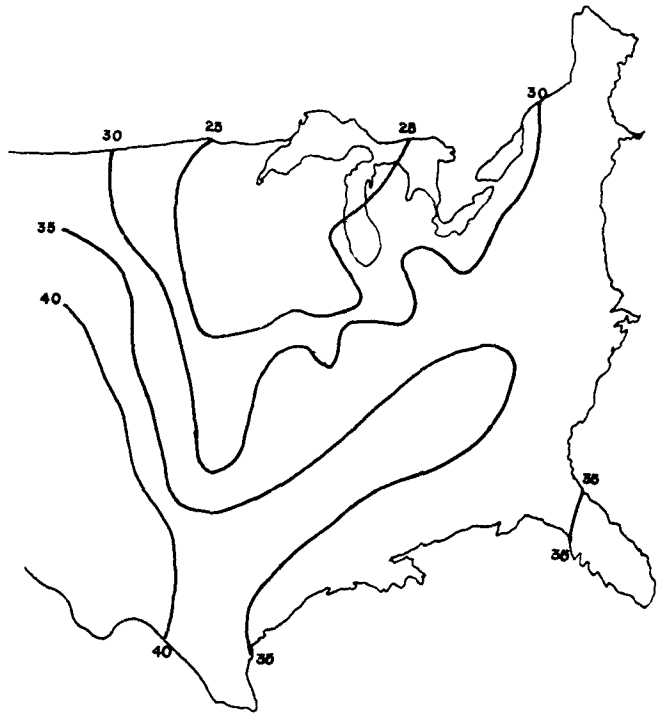

(b)

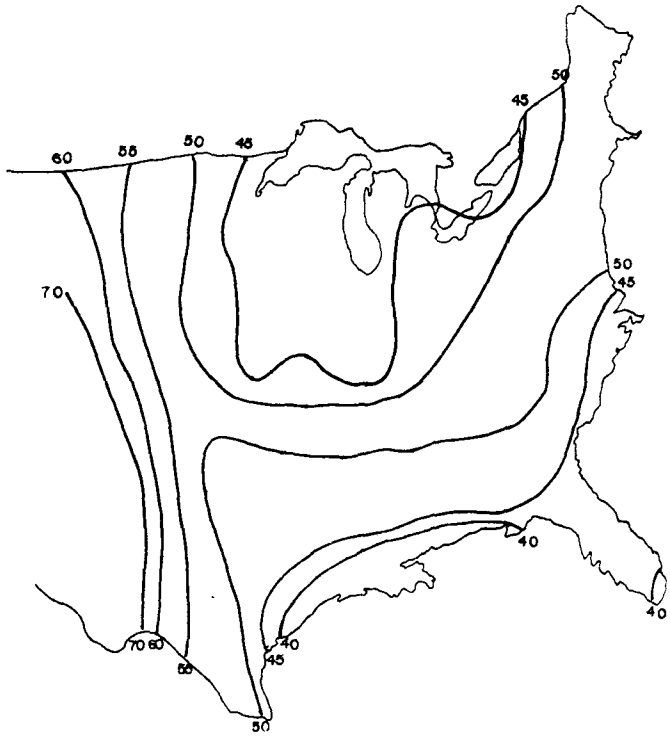

Figure 17. The residence time (in hours) due to dry deposition, t_d, (a) for the cold season, and (b) for the warm season.

(a)

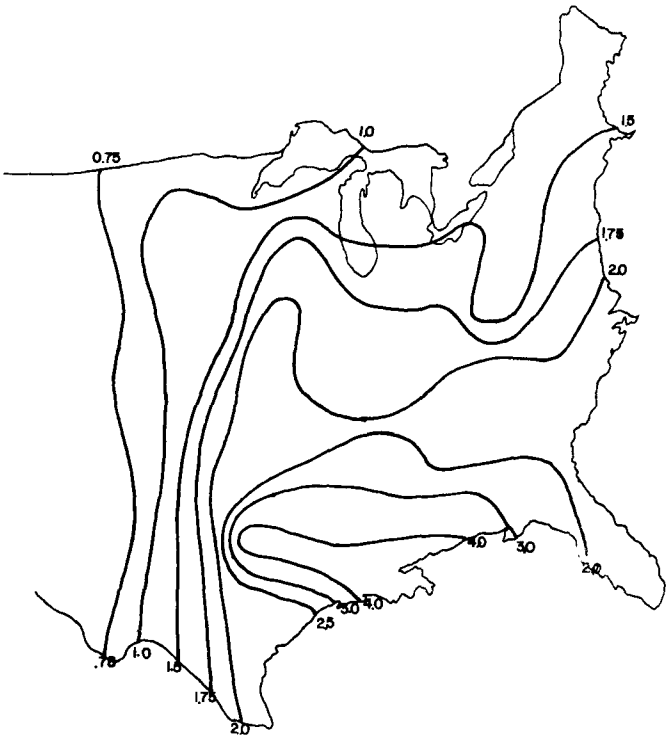

(b)

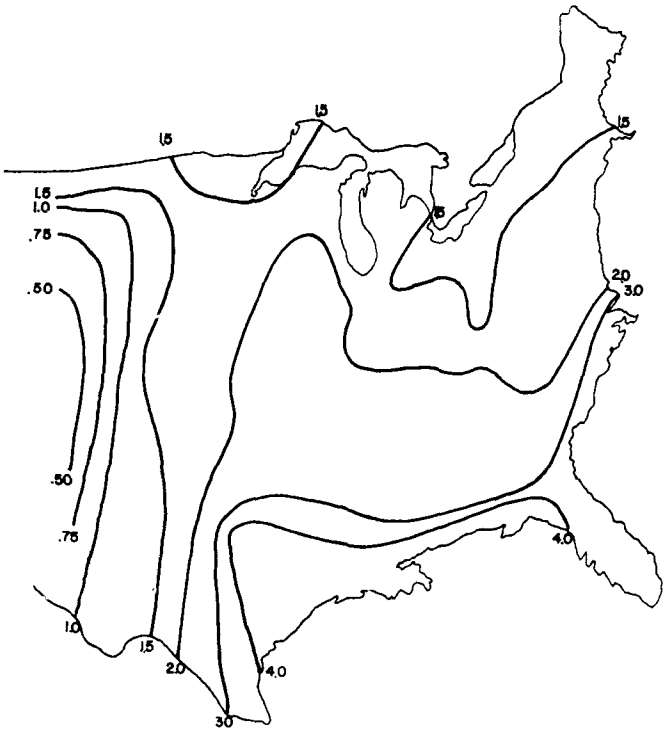

Figure 18. Climatological scavenging coefficient, $\overline{\lambda}$, (x 10^{-5}sec) for SO_2, (a) for the cold season and (b) for the warm season.

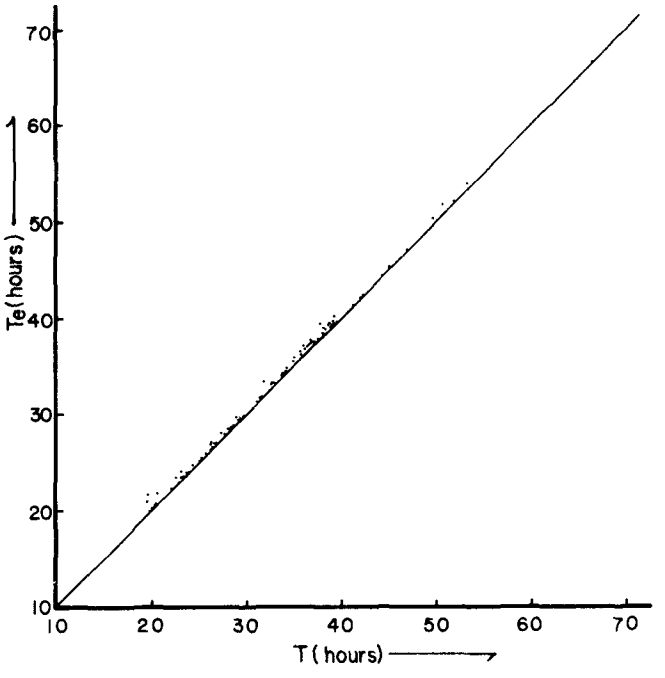

Figure 19. Turnover time, Te, versus residence time, T.

(a)

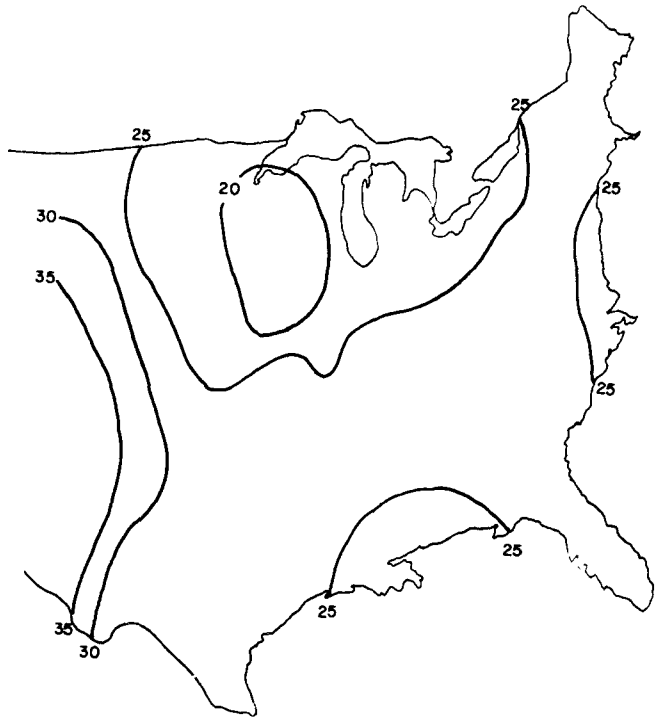

(b)

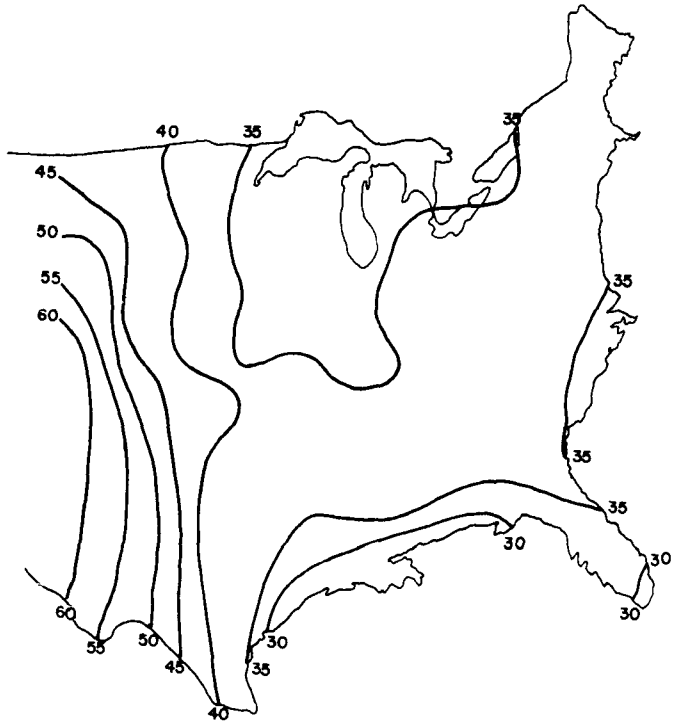

Figure 20. The regional residence time, T (in hours), for SO_2, (a) for the cold season, and (b) for the warm season.

are calculated for each station. In Fig. 19, Te versus T is plotted using the values for both the cold season and the warm season at each station. It can be easily seen that Te is slightly larger than T, and that, for practical use, either Te or T can be calculated to represent the residence time for the studied area.

Because of the close coincidence between Te and T, only the regional residence times T for the cold season and the warm season are shown in Fig. 20(a) and (b).

The following can be seen from these diagrams;

1. The residence time is, in general, longer in the warm season than in the cold season over the whole region studied. This is due to shorter dry periods in the cold season than in the warm season, and due to the shallower depth of the mixing layer in the cold season than in the warm season.

2. Short residence times characterize the region surrounding the Great Lakes and the southern part of the United States.

3. Long regional residence times are found in the western parts of the studied area, where the mixing layer height is large, the precipitation frequency is small.

4. In the studied area, the regional residence time lies in the range between 20 and 40 hours for the cold season and in the range between 30 and 60 hours for the warm season.

5. A comparison of Fig. 20 with Fig. 17 shows a similar pattern of the isolines, implying that in the studied area the dry deposition is the most dominant removal mechanism.

As mentioned previously, Junge (1960) arrived at a residence time for anthropogenic SO_2 of about five days over the United States. This value is much larger than the values we obtained. The reason for this discrepancy is that Junge did not take into account the removal due to deposition. Comparisons with the results obtained in Europe are difficult because of the different methods of estimation and because of the different climate. However, it should be noted that the residence times for SO_2 in the present study are in agreement with those over Europe within a factor of two to three.

Our study has been based on the observed data available for v_d, $\left(\frac{\kappa}{\chi}\right)_v$ and λ_c. These parameters have been assumed to be constant over the studied region, regardless of the season and the location. In reality, these parameters are, as has been mentioned previously, dependent on temperature, humidity, wind speed, location and other factors. Therefore, the residence times presented in the present paper should be regarded as approximate.

5.5. Summary

Assuming that sulfur dioxide in the mixing layer is removed from the atmosphere by dry deposition, by precipitation scavenging, and by transformation into SO_4^-, the regional residence time is defined and calculated for the region of the United States east of 105°W longitude. The results have been shown as the isopleths of the residence time. However, because of the assumptions that v_d = 1 cm/sec, $\left(\frac{K}{\chi}\right)_v = 5 \times 10^4$ and $k_c = 1 \times 10^6$ regardless of season and location, the results should be regarded as approximate. Further improvements must be delayed until these values are specified in more detail for each season and location.

SECTION 6

SCAVENGING OF AEROSOL POLLUTANTS IN CUMULUS CLOUDS

6.1. Introduction

Cumulus clouds are an important mechanism not only for transporting air pollutants from the boundary layer into the free atmosphere, but also for cleansing the atmosphere by precipitation processes.

Pollutants are removed by precipitation through rainout and washout processes. "Rainout" comprises all processes within the clouds, and "washout" constitutes the removal by precipitation below the clouds. It is important to study the effects of the physical characteristics of clouds on rainout and washout of pollutants. By understanding these effects, the vertical transport processes of pollutants from the planetary boundary layer into the free atmosphere and the cleansing mechanisms of the atmosphere will be estimated quantitatively.

Recent studies by Dingle and Lee (1973) on rainout processes and by Dana and Hales (1976) on washout processes of polydispersed aerosols make it possible to investigate in detail the removal mechanisms of aerosol pollutants by precipitation.

The study in this section is concerned with the rainout process in cumulus clouds. A cumulus cloud model developed by Cotton (1972a,b) is combined with the multi-rate model of in-cloud scavenging (Dingle and Lee, 1973), in order to investigate the effects of the physical characteristics of clouds on in-cloud scavenging, particularly the characteristics of continental and maritime cumulus clouds. The rain-out process in other types of clouds, such as clouds associated with front formation must be studied in the future.

Studies carried out by Howell (1949), Mordy (1960) and Neiburger and Chien (1960) have shown that the influence of cloud nuclei in determining the number and size of cloudwater droplets is restricted to the lowest few meters above cloud base. It is only in the base region that cloud nuclei are activated. Hence it is there that the concentration of cloudwater droplets is determined. Subsequent condensation merely serves to increase the size of droplets which are already present. In this study, we define a continental cumulus as having a concentration of 300 droplets per cm^3 and a radius dispersion of 0.25, and a maritime cumulus as having a concentration of 100 droplets per cm^3 and a radius dispersion of 0.25. Here "radius dispersion" is defined as the ratio of the standard deviation of droplet size to the mean radius.

The multi-rate model incorporates explicitly the rate of progress of each process which contributes to the ultimate removal of contaminants from clouds. The attachment of aerosols to cloudwater droplets and to rainwater droplets, and the conversion of cloudwater droplets to rainwater droplets by autoconversion and accretion are incorporated in the model. Water droplets in the cloud are classified into two classes: cloudwater droplets refer to water droplets having a diameter of smaller than 100 μm, and rainwater droplets refer to water droplets having a diameter of larger than 100 μm. In the present study, it is assumed that cloudwater droplets and rainwater droplets are kept unfrozen even under temperatures below freezing.

In the case of a precipitating cumulus cloud, the discrete particle sizes of importance range from aerosol particles of the order of 10^{-2} μm in diameter to precipitation drops as large as 5×10^{3} μm in diameter. Therefore, in order to study the interaction of pollutant particles and cloudwater droplets, a model must be chosen in which the microphysical processes are incorporated in as much detail as possible. One such model is the one-dimensional cumulus model by Cotton (1972a,b). The model involves upward integration with height following the rise of the convective bubble or plume. Although this cumulus model deals only with the actively growing phase of a cloud, it is useful to study the gross aspects of in-cloud scavenging in different clouds with different physical characteristics.

6.2. The Model

6.2.1. Cumulus cloud.

In the following, the equations used in the model are cited. The details will be found in Cotton (1972b).

1. Moisture continuity

The continuity equation of the total moisture mixing ratio Q_T

$$Q_T = q_v + Q_c + Q_H \tag{31}$$

Q_T = total moisture mixing ratio

q_v = cloud vapor mixing ratio

Q_c = cloudwater mixing ratio

Q_H = rainwater mixing ratio

$$\frac{dQ_T}{dz} = \frac{dq_v}{dz} + \frac{dQ_c}{dz} + \frac{dQ_H}{dz} - \mu(q_v - q_e + Q_c + Q_H) - \text{fallout} \tag{32}$$

q_e = environmental vapor mixing ratio

μ = entrainment parameter

$$\mu = \frac{1}{M}\frac{dM}{dz} \tag{33}$$

M = cloud mass

$$\frac{dq_v}{dz} = \frac{\varepsilon L_c q_s}{R_a T^2}\left(\frac{dT_c}{dz}\right) + \frac{g}{R_a T} q_s - \mu(q_v - q_e) \tag{34}$$

q_s = saturation mixing ratio with respect to water

ε = ratio of the density of water to that of air

L_c = latent heat of condensation

R_a = gas constant of air

g = acceleration of gravity

Here dT_c/dz is calculated from Eq. (39) below.

The continuity equation for Q_c is

$$\frac{dQ_c}{dz} = -\frac{dq_s}{dz} - \mu Q_c - \text{conversion} - \text{accretion} \tag{35}$$

$$\text{Conversion} = \frac{\frac{1}{\rho_a}\frac{dM}{dt}\Big|_{\text{auto}}}{w} \tag{36}$$

$$\text{Accretion} = \frac{\frac{1}{\rho_a}\frac{dM}{dt}\Big|_{\text{accr}}}{w} \tag{37}$$

ρ_a = density of cloud air

The continuity equation of Q_H is

$$\frac{dQ_H}{dz} = -\mu Q_H + \text{conversion} + \text{accretion} \tag{38}$$

2. Cloud thermodynamics

The equation for the vertical lapse in temperature of a water-saturated cloud is

$$\frac{dT_c}{dz} = \frac{-\frac{g}{C_p}\left(\frac{L_c q_s}{R_a T_c} + 1\right) - \mu(T_c - T_{en})}{1 + \frac{\varepsilon L_c^2 q_s}{C_p R_a T_c^2}} \qquad (39)$$

C_p = specific heat at constant pressure

T_{en} = environmental temperature

3. Dynamics

The vertical motion equation used in the model is based on the derivation by Squires and Turner (1962). The vertical change in momentum flux due to buoyancy forces is

$$\frac{d}{dz}(\pi R^2 w^2 \rho_a) = \pi R^2 g \rho_a \left(\frac{\rho_e - \rho_a}{\rho_a} - Q_s\right) \qquad (40)$$

ρ_a = density of cloud air

ρ_e = density of the environmental air

Q_s = total mixing ratio of condensed water substance

($Q_s = Q_c + Q_H$)

This equation can be rearranged as

$$w \frac{dw}{dz} = g\left(\frac{T_{vc} - T_{ve}}{T_{vc}} - Q_s\right) - \mu w^2 \qquad (41)$$

If we let

$$F_\alpha = \left(\frac{T_{vc} - T_{ve}}{T_{ve}} - Q_s\right) g \qquad (42)$$

and

$$K_\alpha = 2\mu, \qquad (43)$$

equation (41) can be integrated analytically from z_1 to z_2, assuming F_α and K_α are constant in the layer.

$$w_2 = \left[\frac{2F_\alpha}{K_\alpha} + \left(w_1^2 - \frac{2F_\alpha}{K_\alpha} \right) \exp\ (-K_\alpha \Delta z) \right]^{\frac{1}{2}} \qquad (44)$$

$$\Delta z = z_n - z_{n-1}.$$

4. Autoconversion and accretion

The numerical calculations of Howell (1949), Mordy (1959) and Neiburger and Chien (1960) show that droplet growth by condensation produces only a relatively narrow distribution of small droplets during the lifetime of one to two hours of a typical cumulus cloud. In warm clouds, a broadening of this distribution to include some larger droplets can occur by collision and coalescence. The occurrence of collision and coalescence among cloud particles is called "autoconversion".

Kessler (1967) hypothesized that the water converted to rainwater droplets is size-distributed in the inverse exponential distribution formulated by Marshall and Palmer (1948), given by

$$F(R) = N_o e^{-2\gamma R} = N_o e^{-\gamma D} \qquad (45)$$

where γ is a coefficient. Once these rainwater droplets have formed, they can grow very rapidly by accretion of cloudwater droplets.

Using the stochastic collection model by Berry (1965), and assuming a gamma distribution for cloudwater droplets, Cotton (1972a) derived the following equation for the autoconversion rate of cloudwater droplets to rainwater:

$$\left.\frac{dM}{dt}\right|_{auto} = \exp\left[k' - \frac{1}{4a'} (t - h')^2 \right] \qquad (46)$$

where t represents the age of a parcel of droplets and a', k' and h' are coefficients which are functions of the cloudwater content for a given initial concentration and dispersion.

When $n_o = 100\ cm^{-3}$ and $\nu_r = 0.25$

$$\left.\begin{aligned} h' &= e^{7.13\ m^{-1.44}} \\ k' &= -e^{2.001\ m^{-0.478}} \\ a' &= e^{9.63\ m^{-2.59}}, \end{aligned}\right\} \qquad (47a)$$

and when $n_o = 300\ cm^{-3}$ and $\nu_r = 0.25$

$$\left.\begin{aligned} h' &= e^{6.548}\, m^{-1.75} \\ k' &= -e^{2.46}\, m^{-0.779} \\ a' &= 15.6 \times 10^{4} - 4.8 \times 10^{4}\ m. \end{aligned}\right\} \qquad (47b)$$

Here n_o is the concentration of cloudwater droplets, ν_r the radius dispersion and m is the liquid water content in $gm \cdot m^{-3}$. The former set of parameters is used for the maritime cloud and the latter is used for the continental cloud.

Kessler derived the following equation describing the accretion rate of cloudwater droplets by rainwater droplets:

$$\left.\frac{dM}{dt}\right|_{accr} = \frac{130\pi}{4}\left[\frac{\pi\rho_\ell \Gamma(4)}{6}\right]^{-0.875} N_o^{0.125}\, \overline{E(D/C)}\, \Gamma(3.5) m M^{0.875} \qquad (48)$$

where ρ_ℓ is the density of water, $\overline{E(D/C)}$ represents an average collection efficiency between the rainwater droplets and cloudwater droplets, Γ is the gamma function, and M is the rainwater content in $gm \cdot m^{-3}$.

5. Fallout of rainwater

Cotton (1972b) used the scheme suggested by Howell and Lopez (1968). The scheme is to drop out the portion of water droplets that has a terminal velocity larger than the updraft velocity, w. If D_w represents the raindrop diameter falling at a terminal velocity equivalent to the updraft velocity, then the water content that falls out is

$$M_H(> D_w) = \int_{D_w}^{\infty} \frac{\pi\rho_\ell D^3}{6} N_o e^{-\gamma D} dD \qquad (49)$$

6.2.2. Rainout model.

In the present model, the aerosols in the planetary boundary layer are transported up into the cumulus cloud by convection. The cloud is envisaged as an assembly of cloudwater droplets and rainwater droplets intermingled with aerosol pollutants, some of which are free-floating in the cloud air and some of which are collected by the droplets. Aerosol pollutants in the cloud air and in the droplets are injected into the environmental air by detrainment. Precipitating rainwater droplets also remove aerosol pollutants from the cloud.

After modifying the equations by Dingle and Lee (1973), the spatial variation of the aerosol concentration in each category, while the aerosols are carried up through the cloud, can be described by the following equations:

$$\frac{dN_{a_i}}{dz} = -\left[\sum_{j=1}^{M} \Lambda_{1ij} + \sum_{k=1}^{N} \Lambda_{2ik}\right] \frac{N_{a_i}}{w} - \mu N_{a_i} \quad \text{for each } i \qquad (50)$$

$$\frac{dN_{c_i}}{dz} = \left[N_{a_i} \sum_{j=1}^{M} \Lambda_{1ij} - \lambda N_{c_i}\right] \frac{1}{w} - \mu N_{c_i} \qquad (51)$$

$$\frac{dN_{r_i}}{dz} = \left[\lambda N_{c_i} + \sum_{k=1}^{N} \Lambda_{2ij} \cdot N_{a_i} \frac{1}{w} - \mu N_{r_i}\right] \qquad (52)$$

where

N_a = number concentration of aerosol pollutants in the cloud air (cm^{-3})

N_c = number concentration of aerosol pollutants attached to cloudwater droplets (cm^{-3})

N_r = number concentration of aerosol pollutants attached to the rainwater droplets (cm^{-3})

Λ_1 = scavenging rate of aerosols by cloudwater droplets (sec^{-1})

Λ_2 = scavenging rate of aerosols by rainwater droplets (sec^{-1})

λ = conversion rate of cloudwater droplets into rainwater droplets by autoconversion and by accretion (sec^{-1})

i = aerosol size index

j = cloudwater droplet size index

k = rainwater droplet size index.

If Λ_1, Λ_2 and λ (the indices are omitted for brevity) are considered constants in a single height interval, Eqs. (50), (51), and (52) can be integrated with height, yielding the following solutions:

$$N_a = N_{a_o} \exp\left\{-\left(\frac{\Lambda_1 + \Lambda_2}{w} + \mu\right)\Delta z\right\} \qquad (53)$$

$$N_c = \frac{\Lambda_1}{\lambda - (\Lambda_1 + \Lambda_2)} N_{a_o} \exp\left\{-\left(\frac{\Lambda_1 + \Lambda_2}{w} + \mu\right)\Delta z\right\} \qquad (54)$$

$$+\left(N_{c_o} - \frac{\Lambda_1 N_{a_o}}{\lambda - (\Lambda_1 + \Lambda_2)}\right) \exp\left\{-\frac{\lambda}{w} + \mu \Delta z\right\}$$

and

$$N_r = \left((N_{r_o} + N_{c_o} + N_{a_o})\right)\exp(-\mu\Delta z)$$

$$- N_{a_o}\left(\frac{\Lambda - \Lambda_2}{\lambda - (\Lambda_1 + \Lambda_2)}\right)\exp\left\{-\left(\frac{\Lambda_1 + \Lambda_2}{w} + \mu\right)\Delta z\right\} \qquad (55)$$

$$-\left(N_{c_o} - \frac{\Lambda_1}{\lambda - (\Lambda_1 + \Lambda_2)} N_{a_o}\right)\exp\left\{-\frac{\lambda}{w} + \mu \Delta z\right\}$$

Here $\Delta z = z_n - z_{n-1}$, N_{a_o}, N_{c_o}, and N_{r_o} are the concentrations of aerosol in cloud air, cloudwater, and rainwater, respectively. Equations (53), (54) and (55) are evaluated for each size range of aerosol. In the present study, the conversion rate λ is parameterized as described in the next section, so that the individual interactions between rainwater droplets and cloudwater droplets cannot be distinguished. Therefore, it is assumed that aerosol pollutants contained in rainwater are uniformly distributed in rainwater regardless of the size of aerosols.

Based on this assumption, the effect of fallout is treated as follows: In the evaluation of N_r of Eq. (55) at the height z_n, N_{r_o} is replaced by $N_{r_o}(1 - P_r)$, where P_r is the ratio of rainwater fallout to the total rainwater at the height z_{n-1}.

6.2.3. The rate constants Λ_1, Λ_2, and λ.

1. The scavenging rate of aerosols by cloudwater droplets, Λ_1

The scavenging of aerosols by cloudwater droplets occurs by Brownian and turbulent diffusion (Greenfield, 1957, and Dingle and Lee, 1973), and by phoretic diffusion (Slinn and Hales, 1971, and Young, 1974). Howell (1949), Squires (1952), Mordy (1959) and Neiburger and Chien (1960) showed, from theoretical calculations, that peak supersaturation (generally less than 1%) is reached at a few tens of meters above cloud base and thereafter the cloud droplets consume the moisture at such a rate that the supersaturation remains below the 0.2% level. Warner (1968) estimated that the median supersaturation

is 0.1% in small cumuli. The phoretic diffusion (diffusiophoresis plus themophoresis) rate, compared with Brownian and turbulent diffusion rates, is very small in the portion of cloud where the air is slightly supersaturated with respect to water. Therefore, the phoretic diffusion effect is neglected.

The Brownian diffusion scavenging rate, Λ_B, is expressed by

$$\Lambda_B(a,r_s) = \int_0^\infty \frac{k_b T}{3\eta}\left(\frac{a + A\ell}{a^2} + \frac{r + A\ell}{r^2}\right)(a + r)\, f(r)dr \qquad (56)$$

where a and r are aerosol and cloudwater droplet radii, respectively; A the Cunningham correction factor (= 0.9); ℓ the mean free path of air molecules; k_b Boltzmann's constant; T the absolute temperature; and η the dynamic viscosity of air. f(r) is the size distribution of the cloudwater droplet. In Eq. (56) and in the succeeding equations the subscript s refers to "the spectrum of", that is, $\Lambda(a,r_s)$ means the scavenging rate for aerosol of radius "a" by cloudwater droplets having a spectrum defined by f(r)dr.

The turbulent diffusion scavenging rate, Λ_T, is expressed by

$$\Lambda_T(a,r_s) = \int_0^\infty 14.1(a + r)^3 \cdot \left(\frac{\varepsilon'}{\nu}\right)^{\frac{1}{2}} f(r)dr \qquad (57)$$

where ε' is the rate of energy dissipation and ν the kinetic viscosity of air (Levich, 1962, Dingle and Lee, 1973). For a convective cloud such as cumulus, Ackerman (1968) obtained an average value for ε of 46.2 $cm^2 sec^{-3}$.

Considering that Brownian and turbulent diffusions are additive, the scavenging rate of aerosols by cloudwater droplets Λ_1 is given by

$$\Lambda_1(a,r_s) = \Lambda_B(a,r_s) + \Lambda_T(a,r_s) \qquad (58)$$

2. The scavenging rate of aerosols by rainwater droplets, Λ_2

We take into consideration Brownian diffusion, interception collection, and inertial impaction collection. Dana and Hales (1976) cited the following approximate expressions for these collections.

The Brownian diffusion scavenging rate, Λ_B', is expressed as

$$\Lambda_B'(a,R_s) = \int_0^\infty (0.65 \times 10^{-12})\pi R^2 \left[\frac{10^{-7}}{a^2R^2} + \frac{1}{a^{4/3}R}\right] F(R)dR \qquad (59)$$

where R is the radius of rainwater droplets, a the radius of aerosol pollutants, and F(R) the size distribution of rainwater droplets (Slinn, 1971).

The interception collection rate, Λ_I, is

$$\Lambda_I(a,R_s) = \int_0^\infty 3\,\frac{a}{R}\,F(R)dR, \tag{60}$$

according to Fuchs (1964).

The inertial impaction rate, Λ_{II}, is given by

$$\Lambda_{II}(a,R_s) = \int_0^\infty \left[\frac{S - \frac{1}{12}}{S + \frac{7}{12}}\right]^{3/2} F(R)dR \tag{61}$$

where

$$S = \frac{2}{9}\,\frac{a^2\rho_p}{R\rho_a}\,\frac{V_t}{\nu} \tag{62}$$

ρ_p and ρ_a are the mass density of the aerosols and air, respectively, V_t the terminal velocity of rainwater droplets, and ν the kinematic viscosity of air.

Again considering these effects to be additive, the scavenging rate of aerosols by rainwater droplets Λ_2 is given by

$$\Lambda_2(a,R_s) = \Lambda_B'(a,R_s) + \Lambda_I(a,R_s) + \Lambda_{II}(a,R_s) \tag{63}$$

3. The conversion rate of cloudwater droplets into rainwater droplets, λ

In cumulus clouds the rainwater droplets are generated by the processes of autoconversion and accretion, as described previously. The growth due to diffusion is small compared with these processes, so that it can be neglected. Thus, the growth rate of rainwater can be expressed as

$$\frac{dM}{dt} = \left.\frac{dM}{dt}\right|_{auto} + \left.\frac{dM}{dt}\right|_{accr} = \lambda m. \tag{64}$$

Therefore,

$$\lambda = \frac{1}{m}\left(\left.\frac{dM}{dt}\right|_{auto} + \left.\frac{dM}{dt}\right|_{accr}\right) \tag{65}$$

Here, M and m are the contents of rainwater and cloudwater, respectively, in the cloud layer under consideration, and $\left.\frac{dM}{dt}\right|_{auto}$ and $\left.\frac{dM}{dt}\right|_{accr}$ have been given

by Eqs. (47) and (48).

6.2.4. The size distribution of aerosols and cloudwater droplets.

1. The size distribution of cloudwater droplets

As mentioned previously, the size distribution of cloudwater droplets is assumed to be given by a gamma distribution as

$$f(r) = \frac{n_o r^{\alpha-1} e^{-r/\beta}}{p(\alpha)\beta^{\alpha}} \qquad 0 < r < \infty \tag{66}$$

The mean $\bar{r}$ and variance σ^2 of the distribution are given by

$$\bar{r} = \alpha\beta \tag{67}$$

and $$\sigma^2 = \alpha\beta^2 \tag{68}$$

The radius dispersion ν_r specifies the parameter α by

$$\nu_r = \frac{\sigma}{\bar{r}} = \alpha^{-\frac{1}{2}} \tag{69}$$

The mean radius is given by

$$\bar{r} = \left(\frac{3}{4\pi\rho_\ell}\right)\frac{m}{n_o}^{1/3}, \tag{70}$$

and the parameter β is given by

$$\beta = \left[\frac{3m}{4\pi\alpha(\alpha+1)(\alpha+2)\,n_o}\right]^{1/3} \tag{71}$$

Therefore, if the radius dispersion, ν_r, the droplet concentration, n_o, and the cloudwater content, m, are known, Eq. (67) completely specifies the distribution.

2. The size distribution of aerosols

Model aerosol spectra for continental aerosols and for maritime aerosols published by Junge and McLaren (1971) are used as input data for the present study. In Fig. 21, the model aerosol distributions are shown.

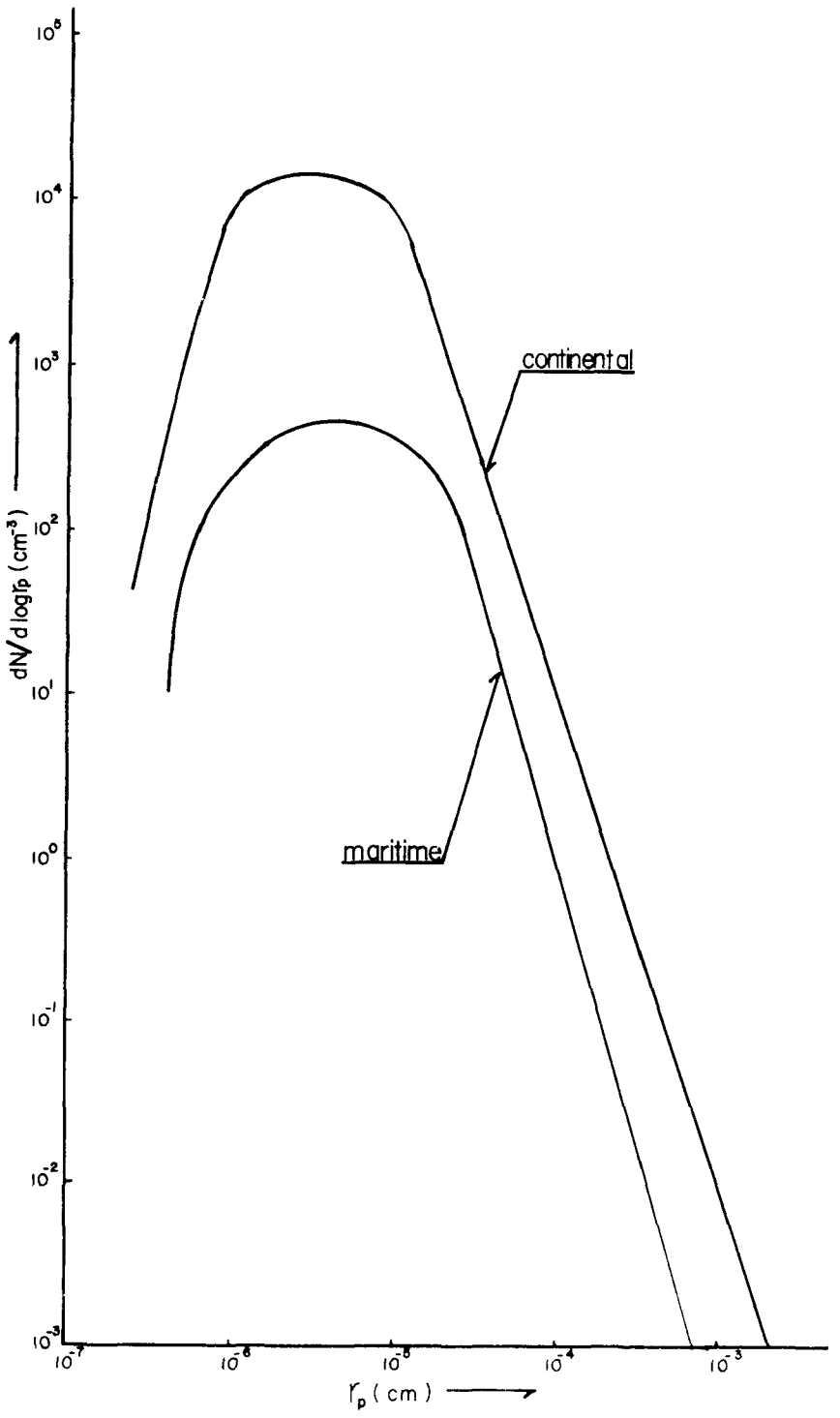

Figure 21. Model size distributions of continental and maritime air. (After Junge and McLaren, 1971.)

6.3. Numerical Procedures

1. In order to generate a cloud, the model sounding data shown in Fig. 22 are used. This sounding is applied to both continental and maritime clouds. In addition, the entrainment constant, $c'(\mu = c'/R_c$, where R_c is the cloud radius); the cloud radius, R_c; the initial temperature perturbation, ΔT; the initial updraft velocity, w_1; the concentration of cloudwater droplets, n_o; the radius dispersion, ν_r; and the concentration of rainwater droplets, N_o, are specified.

2. The vertical numerical integration scheme of the cloud parcel by height steps, Δz, is the same as suggested by Cotton (1972b). The integrations of moisture continuity equations and vertical lapse rates in cloud temperature are performed numerically with a first-order integration. The vertical integration is repeated until the updraft velocity vanishes.

3. After each height step, Q_c (or m) and Q_H (or M) are used to calculate the size distributions of cloudwater droplets and of rainwater droplets, and subsequently the scavenging coefficients, Λ_1, Λ_2, and λ are derived. The calculations of aerosol concentrations in cloud air, cloudwater, and rainwater for each size class then follow.

4. In the next step the mass concentrations of aerosols in cloud air, cloudwater, and rainwater are calculated as

$$M_x = \sum_i \left(\frac{4}{3}\pi\rho a_i^3\right) N_{x,i} \tag{72}$$

where the subscript x stands for cloud air, cloudwater or rainwater, i is the size class of the aerosol and ρ is the density of the aerosols.

5. The next step is to calculate, at each height interval, the mass-integral scavenging coefficients, $\Lambda_1(a_s,r_s)$ and $\Lambda_2(a_s,R_s)$, defined as

$$\Lambda_1(a_s,r_s) = \frac{\int_0^\infty \Lambda_1(a,r_s)\, a^3 f(a)da}{\int_0^\infty a^3 f(a)da} \tag{73}$$

and

$$\Lambda_2(a_s,R_s) = \frac{\int_0^\infty \Lambda_2(a,R_s)\, a^3 f(a)da}{\int_0^\infty a^3 f(a)da} \tag{74}$$

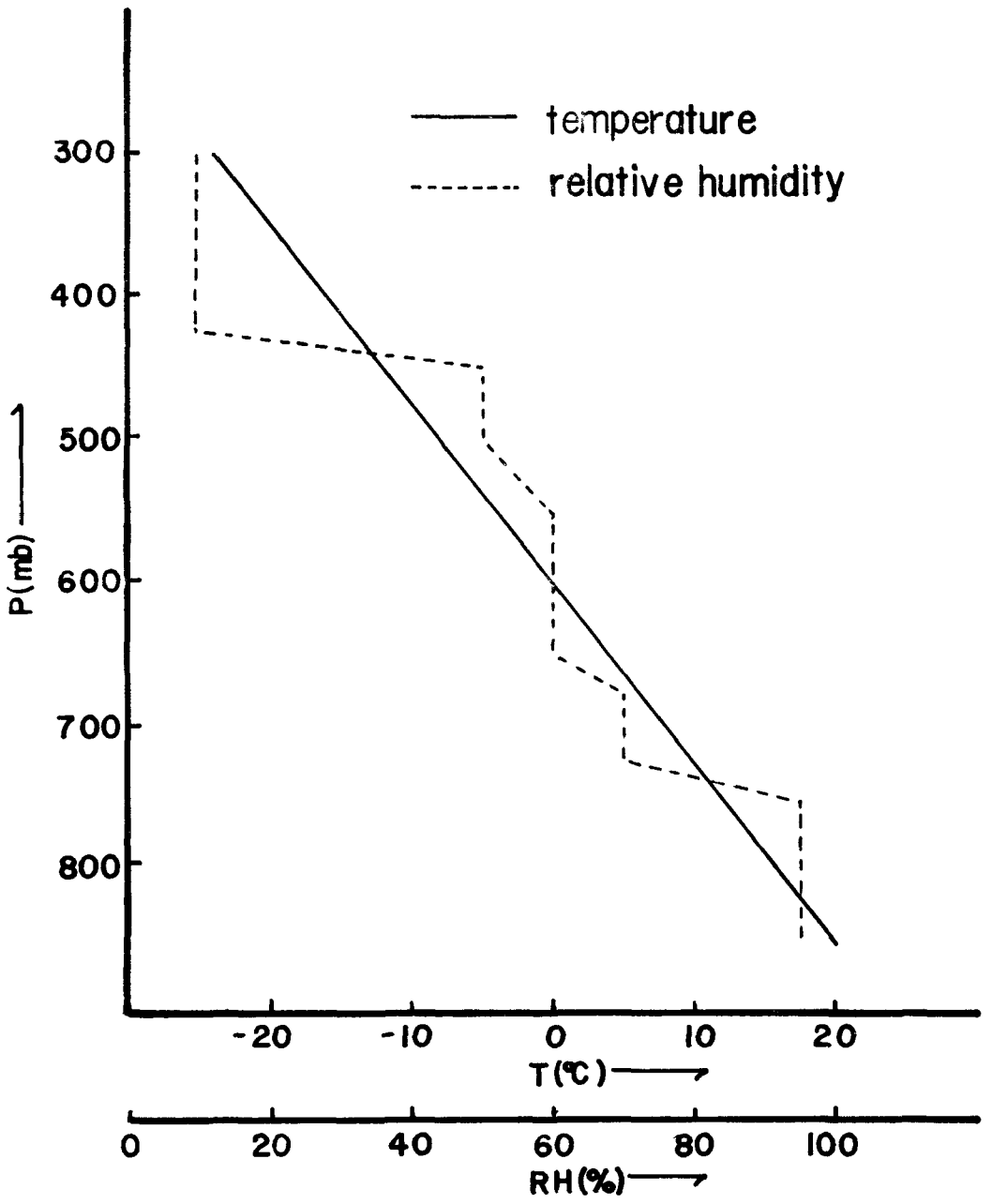

Figure 22. Model sounding used as an input.

Equations (73) and (74) are for the scavenging of aerosols by cloudwater and by rainwater, respectively. $\Lambda_1(a,r_s)$ and $\Lambda_2(a,R_s)$ have been given by Eqs. (58) and (63).

6.4. Results

6.4.1. Liquid water distribution with height in the clouds.

With the initial parameters of $k' = 0.2$, $R_c = 1$ km, $\Delta T = 0.5°C$, and $w_1 = 1$ m/sec, and with the sounding of environmental air shown in Fig. 22, the cloud tops were reached at 8300 m for both continental and maritime cumulus clouds. The cloud bases are at 1500 m. As mentioned previously, for the continental cumulus cloud, the concentration of cloudwater droplets, $n_o = 300$ cm^{-3}; the radius dispersion, $\nu_r = 0.25$; and the parameter set given by (47b) for the autoconversion equation (46) are used. For the maritime cumulus, $n_o = 100$ cm^{-3}, $\nu_r = 0.25$, and (47a) are used.

In Fig. 23, the distributions of cloudwater, Q_c, and rainwater, Q_h, with respect to height, are shown in terms of mixing ratio. The solid lines are for a maritime cloud, and the broken lines are for a continental cloud. From the figure, it can be seen that cloudwater conversion into rainwater is faster in the maritime cloud than in the continental cloud.

6.4.2. The distribution of scavenging rates with height.

The scavenging rates, Λ_1 and Λ_2, defined by Eqs. (73) and (74), and λ, defined by Eq. (65), are shown in Fig. 24(a) and (b). Figure 24(a) is for the continental cloud, and Fig. 24(b) is for the maritime cloud.

From these figures it can be seen that the scavenging rate of aerosols by cloudwater droplets has a peak at a few hundred meters above the cloud base. At this level, the conversion of cloudwater into rainwater has not started, so that the scavenging of aerosols is only by cloudwater droplets. After the rainwater starts to form, the scavenging rate, Λ_1, by cloudwater decreases. The renewed increase in Λ_1 above about 5000 m, for the case of the continental cloud, can be explained by the decrease in the value of the denominator of Eq. (69). In the case of the maritime cloud, a similar increase in Λ_1 can be seen, but it is not as obvious as in the continental cloud.

From a comparison of Fig. 24(a) with 24(b), it becomes clear that the scavenging rate of aerosols by cloudwater droplets, Λ_1, is about one order of magnitude larger in the continental cloud than in the maritime cloud. On the other hand, the scavenging rate by rainwater droplets, Λ_2, is larger in the maritime cloud than in the continental cloud. Similarly, the scavenging rate

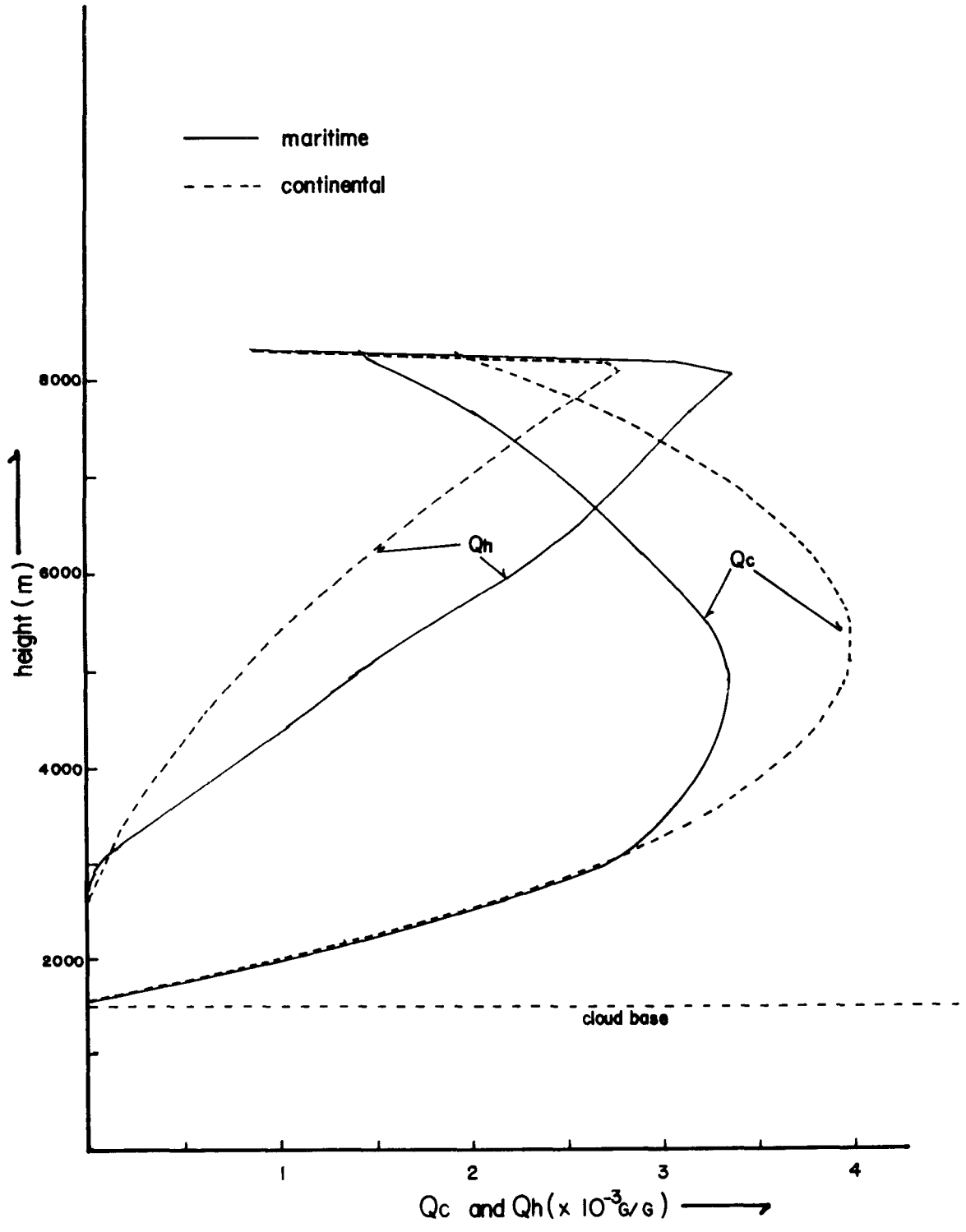

Figure 23. Distribution of cloudwater, Q_c, and rainwater, Q_h with respect to height.

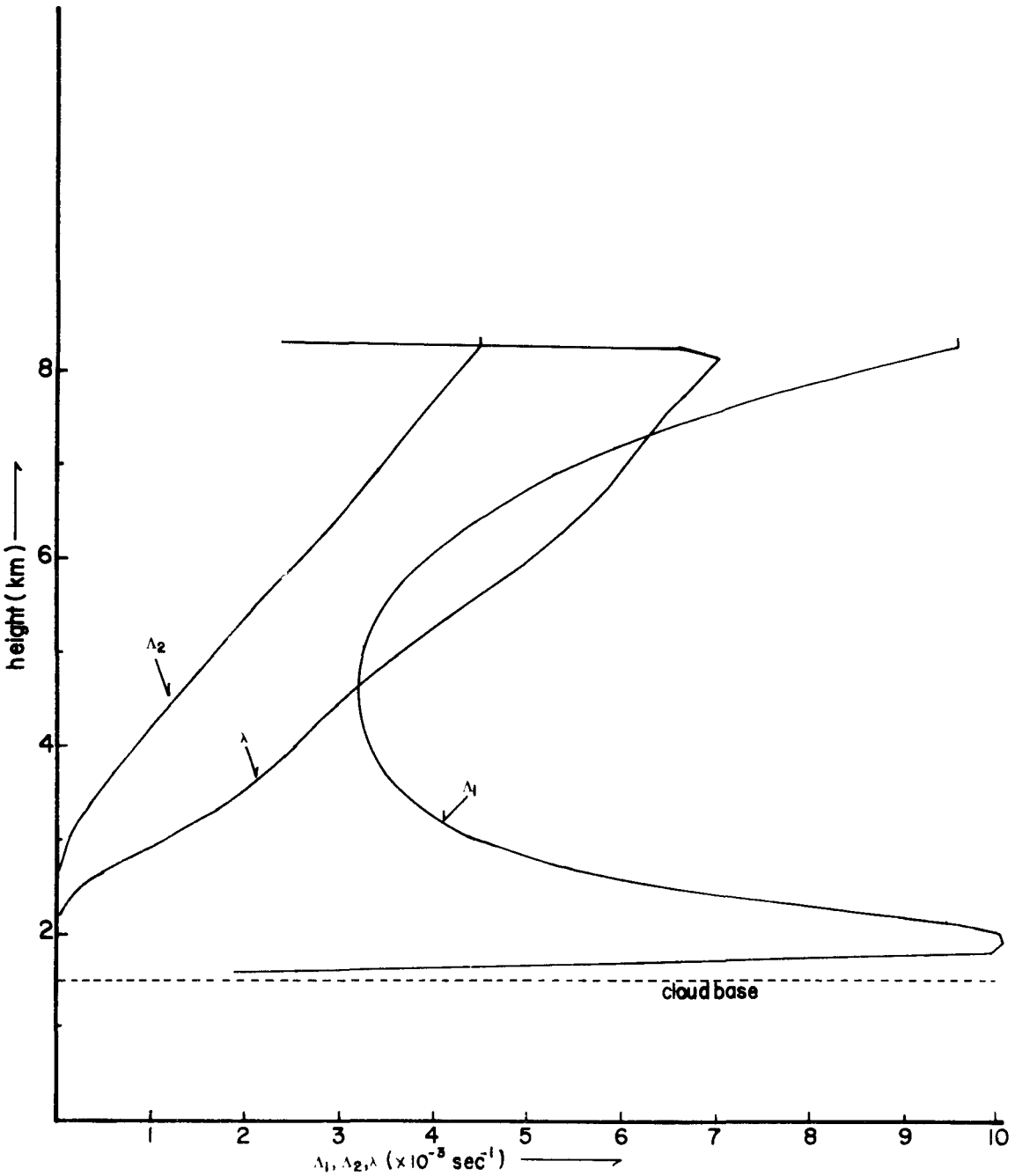

Figure 24 (a). Distributions of scavenging rates, Λ_1, Λ_2 and λ, in the continental cloud.

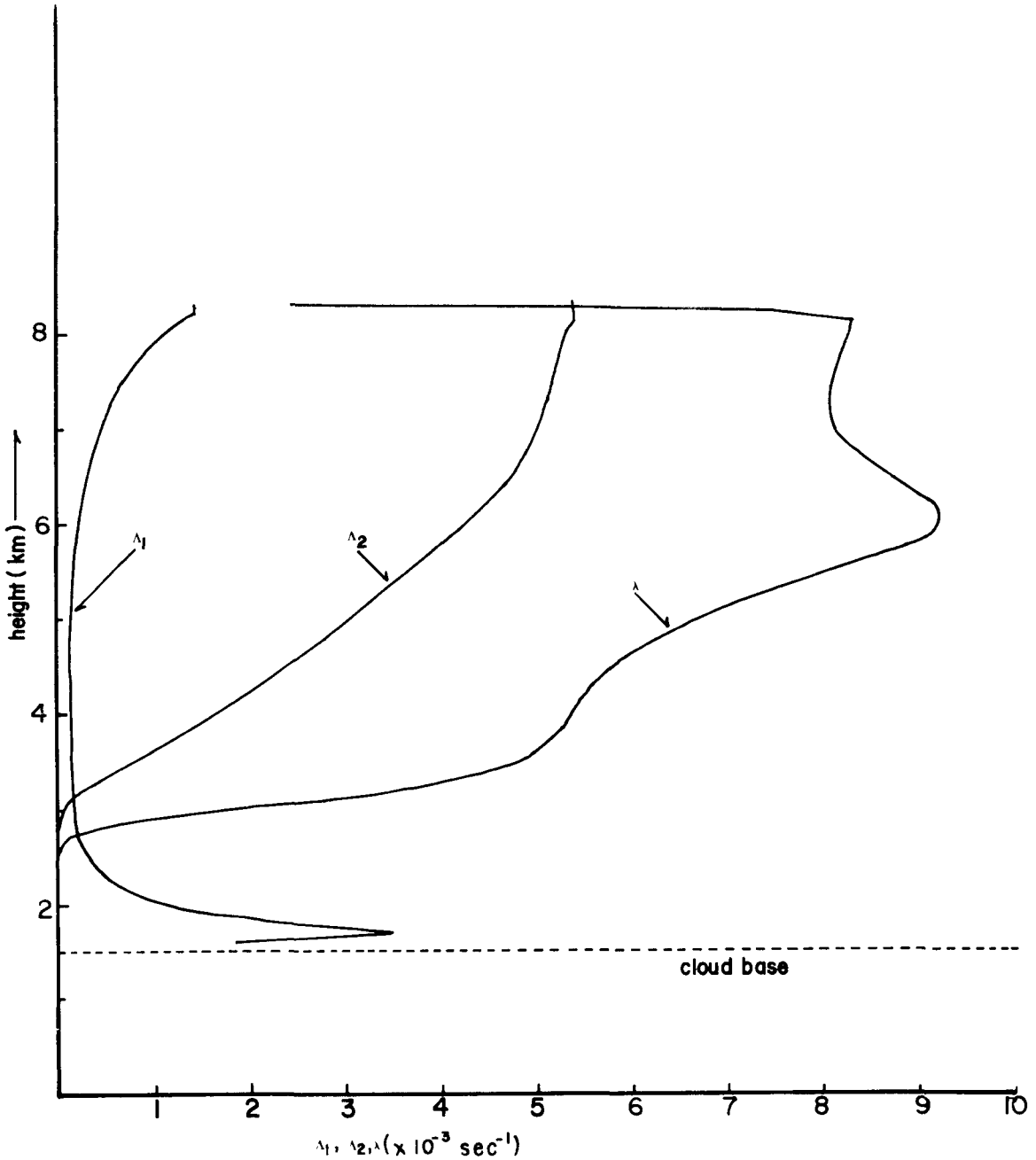

Figure 24(b). Same as Figure 24(a), except in the maritime cloud.

of cloudwater by rainwater, λ, is larger in the maritime cloud than in the continental cloud. In these particular clouds, the average values of Λ_1, Λ_2 and λ over the whole depth of the cloud are as follows:

	Continental	Maritime
Λ_1	5.11×10^{-3} sec^{-1}	4.88×10^{-4} sec^{-1}
Λ_2	1.76×10^{-3} sec^{-1}	2.66×10^{-3} sec^{-1}
λ	3.47×10^{-3} sec^{-1}	5.52×10^{-3} sec^{-1}

Makhon'ko (1967) and Davis (1972) have obtained gross scavenging rates of $10^{-4} \sim 10^{-3}$ sec^{-1}. The values obtained in the present study can be favorably compared with these observed values.

6.4.3. Mass fraction distributions of aerosols with height.

In Fig. 25(a) and (b), the mass fractions of aerosols in cloud air, cloudwater and rainwater divided by the total mass of aerosols in the air below the cloud base are shown. Figures 25(a) and (b) are for the continental cloud and for the maritime cloud, respectively.

The theoretical calculations by Howell (1949), Mordy (1960), and Neiburger and Chien (1960) show that the concentration of cloudwater droplets is determined by the number of effective condensation nuclei in the cloud base region. Furthermore, the particles effective as condensation nuclei are, in general, hygroscopic and larger than 0.1 microns, (Fletcher, 1966). Therefore, the two cases are studied. In the first case, the simple assumption is made that the 300 largest aerosol particles per cm^3 are consumed as condensation nuclei in the continental cloud (and the 100 largest in the maritime cloud) within the first layer of integration above the cloud base. In the second case, condensation nuclei are assumed to be supplied by other sources. In Figs. 25(a) and 25(b), the solid lines are for the case of condensation process assumed, and the broken lines are for the case of no-condensation assumed for the aerosols.

From a comparison of these two figures, the following can be inferred:

1. Aerosols in cloud air in the continental cloud are removed more efficiently than those in the maritime cloud. This is due to more efficient scavenging by cloudwater droplets in the continental cloud than in the maritime cloud.

2. As a consequence, the mass fraction of aerosols in cloudwater is larger in the continental cloud than in the maritime cloud.

3. Because of the more efficient conversion of cloudwater to rainwater in the maritime cloud than in the continental cloud, the mass

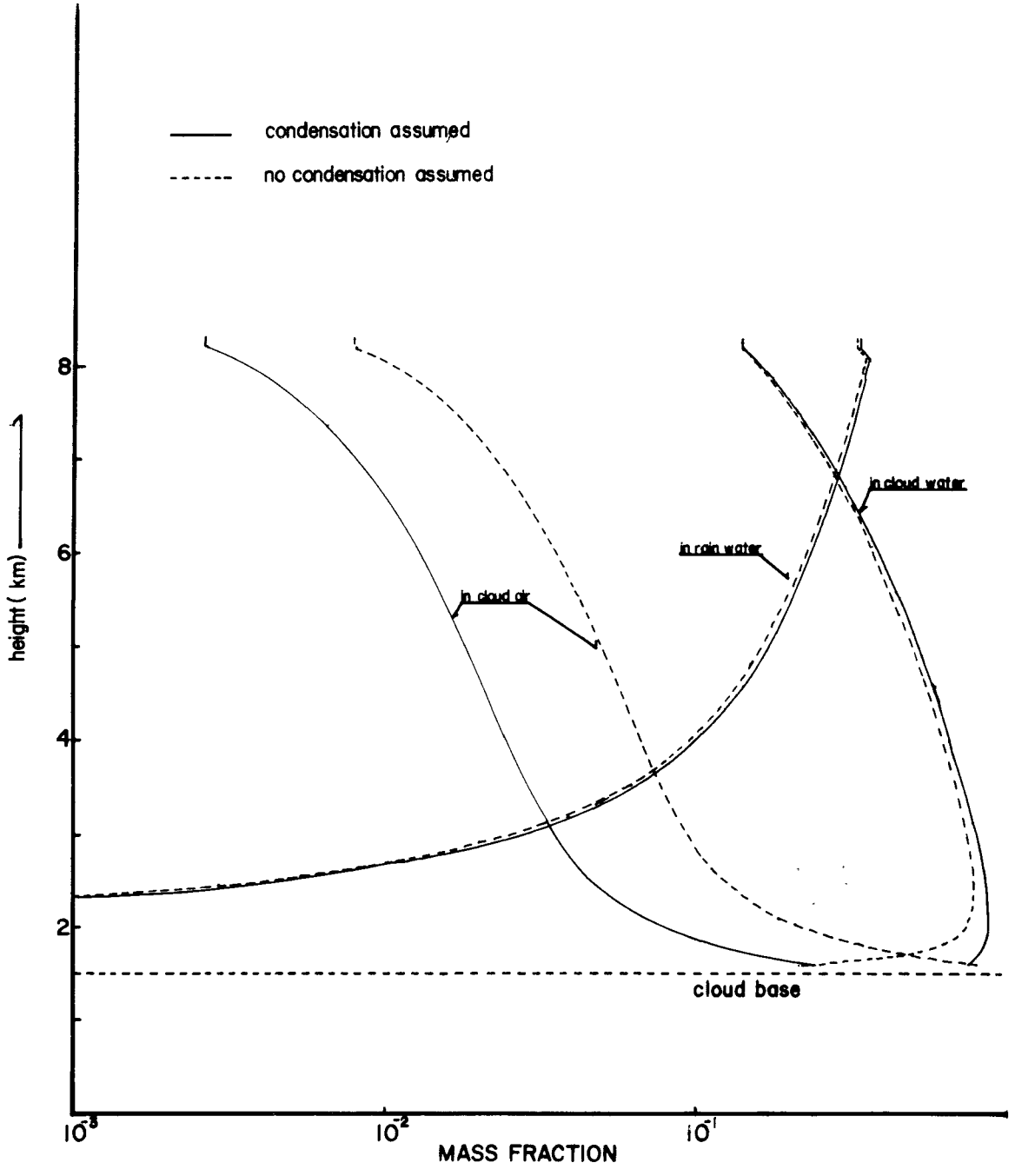

Figure 25(a). Distributions of mass fractions of aerosols in cloud, cloudwater and rainwater in the continental cloud.

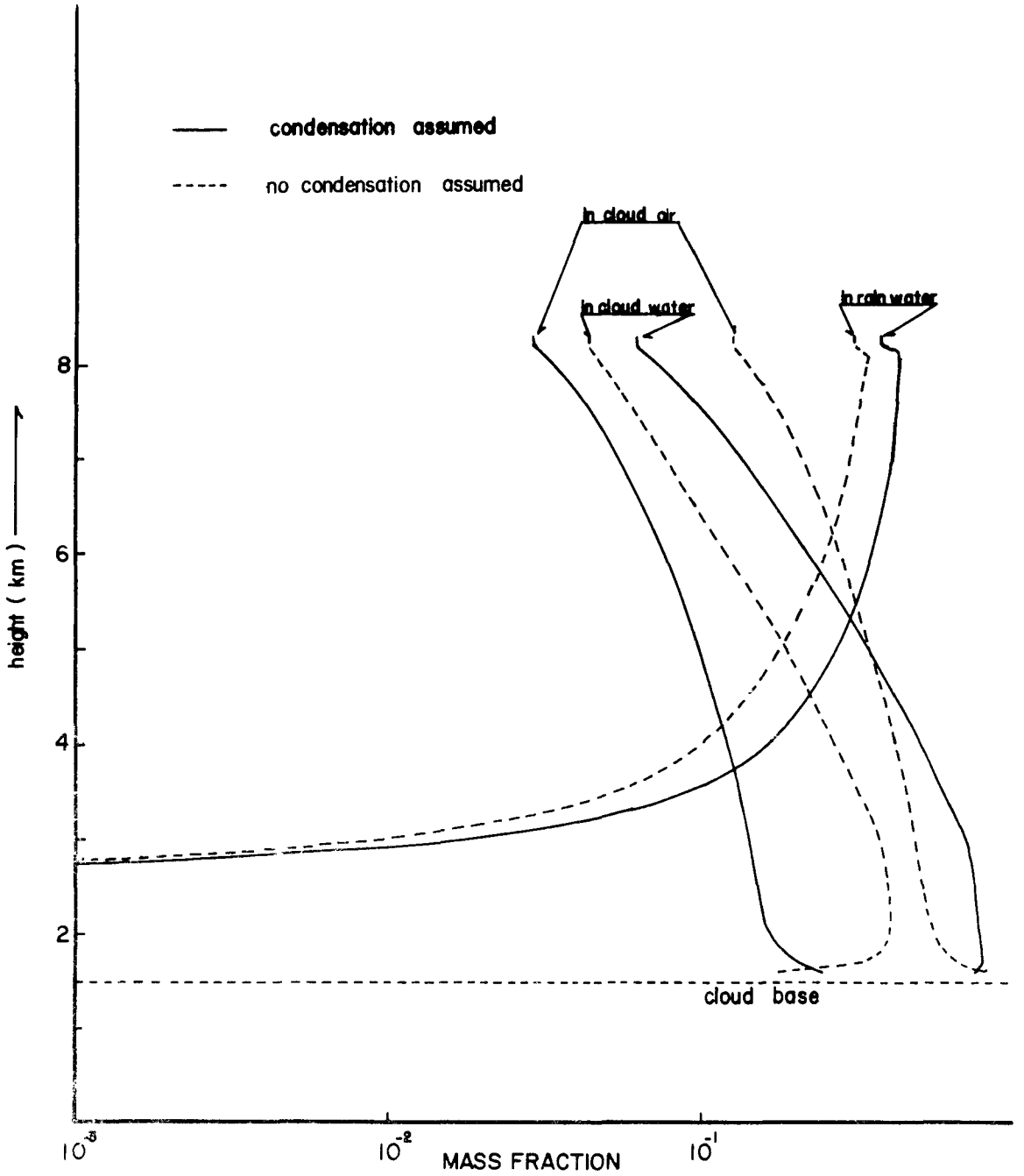

Figure 25(b). Same as Figure 25(a), except in the maritime cloud.

fraction of aerosols in rainwater is larger in the maritime cloud than in the continental cloud.

4. In the continental cloud it does not make a significant difference in the mass fractions of aerosols in cloudwater and in rainwater whether condensation processes are assumed or not. On the other hand, in the maritime cloud, the mass fractions of aerosols in the cloudwater and in rainwater become significantly larger than those of no assumption of condensation. This is again a consequence of the fact that the scavenging rate, Λ_1, is larger in the continental cloud than in the maritime cloud.

6.4.4. The ratio of aerosol mass in rainwater to that in the air at cloud base, $(\kappa/\chi_o)_m$.

Engelmann (1971) defines a "washout ratio" in terms of κ/χ_o, where κ is the concentration of a specific pollutant in rainwater, and χ_o is the concentration of the pollutant in surface air. According to the table of $(\kappa/\chi_o)_m$ for various pollutants summarized by Engelmann, the values of (κ/χ_o) vary, but are within the orders of 10^2 to 10^3. Here, the subscript m means that the ratio is taken on the basis of masses of rainwater and air.

In the present study, the following values of $(\kappa/\chi_o)_m$ are obtained:

	Total Precipitation Per Cloud	$(\kappa/\chi_o)_m$ - Condensation Assumed	$(\kappa/\chi_o)_m$ - No Condensation Assumed
Continental	3.87 mm	203	198
Maritime	5.82 mm	198	161

These values are in good agreement with values observed by various authors (see Table 1, Engelmannn, 1971). It can be seen that $(\kappa/\chi_o)_m$ for the continental cloud is larger than that for the maritime cloud.

6.5. Summary

The purpose of the present study was to investigate the scavenging characteristics of continental and maritime cumulus clouds, based on a numerical model of in-cloud scavenging, combined with a cumulus model. Using identical sounding and initial parameters, w_1, ΔT, and R, two different clouds with different numbers of cloudwater droplets (300 cm^{-3} for the continental cloud,

and 100 cm^{-3} for the maritime cloud) and with different autoconversion rates of cloudwater to rainwater have been studied.

The scavenging rate of aerosols by cloudwater droplets, Λ_1, is one order of magnitude larger in the continental cloud than in the maritime cloud. On the other hand, scavenging rates of aerosols by rainwater droplets, Λ_2, and scavenging rates of cloudwater droplets by rainwater droplets, λ, are larger in the maritime cloud than in the continental cloud.

Because of the larger value of Λ_1 in the continental cloud than in the maritime cloud, the mass fraction of aerosols in cloudwater is larger in the continental cloud than in the maritime cloud, and consequently the ratio of $(\kappa/\chi_o)_m$ is larger in the continental cloud than in the maritime cloud.

The application of results from the model calculation to the transport model described in Section 4 can be made through the relationship

$$V_p = (\kappa/\chi_o)_v \cdot P$$

where V_p is the scavenging velocity in equation 4, and P is the precipitation rate. Therefore, if the precipitation rate in the area where the pollutant plume passes through is known, the removal term of the pollutant due to precipitation can be estimated.

SECTION 7

REFERENCES

Ackerman, B., 1968. The rate of dissipation of turbulent energy in cloudy air. Proc. Intern. Conf. Cloud Physics, Toronto, pp. 564-567.

Andersson, T., 1969. Small-scale variations of the contamination of rain caused by washout from the low layers of the atmospheres. Tellus, 21, 685-692.

Auer, A. H., 1975. The production of cloud and Aitken nuclei by the St. Louis Metropolitan area (Project METROMEX). Journal de Recherches Atmospheriques, 9, 11-12.

Bauer, E., 1973. Dispersion of tracers in the atmosphere: Survey of meteorological data. Institute for Defence Analysis, Science and Technology Division, Paper P-925, Contract DAHC 15 73 C 0300 Task T-90.

Berry, E. X., 1965. Cloud Droplet Growth by Collection. Ph.D. Dissertation, Univ. Nevada, pp 143.

Bufalini, M., 1971. Oxidation of sulfur dioxide in polluted atmospheres. A Review. Env. Sci. & Tech., 5, 685-700.

Csandy, G. T., 1969. Diffusion in an Ekman layer. J. Atmos. Sci., 26, 414-426.

Cotton, W. R., 1972. Numerical simulation of precipitation development in supercooled cumuli - Part I. Mon. Wea. Rev., 100, 757-763.

Cotton, W. R., 1972. Numerical simulation of precipitation development in supercooled cumuli - Part II. Mon. Wea. Rev., 100, 764-784.

Dana, M. T., J. M. Hales, W. G. N. Slinn, and M. A. Wolf, 1973. Natural precipitation washout of sulfur compounds from plumes. Atmos. Sci. Dept., Battelle, Pacific Northwest Laboratories, EPA-R3-73-047.

Dana, M. T., and J. M. Hales, 1976. Statistical aspects of the washout of polydisperse aerosols. Atmos. Env., 10, 45-50.

Dana, M. T., D. R. Drewes, D. W. Glover, and J. M. Hales, 1976. Precipitation scavenging of fossil-fuel effluents. EPA-600/4-76-031. U.S. Environmental Protection Agency.

Davis, F.D., and H. Newstein, 1968. The meteorology and vertical distribution of pollutants in air pollution episodes in Philadelphia. Atmos. Env., 2, 559-574.

Davis, W. E., 1972. A model for in-cloud scavenging of cosmogenic radionuclides. J. Geoph. Res., 77, 2159-2165.

Deardorff, J. W. and G. E. Willis, 1974. Computer and laboratory modeling of the vertical diffusion of nonbuoyant particles in the mixed layer. Advances in Geophysics. 18B, 187-200.

Dingle, A. N., and Y. Lee, 1973. An analysis of in-cloud scavenging. J. Appl. Met., 12, 1295-1302.

Dittenhoeffer, A. C., and B. E. Dethier, 1976. The precipitation chemistry of western New York State: A meteorological interpretation. Research Project Technical completion Report OWRT, Project No. A-044-NY. Agreement No. 14010001-3532, Cornell University Water Resources and Marine Science Center, Ithaca, New York.

Eliassen, A. and J. Saltbones, 1975. Decay and transformation rates of SO_2, as estimated from emission data, trajectories and measured air concentrations. Atmos. Env., 9, 425-430.

Engelmann, R. L., 1971. Scavenging prediction using ratios of concentrations in air and precipitation. J. Appl. Met., 10, 493-497.

Fletcher, N. H., 1966. The Physics of Rainclouds. Cambridge at University Press, pp. 390.

Fuelberg, H. E., and R. E. Turner, 1975. Data for NASA's AVE III experiments: 25-mb sounding data and synoptic charts. NASA Technical Memorandum NASA TMX-64938.

Garland, J. A., D. H. F. Atkins, C. J. Readings, and S. J. Coughey, 1974: Deposition of gaseous sulphur dioxide to the ground. Atmos. Env., 8, 75-79.

Garland, J. A. and J. R. Branson, 1976. The mixing height and mass balance of SO_2 in the atmosphere above Great Britain. Atmo. Env., 10, 353-362.

Garland, J. A., W. S. Clough, and D. Fowler, 1973. Deposition of sulphur dioxide on grass. Nature, 242, 256-257.

Georgii, H. -W., 1969. Note on the vertical distribution of pollutants in stagnating air. Atmos. Env., 3, 238-239.

Greenfield, S. M., 1957. Rain scavenging of radioactive particle matter from the atmosphere. J. Met., 14, 115-125.

Harrison, H., T. V. Larsen, and P. V. Hobbs, 1975. Oxidation of sulfur dioxide in the atmosphere: A review. Proc. Int'l. Conf. on Enviromental Sensing and Assessment, Las Vegas, Nevada, Sept. 14-19, 1975.

Heffter, J. L., and A. D. Taylor, 1975. A regional-continental scale transport, diffusion and deposition model. NOAA Technical Memorandum ERL ARL-50.

Holzworth, G. C., 1967. Mixing depths, wind speeds, and air pollution potential for selected locations in the United States. J. Appl. Meteor., 6, 1039-1044.

Holzworth, G. C., 1972. Mixing heights, wind speeds, and potential for urban air pollution throughout the contiguous United States. EPA Office of Air Programs Publication, No. AP-101.

Howell, W. E., 1949. The growth of cloud drops in uniformly cooled air. J. Met., 6, 134-149.

Howell, W. E., and M. Lopez, 1968. "Project Rainstart" Interim Report. Contract No. NSF-C453, E. Bollay Associates, Inc., Boulder, Colo., pp. 66.

Junge, C. E., 1960. Sulfur in the atmosphere. J. Geophys. Res., 65, 227-237.

Junge, C., and E. McLaren, 1971. Relationship of cloud nuclei spectra to aerosol size distribution and composition. J. Atmos. Sci., 28, 382-390.

Kessler, E., 1967. On the continuity of water substance. ESAS Technical Memorandom IERTM-NSSL33, U.S. Dept. Commerce, National Severe Storms Laboratory, Norman, Okla., pp. 125.

Kocmond, W. C. and E. J. Mack, 1972. The vertical distribution of cloud and Aitken nuclei downwind of urban pollution sources. J. Appl. Meteor., 11, 141-148.

Levich, V. G., 1962. Physico-Chemical Hydrodynamics. Englewood Cliffs, New Jersey, Prentice-hall, pp. 700.

Lodge, J. P., Jr., et al., 1968. Chemistry of United States precipitation. Final Report on the National Precipitation Sampling Network, National Center for Atmospheric Research, Boulder, Colorado.

Makhon'ko, K. P., 1967. Simplified theoretical notion of contaminant removal by precipitation from the atmosphere. Tellus, 19 467-476.

Marshall, J. S., and W. M. Palmer, 1948. The distribution of raindrops with size. J. Met., 5, 165-166.

Meetham, A. R., 1950. Natural removal of pollution from the atmosphere. Quart. J. Roy. Meteor. Soc., 76, 359-371.

Meetham, A. R., 1954. Natural removal of atmospheric pollution during fog. Quart. J. Roy. Meteor. Soc., 80, 96-99.

Mordy, W. A., 1959. Computations of the growth by condensation of a population of cloud droplets. Tellus, 11, 16-44.

Neiburger, M., and C. W. Chien, 1960. Computations of the growth of cloud drops by condensation using an electronic digital computer. Physics of Precipitation, Geophysical Monograph Series, 5, 191-208, AGU, Washington, D.C.

Owers, M. J. and A. W. Powel, 1974. Deposition velocity of sulphur dioxide on land and water surfaces using a ^{35}S tracer method. Atmos Env., 8, 63-67.

Pasquill, F., 1974. Atmospheric Diffusion, 2nd Edition, Halsted Press: A Division of John Wiley & Sons, pp. 429.

Prahm, L. P., U. Torp and R. M. Stern, 1976. Deposition and transformation rates of sulphur oxides during atmospheric transport over the Atlantic. Tellus, 28, 355-372.

Rao, K. S., J. S. Lague, and B. A. Egan, 1976. An air trajectory model for regional transport of atmospheric sulfates. Preprints of Third Symposium on Atmospheric Turbulence, Diffusion and Air Quality, American Meteorologican Society, 325-331.

Rodhe, H., 1970. On the residence time of anthropogenic sulfur in the atmosphere. Tellus, 22, 137-139.

Rodhe, H., 1972. A study of the sulfur budget for the atmosphere over Northern Europe. Tellus, 26, 128138.

Rodhe, H. and J. Grandell, 1972. On the removal time of aerosol particles from the atmosphere by precipitation scavenging. Tellus, 26, 442-454.

Scoggins, J. R., and R. E. Turner, 1974. Data for NASA's AVE II pilot experiment, Part I: 25-mb sounding data and synoptic charts. NASA Technical Memorandum NASA TMX - 64877.

Scriven, R. A. and B. E. A. Fisher, 1974. The long range transport of airborne material and its removal by deposition and washout - 1. General considerations. Atmos. Env., 9, 49-58.

Shepherd, J. A. 1974. Measurements of the direct deposition of sulfur dioxide onto grass and water by the profile method. Atmos. Env, 8, 69-74.

Slinn, W. G. N., 1971. Numerical explorations of washout of aerosol particles. Pacific Northwest Laboratory Annual Report for 1970 to the USAEC Division of Biology and Medicine, Vol. II: Physical Sciences, Part I, Atmospheric Sciences, p. 75. BNWL-1551 (II,I), Battele Pacific Northwest Laboratories Richland, Wash.

Slinn, W. G. N., and J. M. Hales, 1971. A reevaluation of the role of thermophoresis as a mechanism of in- and below-cloud scavenging. J. Atmos. Sci., 28, 1465-1471.

Smith, F. A. and F. H. Jeffrey, 1975. Airborne transport of sulfur dioxide from the U.S. Atmos. Env., 9, 643-659.

Squires, P., and J. S. Turner, 1962. An entertaining jet model for cumulonimbus updraughts. Tellus, 14, 422-434.

Stevenson, C. M., 1968. An analysis of the chemical composition of rainwater and air over the British Isles and Eire for the years 1959-1964. Quart. J. Roy. Meteor. Soc., 94, 56-70.

Summers, P. W., 1970. Scavenging of SO_2 by convective storms. Precipitation Scavenging 1970, U.S. Atomic Energy Commission Symposium Series.

Tyldesley, J. B., and C. E. Wallington, 1965. The effects of wind shear and vertical diffusion on horizontal dispersion. Quart. J. Roy. Meteor. Soc., 91, 158-174.

Urone, P. and W. H. Schroeder, 1969. SO_2 in the atmosphere: A wealth of monitoring data, but few reaction rate studies. Env. Sci. & Tech., 3, 436445.

U.S. Department of Commerce, National Oceanic and Atmospheric Administration, Environmental Data Service, 1974; Hourly Precipitation Data.

Warner, J., 1968. The supersaturation in natural clouds. J. de Recherches Atmospheriques, 3, 233-237.

Whelpdale, D. M. and R. W. Shaw, 1974. Sulphur dioxide removal by turbulent transfer over grass, snow, and water surfaces. Tellus, 26, 196-204.

Young, K. C. 1974. The role of contact nucleation in ice phase initiation in clouds. J. Atmos. Sci., 31, 768-776.

TECHNICAL REPORT DATA
(Please read Instructions on the reverse before completing)

1 REPORT NO	2	3. RECIPIENT'S ACCESSION NO.
EPA-600/4-78-003		

4 TITLE AND SUBTITLE	5. REPORT DATE
RESIDENCE TIME OF ATMOSPHERIC POLLUTANTS AND LONG-RANGE TRANSPORT	January 1978
	6. PERFORMING ORGANIZATION CODE
7 AUTHOR(S)	8. PERFORMING ORGANIZATION REPORT NO.
Teizi Henmi, Elmar R. Reiter and Roger Edson	
9 PERFORMING ORGANIZATION NAME AND ADDRESS	10. PROGRAM ELEMENT NO.
Colorado State University Fort Collins, CO 80523	1AA603 AG-03 (FY-77)
	11. CONTRACT/GRANT NO.
	803685
12. SPONSORING AGENCY NAME AND ADDRESS	13. TYPE OF REPORT AND PERIOD COVERED
Environmental Sciences Research Laboratory - RTP, NC Office of Research and Development U.S. Environmental Protection Agency Research Triangle Park, NC 27711	Final 5/75-4/77
	14 SPONSORING AGENCY CODE
	EPA/600/09

15 SUPPLEMENTARY NOTES

16. ABSTRACT

The Lagrangian trajectory model which is suitable for the study of long-range transport of pollutants is developed. The computer program is capable of calculating trajectories over the region of the U.S. using routine sounding data. The output consists of tables of locations of trajectory end points at each time-step, dispersion widths along a trajectory, and the plotting of trajectories. The regional residence times, T, of SO_2 in the mixing layer are calculated for the region of the United States east of 105°W longitude, based on climatological data of the mixing layer depth and hourly precipitation data. The results are shown as isopleths of T over the studied area for the cold season (November to April) and for the warm season (May to October). Taking detailed microphysical processes into consideration, the scavenging due to cumulus cloud precipitation is studied. The results can be summarized as follows: The scavenging coefficient of aerosols by cloudwater droplets is one order of magnitude larger in the continental cloud than in the maritime cloud. On the other hand, the scavenging coefficient of aerosols by rainwater droplets is slightly larger in maritime clouds than in continental clouds. As a whole, aerosols are more efficiently scavenged in the continental cloud than in the maritime cloud.

17. KEY WORDS AND DOCUMENT ANALYSIS

a DESCRIPTORS	b. IDENTIFIERS/OPEN ENDED TERMS	c COSATI Field/Group
* Air pollution		13B
* Transport properties		04B
Meteorological data		14A
* Atmospheric models		07D
* Aerosols		07B
* Sulfur dioxide		

18 DISTRIBUTION STATEMENT	19. SECURITY CLASS *(This Report)*	21. NO. OF PAGES
RELEASE TO PUBLIC	UNCLASSIFIED	103
	20. SECURITY CLASS *(This page)*	22. PRICE
	UNCLASSIFIED	

EPA Form 2220-1 (9-73)